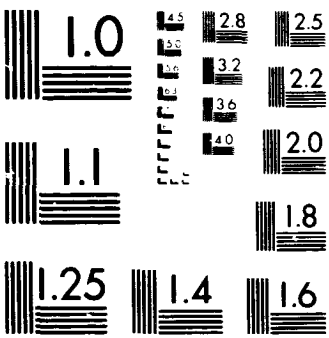

NASA

Technical Memorandum **82046**

Magsat Vector Magnetometer Calibration Using Magsat Geomagnetic Field Measurements

E. R. Lancaster, Timothy Jennings, Martha Morrissey and Robert Langel

NOVEMBER 1980

National Aeronautics and Space Administration

Goddard Space Flight Center
Greenbelt, Maryland 20771

MAGSAT VECTOR MAGNETOMETER CALIBRATION USING MAGSAT GEOMAGNETIC FIELD MEASUREMENTS

E. R. Lancaster, Timothy Jennings, Martha Morrissey
and Robert Langel

ABSTRACT

The Magnetic Field Satellite (Magsat) was launched on Oct. 30, 1979 into a nearly polar, sun-synchronous orbit, carrying a scalar magnetometer and a vector magnetometer. The satellite re-entered the earth's atmosphere on June 11, 1980, having measured and transmitted more than three complete sets of global magnetic field data. The data obtained from the mission will be used primarily to compute a currently accurate model of the earth's main magnetic field, to update and refine world and regional magnetic charts, and to develop a global scalar and vector crustal magnetic anomaly map.

This report describes the in-flight calibration procedure used for 39 vector magnetometer system parameters and gives results obtained from some data sets and the numerical studies designed to evaluate the results.

CONTENTS

MAGSAT VECTOR MAGNETOMETER CALIBRATION USING MAGSAT GEOMAGNETIC FIELD MEASUREMENTS

INTRODUCTION

The Magnetic Field Satellite (Magsat) was launched from the Western Test Range at Vandenberg Air Force Base in California into a nearly polar, sun-synchronous orbit on October 30, 1979. The orbit initially had a perigee of 352 km (219 miles) and an apogee of 578 km (359 miles). The satellite reentered the earth's atmosphere on June 11, 1980, having measured and transmitted more than three complete sets of global magnetic field data.

Magsat carried a scalar magnetometer and a vector magnetometer. The scalar magnetometer was an optically pumped, atomic resonance, dual-cell, self-oscillating cesium vapor magnetometer, capable of measuring the magnitude of the earth's magnetic field with a resolution of about ±0.6 gamma (1 gamma = 1 nanoTesla). The vector magnetometer consisted of three fluxgate sensing elements aligned along nearly orthogonal axes, capable of measuring each component of the earth's magnetic field with a resolution of ±0.5 gamma.

The data obtained from the mission will be used primarily to compute a currently accurate model of the earth's main magnetic field, to update and refine world and regional magnetic charts, and to develop a global scalar and vector crustal magnetic anomaly map. Details concerning the mission and its objectives have been given by Langel, Reagan, and Murphy (1).

Prior to the launch of Magsat, the values of thirty-nine parameters associated with the vector magnetometer were determined in the laboratory at Goddard Space Flight Center. It could not be assumed, however, that these values would remain unchanged after launch and under space conditions. Because of this a statistical procedure was developed for estimating the system parameters from the data taken by the scalar and vector magnetometers in space. A computer program was written and the procedure was tested on measurements made by the magnetometers in the magnetic test facility at Goddard Space Flight Center. The procedure has been and is continuing to be applied to the real magnetic field data transmitted from Magsat.

This report describes the in-flight vector magnetometer calibration procedure and gives results obtained from some data sets and the numerical studies designed to evaluate the results. A FORTRAN listing of the calibration program can be obtained upon request.

THE MAGSAT VECTOR MAGNETOMETER

The triaxial fluxgate magnetometer flown aboard the Magsat spacecraft was capable of measuring the earth's magnetic field vector components with a resolution of ±0.5 gamma. It was developed at NASA's Goddard Space Flight Center by M. H. Acuna and co-workers (2). A basic triaxial fluxgate magnetometer with 7-bit analog-to-digital converter had a dynamic range of ±2000 gammas. This range was increased to ±64,000 gammas in steps of approximately ±1000 gammas by using three 7-bit digital-to-analog converters as field offset generators, one for each sensor axis. Ground command could select either of two redundant configurations (A or B) for the magnetometer electronics; an additional ground command could select one of two configurations for analog-to-digital converter, field offset generators, digital interface, and power converter. A feedback coil nulled the ambient field independently along each sensor axis. The reader is referred to a report by Acuna et al (2) for details of the design of the Magsat vector magnetometer.

The magnetic field values (y_1, y_2, y_3) associated with the three sensor axes are computed from the equations

$$y_j = u_{j7} w_{j7} - \sum_{k=1}^{6} u_{jk} w_{jk} + w_{j8} (64 - K_j)^3 + w_{j9} (64 - K_j)^5 + a_j (f_j - b_j); j = 1, 2, 3 \qquad (1)$$

f_j = (integer given by A/D converter) minus (zero level value)

= fine measurement ($-2048 \leq f_j \leq 2047$) (zero level value = 2048)

K_j = integer from 7-bit D/A converter

= coarse measurement ($0 \leq K_j \leq 127$)

b_j = bias in f_j

a_j = scale factor

w_{jk} = value associated with kth step of offset generator

$\approx 1000 \times 2^{k-1}$; k = 1 to 7

u_{jk} = 0 or 1

u_{j7} = 0 if the most significant bit of K_j is 1

u_{j7} = 1 if the most significant bit of K_j is 0

u_{jk} = the kth bit of K_j, u_{j0} being the least significant.

For a detailed explanation of equation (1), the reader is referred to Acuna (3). Nominal values were determined for the 33 parameters w_{jk}, a_j, b_j (j = 1, 2, 3; k = 1, 2, . . . , 9) by various calibration procedures prior to launch (2, 3). The values for the A-configuration are given in Table 1. The cubic and quintic terms take into account small non-linearities in the vector magnetometer response function.

An orthogonal reference frame was defined in the sensor assembly such that the angle between a magnetic sensor axis and the corresponding axis in the orthogonal frame was not more than 1 minute of arc. Let (x_1, x_2, x_3) be the components of the magnetic field vector in the orthogonal frame and a_{ij} the cosine of the angle between the ith sensor axis and the jth axis of the orthogonal system at the common origin of the two systems. The vector components (x_1, x_2, x_3) in the orthogonal system and the magnetic field values (y_1, y_2, y_3) computed from (1) for the non-orthogonal axes of the sensors are related by the equations

$$y_1 = a_{11}x_1 + s_1 a_{12}x_2 + a_{13}x_3 \tag{2}$$

$$y_2 = s_2 a_{21}x_1 + a_{22}x_2 + a_{23}x_3 \tag{3}$$

$$y_3 = a_{31}x_1 + s_3 a_{32}x_2 + a_{33}x_3 \tag{4}$$

$$s_1 = \sin v_1 / v_1 \tag{5}$$

$$s_2 = \sin v_2 / v_2 \tag{6}$$

$$s_3 = \sin v_3 / v_3 \tag{7}$$

$$v_1 = a_{12}x_2 / r_1 \tag{8}$$

$$v_2 = a_{21} x_1 / r_2 \tag{9}$$

$$v_3 = a_{32} x_2 / r_3 \tag{10}$$

$$r_1 = h_{11} + \delta_2 h_{12} x_1 + h_{13} \exp(\delta_2 h_{14} x_1) \tag{11}$$

$$r_2 = h_{21} + \delta_1 h_{22} x_2 + h_{23} \exp(\delta_1 h_{24} x_2) \tag{12}$$

$$r_3 = h_{31} + \delta_2 h_{32} x_3 + h_{33} \exp(\delta_2 h_{34} x_3) \tag{13}$$

$$\delta_1 = 1 \text{ if } x_1 > 0 \tag{14}$$

$$= 0 \text{ if } x_1 = 0$$

$$= -1 \text{ if } x_1 < 0$$

$$\delta_2 = 1 \text{ if } x_2 > 0 \tag{15}$$

$$= 0 \text{ if } x_2 = 0$$

$$= -1 \text{ if } x_2 < 0$$

$$a_{11} = (1 - a_{12}^2 - a_{13}^2)^{1/2} \tag{16}$$

$$a_{22} = (1 - a_{21}^2 - a_{23}^2)^{1/2} \tag{17}$$

$$a_{33} = (1 - a_{31}^2 - a_{32}^2)^{1/2} \tag{18}$$

Nominal values were determined in the laboratory at GSFC prior to launch for the 6 parameters a_{jk} ($j \neq k$) and for the 12 parameters h_{jk}. The values for the A-configuration are given in Table 1. For further details see Acuna (2,3).

The s_1, s_2, and s_3 factors in equations (2), (3), and (4) and equations (5) through (15) by which they are computed are designed to model non-linearities in the vector magnetometer.

PARAMETER ESTIMATION PROCEDURE

The parameters to be estimated are w_{jk} ($j = 1, 2, 3$; $k = 1, 2, \ldots, 9$), a_j, b_j ($j = 1, 2, 3$), a_{12}, a_{13}, a_{21}, a_{23}, a_{31}, a_{32}, and x_{ij} ($i = 1, 2, \ldots, n$; $j = 1, 2, 3$) where n = the number of vector-scalar sets of measurements used in the estimation. If (x_{i1}, x_{i2}, x_{i3}) are the true vector components at time τ_i, then the corresponding true magnitude is given by

$$f_{i4} = (x_{i1}^2 + x_{i2}^2 + x_{i3}^2)^{1/2}. \tag{19}$$

If $(f_{i1}, f_{i2}, f_{i3}, f_{i4})$ is a true set of values at time τ_i, we let $(\bar{f}_{i1}, \bar{f}_{i2}, \bar{f}_{i3}, \bar{f}_{i4})$ be the corresponding set of field measurements at time τ_i. If (y_{i1}, y_{i2}, y_{i3}) are the true values of the magnetic field along the sensor axes at time τ_i, then from equation (1) we have

$$f_{ij} = [y_{ij} - u_{ij7} w_{j7} + \sum_{k=1}^{6} u_{ijk} w_{jk} - w_{ij8} (64 - K_{ii})^3$$

$$- w_{i,9} (64 - K_{ij})^5] / a_j + b_j; i = 1 \text{ to } n; j = 1, 2, 3; \tag{20}$$

where the y_{ij}'s are computed from equations (2) through (18). We abbreviate equations [(20), (2) through (18)] by

$$f_{ij} = g_j(x_i, p); j = 1, 2, 3; \tag{21}$$

and equation (19) by

$$f_{i4} = g_4(x_i), \tag{22}$$

where g_j (j = 1, 2, 3, 4) are function symbols, $x_i = (x_{i1}, x_{i2}, x_{i3})'$, using' as a symbol for matrix transpose, and p is a column vector with elements w_{jk} (j = 1, 2, 3; k = 1 to 9), $a_1, a_2, a_3, b_1, b_2, b_3, a_{12}, a_{13}, a_{21}, a_{23}, a_{31}, a_{32}$ in the order given. We further abbreviate for i = 1 to n

$$f_i = (f_{i1}, f_{i2}, f_{i3}, f_{i4})', \tag{23}$$

$$\bar{f}_i = (\bar{f}_{i1}, \bar{f}_{i2}, \bar{f}_{i3}, \bar{f}_{i4})', \tag{24}$$

$$\tilde{f}_i = (\tilde{f}_{i1}, \tilde{f}_{i2}, \tilde{f}_{i3}, \tilde{f}_{i4})', \tag{25}$$

$$\hat{f}_i = (\hat{f}_{i1}, \hat{f}_{i2}, \hat{f}_{i3}, \hat{f}_{i4})', \tag{26}$$

$$\tilde{f}_{ij} = g_j(\tilde{x}_i, \tilde{p}), j = 1, 2, 3, \tag{27}$$

$$\tilde{f}_{i4} = g_4(\tilde{x}_i), \tag{28}$$

$$\hat{f}_{ij} = g_j(\hat{x}_i, \hat{p}), j = 1, 2, 3, \tag{29}$$

$$\hat{f}_{i4} = g_4(\hat{x}_i), \tag{30}$$

where $\tilde{x}_i$ and $\tilde{p}$ are guesses and $\hat{x}_i$ and $\hat{p}$ are estimates for the true values of the parameters x_i and p. By an estimate of a parameter we mean a value obtained with a statistical estimation procedure.

We assume that all sets of vector-scalar measurements $\bar{f}_i$ have the same error distribution with 0 means, 0 correlations, and standard deviations $(\sigma_1, \sigma_2, \sigma_3, \sigma_4)$, and that the a priori values of p_k (k = 1 to 39) are samples of size 1 with error distributions whose means are all 0 and whose standard deviations are ω_k (k = 1 to 39).

Suppose the true value associated with the ith measurement is ψ_i, that ψ_i is given as a function of the complete set of true parameters $\theta = (\theta_1, \theta_2, \ldots \theta_m)$ by $\psi_i = g_i(\theta)$, and that errors in measurements of ψ_i have mean 0 and standard deviation σ_i. Then the "weighted sensitivity matrix" Γ is defined as the matrix whose element in the ith row and jth column is $(\partial \psi_i/\partial \theta_j)/\sigma_i$. Since we will have only a guess for θ, $\tilde{\psi}_i = g_i(\tilde{\theta})$ and Γ is approximated by $\tilde{\Gamma}$. We see that Γ for our estimation will have 4n rows and 3n + 39 columns.

Since many of the partial derivatives for our calibration problem are 0, it will be convenient to partition Γ.

$$\Gamma = [R \; S], \tag{31}$$

$$R = \begin{bmatrix} R_1 & O & \ldots & O \\ O & R_2 & \ldots & O \\ \vdots & \vdots & & \vdots \\ O & O & \ldots & R_n \end{bmatrix}, \quad S = \begin{bmatrix} S_1 \\ S_2 \\ \vdots \\ S_n \end{bmatrix}, \tag{32}$$

and O is a 4 × 3 matrix all of whose elements are 0. $R_i = [r_{ijk}]$ (i = 1 to n) are 4 × 3 matrices with r_{ijk} (j = 1 to 4, k = 1 to 3) as the element in the jth row and kth column with

$$r_{ijk} = (\partial f_{ij}/\partial x_{ik})/\sigma_j.$$

The O's are zero submatrices of R because $\partial f_{ij}/\partial x_{hk} = 0$ unless i = h. $S_i = [s_{ijk}]$ (i = 1 to n) are 4× 39 matrices with s_{ijk} (j = 1 to 4, k = 1 to 39) as the element in the jth row and kth column with

$$s_{ijk} = (\partial f_{ij}/\partial p_k)/\sigma_j. \tag{33}$$

Note that all the elements in the 4th row are 0 for i = 1 to n.

Let z be a column vector of the true values of the estimated parameters and Ω a diagonal matrix whose diagonal elements are the variances for the elements of $\bar{z}$, the a priori approximation of z. We define

$$d = \begin{bmatrix} d_1 \\ d_2 \\ \vdots \\ d_n \end{bmatrix}, \quad d_i = \begin{bmatrix} d_{i1} \\ d_{i2} \\ d_{i3} \\ d_{i4} \end{bmatrix}, \quad d_{ij} = (\bar{f}_{ij} - f_{ij})/\sigma_j. \tag{34}$$

Thus d is the weighted vector of residuals. Also

$$\tilde{d}_{ij} = (\bar{f}_{ij} - \tilde{f}_{ij})/\sigma_j. \tag{35}$$

The weighted least squares estimate of z is

$$\hat{z} = \bar{z} + K^{-1} [\tilde{\Gamma}' \tilde{d} + \Omega^{-1} (\bar{z} - \tilde{z})], \tag{36}$$

$$K = \tilde{\Gamma}' \tilde{\Gamma} + \Omega^{-1}. \tag{37}$$

For the Magsat calibration problem, we assume infinite standard deviations for a priori values of x_{ij}. This means the first 3n diagonal elements of Ω^{-1} are 0 and the remaining 39 are $1/\omega_k^2$ (k = 1 to 39). Thus $\Omega^{-1} (\bar{z} - \tilde{z})$ is a column vector whose first 3n elements are 0 with the remaining elements given by

$$\tilde{t}_k = (\bar{p}_k - \tilde{p}_k)/\omega_k^2; \; k = 1 \text{ to } 39. \tag{38}$$

We note that

$$t_k = (\bar{p}_k - p_k)/\omega_k^2$$

and define a column vector t with 39 elements whose kth element is given by (39). We also define a 39 × 39 diagonal matrix J with kth diagonal element equal to $1/\omega_k^2$. Thus

$$\Omega^{-1} = \begin{bmatrix} O_1 & O_2 \\ O_2' & J \end{bmatrix}, \tag{40}$$

where O_1 and O_2 are 3n × 3n and 3n × 39 zero matrices. For our calibration problem we also have

$$z = \begin{bmatrix} x \\ p \end{bmatrix}, \quad x = \begin{bmatrix} x_1 \\ x_2 \\ \vdots \\ x_n \end{bmatrix}, \quad x_i = \begin{bmatrix} x_{i1} \\ x_{i2} \\ x_{i3} \\ x_{i4} \end{bmatrix}. \tag{41}$$

K can be written in partitioned form as

$$K = \begin{bmatrix} R' \\ S' \end{bmatrix} [R \; S] + \begin{bmatrix} O & O \\ O & J \end{bmatrix}$$

$$= \begin{bmatrix} R'R & R'S \\ S'R & S'S + J \end{bmatrix} = \begin{bmatrix} A & B \\ B' & C \end{bmatrix}, \tag{42}$$

where $A = R'R$, $B = R'S$, and $C = S'S + J$. Note that A, C, and K are symmetric. We also have

$$A = \begin{bmatrix} A_1 & O & \cdots & O \\ O & A_2 & \cdots & O \\ \vdots & \vdots & & \vdots \\ O & O & \cdots & A_n \end{bmatrix}, \quad B = \begin{bmatrix} B_1 \\ B_2 \\ \vdots \\ B_n \end{bmatrix} \tag{43}$$

$$A_i = R_i' R_i, \quad B_i = R_i' S_i \quad (i = 1 \text{ to } n) \tag{44}$$

$$C = \sum_{i=1}^{n} S_i' S_i + J \tag{45}$$

A_i is 3×3, B_i is 3×39, C is 39×39, A is $3n \times 3n$, B is $3n \times 39$, K is $(3n + 39) \times (3n + 39)$. Since n is typically several thousand, a direct inversion of K is impractical. The inversion problem is manageable, however, if we take advantage of the structure of A in a partitioned form of the inverse.

We can now write the bracketed part of equation (36) in the form

$$\tilde{\Gamma}' \tilde{d} + \Omega^{-1} (\tilde{z} - \tilde{z}) = \begin{bmatrix} \tilde{R}^1 \\ \tilde{S}^1 \end{bmatrix} \tilde{d} + \begin{bmatrix} O \\ \tilde{t} \end{bmatrix} = \begin{bmatrix} \beta \\ \gamma \end{bmatrix} \tag{46}$$

with the definitions

$$\beta = \tilde{R}' \tilde{d}, \tag{47}$$

$$\gamma = \tilde{S}' \tilde{d} + \tilde{t}, \tag{48}$$

where β is a column vector with 3n components, γ is a column vector with 39 components, and t is defined by equation (39).

Equation (36) becomes

$$\begin{bmatrix} \hat{x} \\ \hat{p} \end{bmatrix} = \begin{bmatrix} \tilde{x} \\ \tilde{p} \end{bmatrix} + \begin{bmatrix} A & B \\ B' & C \end{bmatrix}^{-1} \begin{bmatrix} \beta \\ \gamma \end{bmatrix}, \tag{49}$$

and we recall that $A' = A$ and $C' = C$.

If we express the inverse in the form

$$\begin{bmatrix} A & B \\ B' & C \end{bmatrix}^{-1} = \begin{bmatrix} D & E \\ E' & G \end{bmatrix} \tag{50}$$

and recall the well-known formulas for the inverse of a partitioned matrix, we have

$$H = -A^{-1} B, \tag{51}$$

$$G = (C + B' H)^{-1}, \tag{52}$$

$$E = HG, \tag{53}$$

$$D = A^{-1} + EH'. \tag{54}$$

Partitioning H, E, and D as

$$H = \begin{bmatrix} H_1 \\ H_2 \\ \vdots \\ H_n \end{bmatrix}, \quad E = \begin{bmatrix} E_1 \\ E_2 \\ \vdots \\ E_n \end{bmatrix}, \quad D = \begin{bmatrix} D_{11} & D_{12} & \cdots & D_{1n} \\ D_{21} & D_{22} & \cdots & D_{2n} \\ \vdots & \vdots & & \\ D_{n1} & D_{n2} & \cdots & D_{nn} \end{bmatrix}, \tag{55}$$

$D'_{ij} = D_{ji}$, i = 1 to n, j = 1 to n, and using (43) we have

$$H_i = -A_i^{-1} B_i; \quad i = 1 \text{ to } n. \tag{56}$$

$$G = (C + \sum_{i=1}^{n} B'_i H_i)^{-1}. \tag{57}$$

$$E_i = H_i G; \quad i = 1 \text{ to } n. \tag{58}$$

$$D_{ii} = A_i^{-1} + E_i H'_i; \quad i = 1 \text{ to } n. \tag{59}$$

$$D_{ij} = E_i H'_i; \quad i = 1 \text{ to } n-1; j = i+1 \text{ to } n. \tag{60}$$

Equation (49) can be written as two equations

$$\hat{x} = \tilde{x} + D\beta + E\gamma, \tag{61}$$

$$\hat{p} = \tilde{p} + E'\beta + G\gamma. \tag{62}$$

From equation (47) we obtain

$$\beta = \begin{bmatrix} \beta_1 \\ \beta_2 \\ \vdots \\ \beta_n \end{bmatrix}, \quad \beta_i = \begin{bmatrix} \beta_{i1} \\ \beta_{i2} \\ \beta_{i3} \end{bmatrix} = \tilde{R}'_i \tilde{d}_i. \tag{63}$$

We can now write (61) and (62) in the forms

$$\hat{x}_i = \tilde{x}_i + E_i \gamma + \sum_{j=1}^{n} D_{ij}\beta_j, \quad i = 1 \text{ to } n \tag{64}$$

$$\hat{p} = \tilde{p} + G\gamma + \sum_{i=1}^{n} E'_i \beta_i. \tag{65}$$

We note that E_i is 3 × 39, D_{ij} is 3 × 3, G is 39 × 39, G′ = G, and recall that $D'_{ij} = D_{ij}$ for all i's and j's.

The covariance matrices associated with the estimates $\hat{x}_i$ (i = 1 to n) and $\hat{p}$ are given by

$$\text{cov}(\hat{x}_i, \hat{x}_j) = D_{ij}, \tag{66}$$

$$\text{cov}(\hat{x}_i, \hat{p}) = E_i, \tag{67}$$

$$\text{cov}(\hat{p}, \hat{p}) = G. \tag{68}$$

Correlation matrices can be obtained from the covariance matrices.

RESULTS OF A CALIBRATION

The calibration results given below were obtained by exercising the computer program on a small subset of the data recorded on Nov. 5, 1979. The number of vector-scalar sets used in the calibration was 1247, approximately equally spaced in time. Table 1 gives the ground-based calibration values for the system parameters along with the standard deviations used to compute the weights for these a priori values in the least-squares algorithm. Except for the a_{ij} parameters, these standard deviations are larger than the realistic ones for the ground-based calibrations. This allows for the fact that the true values of the parameters may be significantly different after launch than before launch. The standard deviations for the a priori values of $a_{12}, a_{13}, a_{21}, a_{23}, a_{31}, a_{32}$ are held at the ground-based calibration values because of strong correlations between the errors in the least squares solutions for these parameters. Table 1 also shows the differences between the ground-based calibration values and the values estimated from the Nov. 5th ('79) data. The final column of Table 1 gives the standard deviations of the estimated parameters. The three parameters w_{25}, w_{26}, and w_{27} enter the least squares procedure only as the linear combination $w_{27} - w_{26} - w_{25}$, due to the fact that the magnetic field components along the second sensor axis had maximum and minimum values of 10228.5 and -15246.1. To obtain a solution, w_{25} and w_{26} were held fixed by giving them very small a priori standard deviations.

Table 2 gives 5 examples from the 1247 sets of vector-scalar measurements used in the least-squares calibration for Nov. 5, 1979. K_i and $\bar{f}_i$ (i = 1, 2, 3) are the coarse and fine values recorded for the three magnetic field components and $\bar{f}_4$ is the field magnitude measurement. The K_i's are error-free and are not considered as measurements in the least-squares estimation.procedure.

Table 1

Parameter	Pre-launch Value	Standard Deviation	Estimated Correction	Standard Deviation
w_{11}	999.7	20	-0.5	.05
w_{12}	1998.7	20	-0.3	.05
w_{13}	3996.7	20	-0.4	.06
w_{14}	7993.3	20	-1.1	.08
w_{15}	15986.1	20	-1.9	.14
w_{16}	31973.8	20	-4.5	.29
w_{17}	63947.5	20	-10.2	.25
w_{18}	.963 E-5	.32 E-5	-0.4 E-6	.31 E-5
w_{19}	-.603 E-9	.32 E-9	-0.5 E-11	.32 E-9
w_{21}	1004.3	20	0.7	.16
w_{22}	2008.7	20	-0.3	.17
w_{23}	4016.8	20	-0.5	.25
w_{24}	8037.6	20	-2.9	.34
w_{25}	16069.6	1 E-12	0.0	1 E-12
w_{26}	32143.9	1 E-12	0.0	1 E-12
w_{27}	64287.9	20	0.1	.46
w_{28}	.436 E-4	.32 E-4	-0.7 E-5	.31 E-4
w_{29}	-.649 E-9	.32 E-9	-0.3 E-12	.32 E-9
w_{31}	997.3	20	0.5	.03
w_{32}	1995.1	20	1.0	.03
w_{33}	3989.8	20	1.9	.04
w_{34}	7979.6	20	3.0	.05
w_{35}	15958.5	20	4.8	.09
w_{36}	31918.2	20	8.8	.14
w_{37}	63844.2	20	18.5	.12
w_{38}	-.508 E-5	.32 E-6	0.6 E-5	.31 E-6
w_{39}	.167 E-8	.32 E-9	0.3 E-9	.26 E-9
b_1	4.0	20	6.8	.24
b_2	13.0	20	4.6	.48
b_3	12.0	20	0.1	.19
a_1	.98248	1 E-4	0.4 E-4	.5 E-4
a_2	.99226	1 E-4	-2.1 E-4	.9 E-4
a_3	.98322	1 E-4	-1.7 E-4	.4 E-4
$\angle a_{12}$	-228.5	6.5	-16.8	4.2
$\angle a_{13}$	168.0	2.1	1.0	1.5
$\angle a_{21}$	-612.3	6.5	8.0	4.7
$\angle a_{23}$	443.3	2.1	2.7	2.0
$\angle a_{31}$	483.1	2.1	1.0	1.5
$\angle a_{32}$	589.9	6.5	28.0	2.1

Table 1
(unestimated parameters)

h_{11}	-35.28
h_{12}	1.46 E-4
h_{13}	-3.78172
h_{14}	-4.61641 E-5
h_{21}	-116.45
h_{22}	3.35 E-4
h_{23}	-10.832
h_{24}	-3.33 E-5
h_{31}	-127.1
h_{32}	3.2 E-4
h_{33}	-13.3367
h_{34}	-2.9167 E-5

$\angle a_{ij}$ = the complement in arc seconds of the angle associated with the direction cosine a_{ij}

Table 2

K_1	$\bar{f}_1$	K_2	$\bar{f}_2$	K_3	$\bar{f}_3$	$\bar{f}_4$
55	-900	62	-655	14	-563	51453.9
32	-376	59	-417	65	522	32740.9
74	855	49	812	99	-462	38780.4
45	754	61	613	71	719	19981.9
54	136	73	-1012	106	968	44726.4

In the remainder of this section we will present some computer results obtained for these 5 vector-scalar sets as well as for all 1247 sets.

Table 3 gives the distribution of the absolute values of $64\text{-}K_i$ for the 1247 data sets.

Table 3

Number	$64\text{-}K_1$	$64\text{-}K_2$	$64\text{-}K_3$
=0	21	46	11
=1	40	177	14
>1&<3	68	287	22
>3&<7	132	437	65
>7&<15	367	300	131
>15&<31	603	0	339
>31&<63	16	0	665

The values (y_1, y_2, y_3) of the magnetic field along the three sensor axes are obtained by substituting the pre-launch values of 33 parameters and the data in Table 2 into equation (1). The results are given in the first 3 columns of Table 4. The fourth column of Table 4 gives $\bar{f}_4 - f_c$, where f_c is the approximate vector magnitude computed from the components y_1, y_2, y_3, using a non-Pythagorean formula.

Table 4

y_1	y_2	y_3	$\bar{f}_4 - f_c$
-9881.2	-2671.5	-50437.0	15.1
-32347.4	-5447.8	1507.1	1.5
10828.3	-14274.7	34452.8	2.5
-18247.6	-2417.6	7685.7	4.0
-9862.3	8027.5	42840.6	10.0

When the values of y_1, y_2, and y_3 from Table 4 and the pre-launch values of a_{12}, a_{13}, a_{21}, a_{23}, a_{31}, and a_{32} are substituted into equations (2) through (18), the vector components (x_1, x_2, x_3) in the orthogonal system can be computed. They are given in the first three columns of Table 5. The fourth column of Table 5 gives $\bar{f}_4 - \tilde{f}$, where $\tilde{f}$ is the vector magnitude computed from the components $\tilde{x}_1$, $\tilde{x}_2$, $\tilde{x}_3$, using the Pythagorean formula (19). Differences between the fourth columns of Table 4 and Table 5 are due to the fact that s_1, s_2, and s_3 differ slightly from 1.

Table 5

$\tilde{x}_1$	$\tilde{x}_2$	$\tilde{x}_3$	$\bar{f}_4 - \tilde{f}_4$
-9843.0	-2592.1	-50421.7	15.1
-32354.8	-5537.8	1567.1	3.1
10784.8	-14316.9	34387.2	2.0
-13256.7	-2486.7	7721.4	4.2
-9888.6	7906.2	42886.6	10.1

The values of $\tilde{x}_1$, $\tilde{x}_2$, and $\tilde{x}_3$ in Table 5 are used as first guesses in the least squares estimation procedure.

Table 6 gives the values of $\tilde{x}_1 - \hat{x}_1$, $\tilde{x}_2 - \hat{x}_2$, and $\tilde{x}_3 - \hat{x}_3$ in the first three columns, where ($\hat{x}_1$, $\hat{x}_2$, $\hat{x}_3$) are estimated values and ($\tilde{x}_1$, $\tilde{x}_2$, $\tilde{x}_3$) are the initial guesses in Table 5. Column 4 of Table 6 gives the values of $\bar{f}_4 - \hat{f}_4$, where $\hat{f}_4$ was computed from ($\hat{x}_1$, $\hat{x}_2$, $\hat{x}_3$) using the Pythagorean equation. We note that the estimated field vectors have magnitudes much closer to the measured magnitudes than the guesses ($\tilde{x}_1$, $\tilde{x}_2$, $\tilde{x}_3$) computed from the vector field measurements ($\bar{f}_{i1}$, $\bar{f}_{i2}$, $\bar{f}_{i3}$) and the a priori parameter values. The means and root-mean-squares of the 1247 values of $\tilde{x}_1 - \hat{x}_1$, $\tilde{x}_2 - \hat{x}_2$, $\tilde{x}_3 - \hat{x}_3$, and $\bar{f}_4 - \hat{f}_4$ are given in Table 7.

Let ($\breve{x}_1$, $\breve{x}_2$, $\breve{x}_3$) be the values computed by substituting the estimated 39 parameters in equation (1) through (18) and solving for (x_1, x_2, x_3), and let $\breve{f}_4 = (\breve{x}_1^2 + \breve{x}_2^2 + \breve{x}_3^2)^{1/2}$. Table 8 shows the differences between these estimates for (x_1, x_2, x_3, f_4) and the least squares estimates ($\hat{x}_1$, $\hat{x}_2$, $\hat{x}_3$, $\hat{f}_4$).

Table 6

$\tilde{x}_1 - \hat{x}_1$	$\tilde{x}_2 - \hat{x}_2$	$\tilde{x}_3 - \hat{x}_3$	$\bar{f}_4 - \hat{f}_4$
5.1	5.1	14.6	-0.5
2.0	5.6	2.5	0.3
8.9	0.6	-5.9	-1.0
3.7	5.6	-0.7	-0.2
5.6	4.1	-11.0	-1.0

Table 7

	$\tilde{x}_1 - \hat{x}_1$	$\tilde{x}_2 - \hat{x}_2$	$\tilde{x}_3 - \hat{x}_3$	$\bar{f}_4 - \hat{f}_4$
MEAN	7.0	3.2	1.7	-0.001
RMS	3.0	1.8	9.8	0.52

Table 8

$\hat{x}_1 - \check{x}_1$	$\hat{x}_2 - \check{x}_2$	$\hat{x}_3 - \check{x}_3$	$\hat{f}_4 - \check{f}_4$
0.1	0.0	0.4	-0.4
-0.2	-0.1	0.0	0.2
-0.2	0.3	-0.6	-0.7
0.1	0.0	0.0	-0.1
0.1	-0.1	-0.7	-0.7

The 1247 values of $\bar{f}_4 - \check{f}_4$ have a mean of -.002 and an RMS of .90, which compare very well with the values of -.001 and .52 in Table 7 for $\bar{f}_4 - \hat{f}_4$. Thus least squares estimation is not needed for every day's data if a loss of about 0.5 gamma in accuracy can be accepted. We must consider that on the GSFC 360/91, full estimation for 1247 data sets required 8 minutes, while computation of (x_1, x_2, x_3) from equations (1) through (18) required 0.4 of a minute, a ratio of 20 to 1.

The first three columns of Table 9 give the residuals $\bar{f}_j - \hat{f}_j$ (j = 1, 2, 3), where the $\bar{f}_j$'s are the fine measurements given in Table 2 and the $\hat{f}_j$ are obtained by substituting the estimated parameters in equation (20) and computing (y_1, y_2, y_3) for (20) by substituting $(\hat{x}_1, \hat{x}_2, \hat{x}_3)$, $\hat{a}_{12}, \hat{a}_{13}, \hat{a}_{21}$,

$\hat{a}_{23}$, $\hat{a}_{31}$, and $\hat{a}_{32}$ in equations (2) through (18). The fourth column of Table 9 repeats the fourth column of Table 6. The 1247 value sets of the numbers given for a sample of 5 in Table 9 have means and RMS's given in Table 10. Table 10 is an indication of the goodness-of-fit of the solution to the measurements.

Table 9

$\bar{f}_1 - \hat{f}_1$	$\bar{f}_2 - \hat{f}_2$	$\bar{f}_3 - \hat{f}_3$	$\bar{f}_4 - \hat{f}_4$
-0.1	-0.0	-0.4	-0.5
0.2	0.0	0.0	0.3
0.2	-0.3	0.6	-1.0
-0.1	0.0	0.0	-0.2
-0.2	0.1	0.7	-1.0

Table 10

$\bar{f}_1 - \hat{f}_1$	$\bar{f}_2 - \hat{f}_2$	$\bar{f}_3 - \hat{f}_3$	$\bar{f}_4 - \hat{f}_4$
-.001	-.0009	.0002	-.001
0.19	0.06	0.32	0.52

FURTHER CALIBRATION RESULTS

Knowing that under space conditions the calibration parameters determined pre-launch would vary, it was necessary to determine criteria for a first in-flight calibration, to be used as a control, to see any trends and shifts in subsequent calibrations typifying changes in the instrument. November 5th data was chosen for the control calibration under the criteria that (1) the instrument should have had time to shift mechanically, due to stresses in a space vacuum system, into some "permanent" position after three days in orbit, and (2) data were taken continuously throughout the day, producing a globally distributed data set for sampling.

The November 5th calibration (see Table 11) shows changes from pre-launch calibration (especially in the z-axis), which illustrate the changes in the instrument. Calibrations were then made at four day intervals beginning November 2, 1979 and ending January 21, 1980 (excluding January 1,

Table 11

Parameter	Pre-Launch Value	November 5th Value	Estimated Correction	Standard Deviation
w_{11}	999.7	999.6	-0.1	0.14
w_{12}	1998.7	1998.3	0.4	0.14
w_{13}	3996.7	3997.0	0.3	0.15
w_{14}	7993.3	7993.2	-0.1	0.16
w_{15}	15986.1	15985.9	-0.2	0.24
w_{16}	31973.8	31973.4	-0.4	0.43
w_{17}	63947.5	63940.0	-7.4	0.39
w_{18}	.963 E-5	.882 E-5	-.803 E-6	.98 E-6
w_{19}	-.603 E-9	-.611 E-9	-.829 E-11	.10 E-9
w_{21}	1004.3	1005.3	1.1	0.42
w_{22}	2008.7	2009.0	0.4	0.41
w_{23}	4016.8	4017.4	0.5	0.43
w_{24}	8037.6	8036.7	-0.9	0.43
w_{25}	16069.6	16068.8	-0.8	0.88
w_{26}	32143.9	32143.2	-0.8	0.88
w_{27}	64287.9	64288.7	0.8	0.88
w_{28}	.436 E-4	.436 E-4	-.910 E-8	.10 E-5
w_{29}	-.649 E-9	-.649 E-9	-.247 E-13	.10 E-9
w_{31}	997.3	997.7	0.4	0.10
w_{32}	1995.1	1996.0	1.0	0.10
w_{33}	3989.8	3991.6	1.8	0.11
w_{34}	7979.6	7982.7	3.0	0.12
w_{35}	15958.5	15963.1	4.6	0.16
w_{36}	31918.2	31926.7	8.5	0.22
w_{37}	63844.2	63862.6	18.4	0.24
w_{38}	-.508 E-5	-.217 E-5	0.291 E-5	.96 E-6
w_{39}	.167 E-8	.173 E-8	0.628 E-10	.10 E-9
b_1	4.0	7.8	3.8	0.35
b_2	13.0	13.9	0.9	0.44
b_3	12.0	12.7	0.7	0.31
a_1	.98248	.98248	0.0	.50 E-5
a_2	.99226	.99226	0.0	.50 E-5
a_3	.98322	.98322	0.0	.50 E-5
$\angle a_{12}$	-228.5	-228.3	-0.2	0.99
$\angle a_{13}$	168.0	168.0	0.01	0.033
$\angle a_{21}$	-612.3	-612.2	-0.1	1.0
$\angle a_{23}$	443.3	443.3	0.01	0.033
$\angle a_{31}$	483.1	483.1	0.01	0.033
$\angle a_{32}$	589.9	595.6	5.7	0.95

1980, at this writing). The first 29 plots following this discussion show graphically the changes from the November 5th calibration for those parameters which changed more than 0.1 gamma (or 0.1 arc-seconds, according to which parameter is being considered). A key to the symbols used in the plots can be located on the page before the plots. Two sets of parameters, $w_{16} - w_{17}$, and $w_{25} - w_{26} - w_{27}$ are plotted together since correlations between these parameters are so large that the parameters are believed to be mathematically inseparable.

Examination of the calibration parameter plots shows trend-line changes with time, usually in one direction (i.e., non-oscillating), with the exception of several days calibrations. Upon further examination, these calibration exceptions are usually found common in several plots. One reason for the offset values is the status of the scalar sensors, A and B. It is found that a different calibration will result for each of the following cases: (1) sensor A on only, (2) sensor B on only, or (3) both sensor A and B on. Examination of the plots implies this to be the case in most instances. For those instances where the sensor status does not apply, other reasons such as diversion in the data distribution, or temperature variation of the sensors and platform may be part of an explanation, but no conclusions have been formalized at this time.

The second set of plots describe some statistics about the relationship between the scalar values and their associated vector magnitudes, for samples of data at four day intervals about the date of the calibration. The data samples had the calibration in question applied to them, and the mean, standard deviation about the mean, and the maximum of the differences between scalars and vector magnitudes were determined. Study of these plots shows conclusively the dependence of the calibration and the calibrated data on the scalar sensor status.

Key to Symbols used in Plots

A: Scalar Sensor A on only

B: Scalar Sensor B on only

C: Scalar Sensors A and B both on

M: Mean of difference values between scalars and vector magnitudes

R: Standard deviation about the mean of difference values between scalars and vector magnitudes

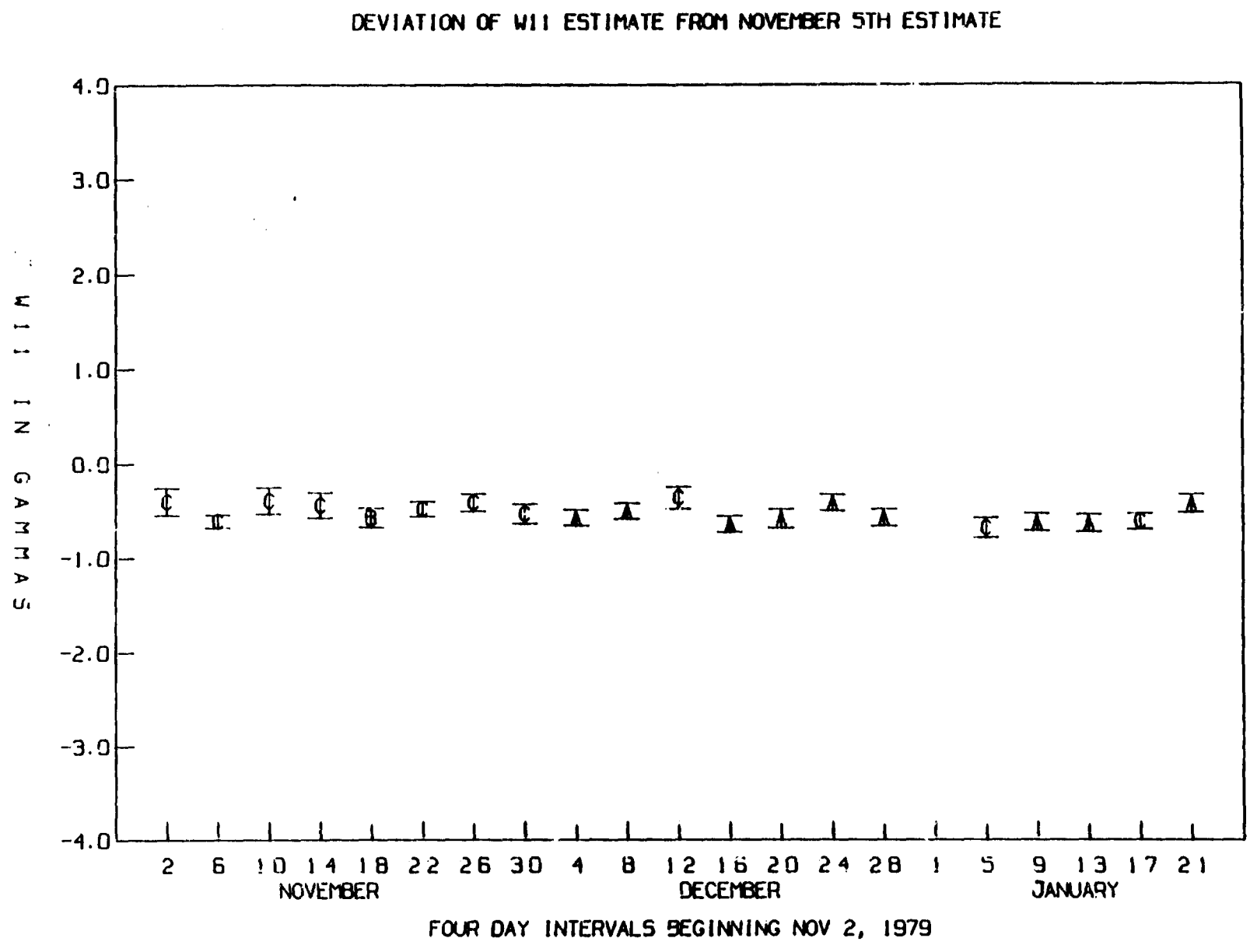
DEVIATION OF W11 ESTIMATE FROM NOVEMBER 5TH ESTIMATE
4.0
3.0
2.0
1.0
0.0
-1.0
-2.0
-3.0
-4.0
W11 IN GAMMAS
2 6 10 14 18 22 26 30 4 8 12 16 20 24 28 1 5 9 13 17 21
NOVEMBER
DECEMBER
JANUARY
FOUR DAY INTERVALS BEGINNING NOV 2, 1979

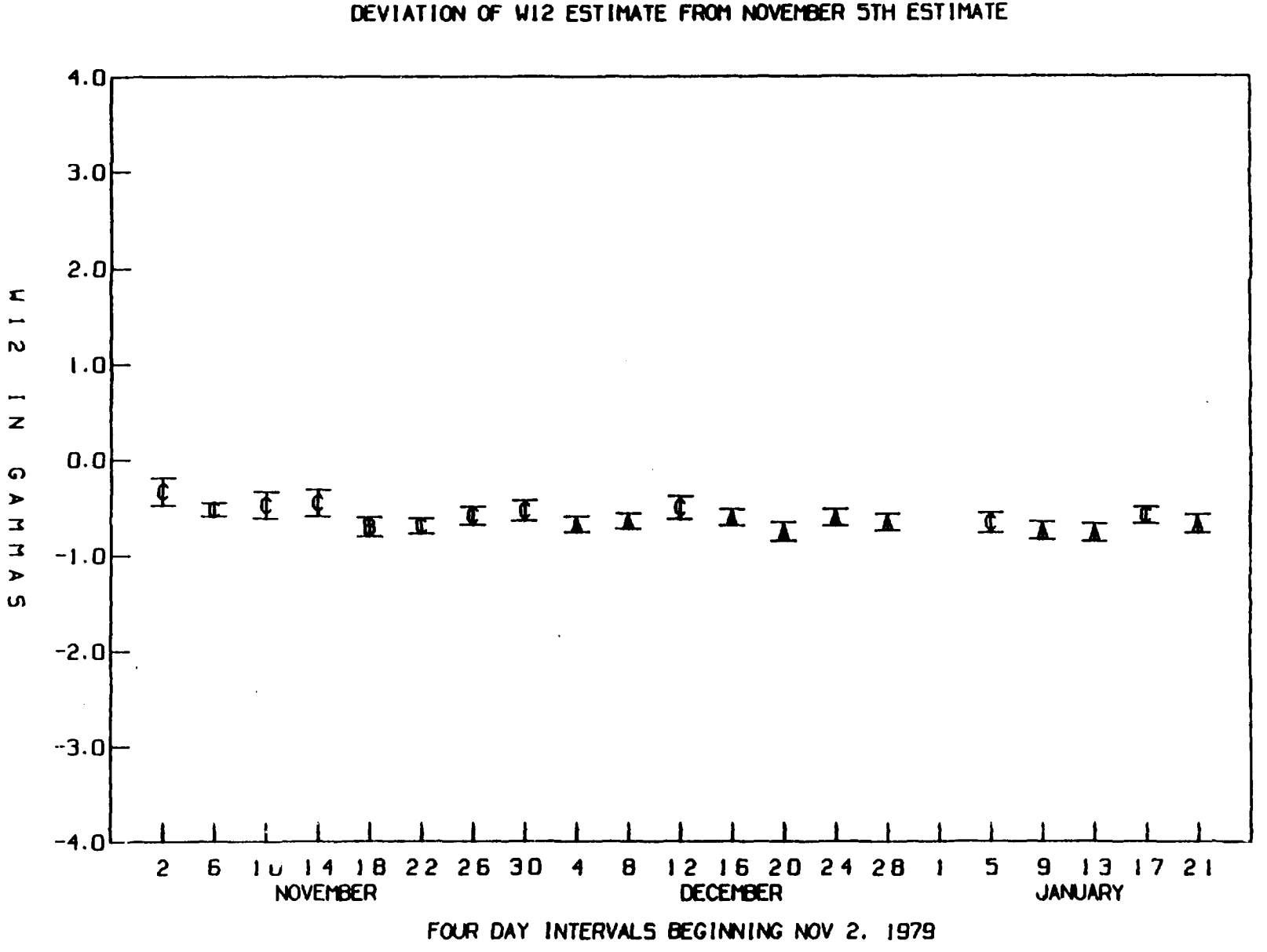
DEVIATION OF W12 ESTIMATE FROM NOVEMBER 5TH ESTIMATE
4.0
3.0
2.0
1.0
0.0
-1.0
-2.0
-3.0
-4.0
W12 IN GAMMAS
2 6 10 14 18 22 26 30 4 8 12 16 20 24 28 1 5 9 13 17 21
NOVEMBER
DECEMBER
JANUARY
FOUR DAY INTERVALS BEGINNING NOV 2. 1979

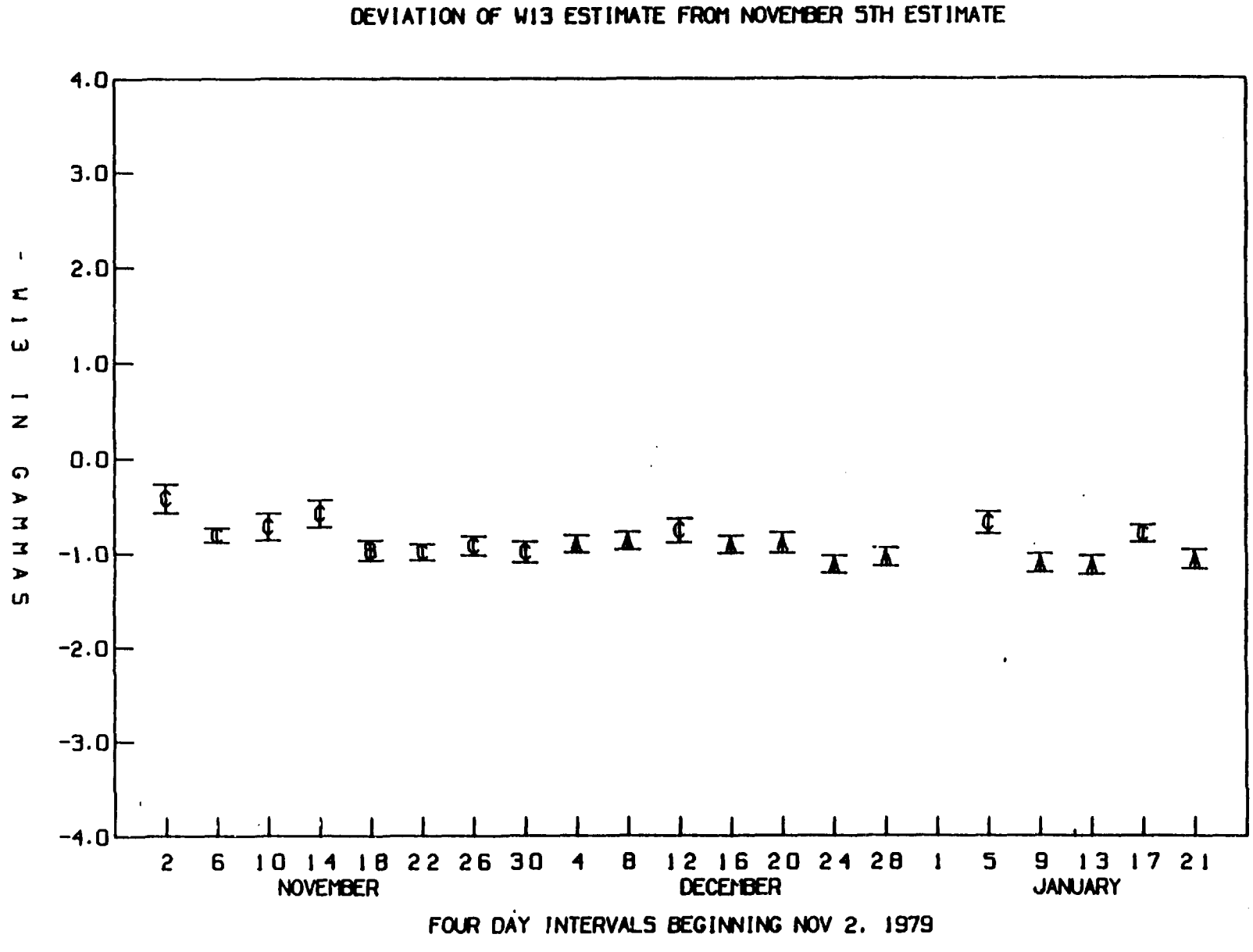
DEVIATION OF W13 ESTIMATE FROM NOVEMBER 5TH ESTIMATE
4.0
3.0
2.0
1.0
0.0
-1.0
-2.0
-3.0
-4.0
- W13 IN GAMMAS
2 6 10 14 18 22 26 30 4 8 12 16 20 24 28 1 5 9 13 17 21
NOVEMBER
DECEMBER
JANUARY
FOUR DAY INTERVALS BEGINNING NOV 2. 1979

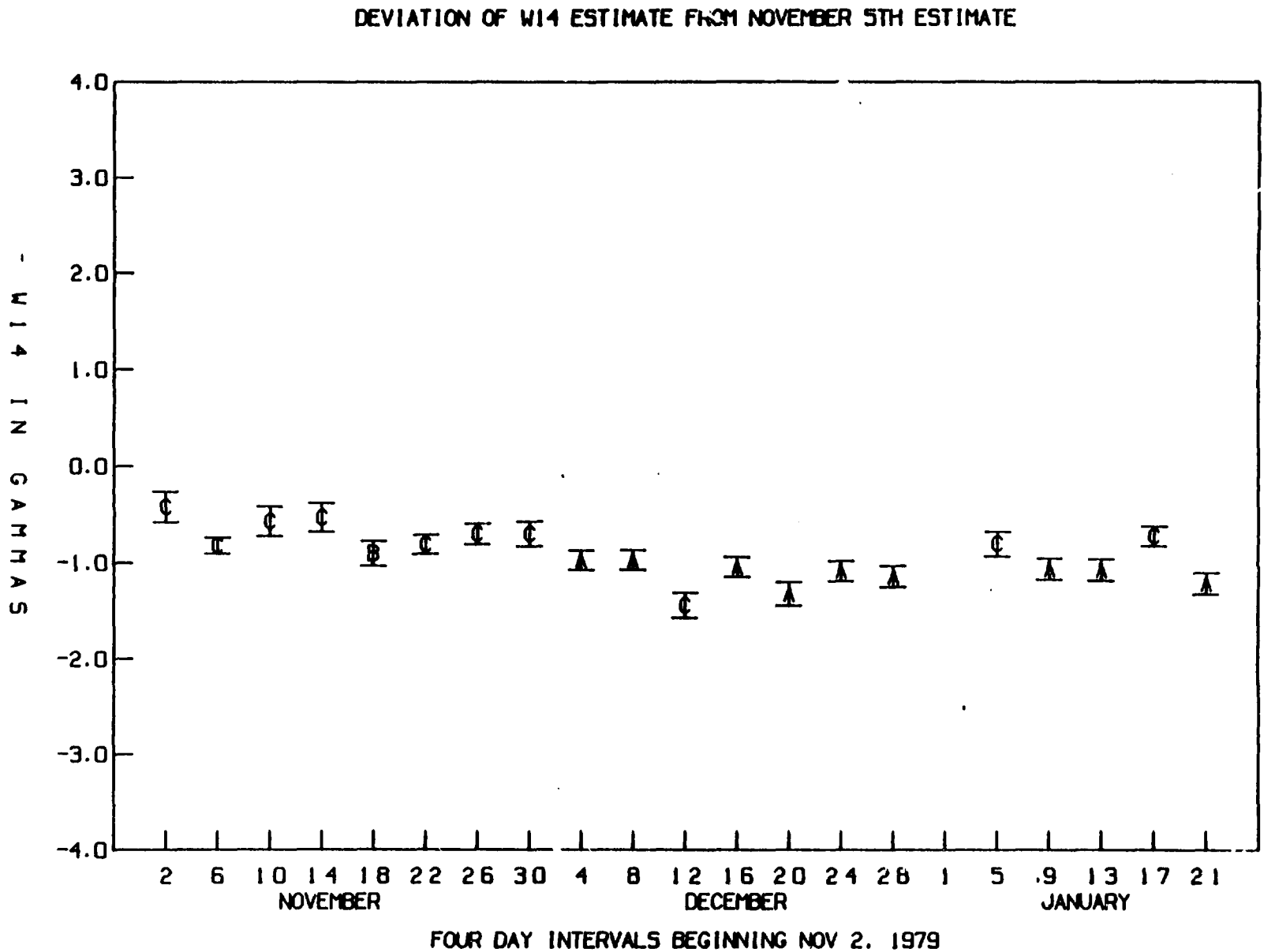
DEVIATION OF W14 ESTIMATE FROM NOVEMBER 5TH ESTIMATE
4.0
3.0
2.0
1.0
0.0
-1.0
-2.0
-3.0
-4.0
- W14 IN GAMMAS
2 6 10 14 18 22 26 30 4 8 12 16 20 24 28 1 5 9 13 17 21
NOVEMBER
DECEMBER
JANUARY
FOUR DAY INTERVALS BEGINNING NOV 2. 1979

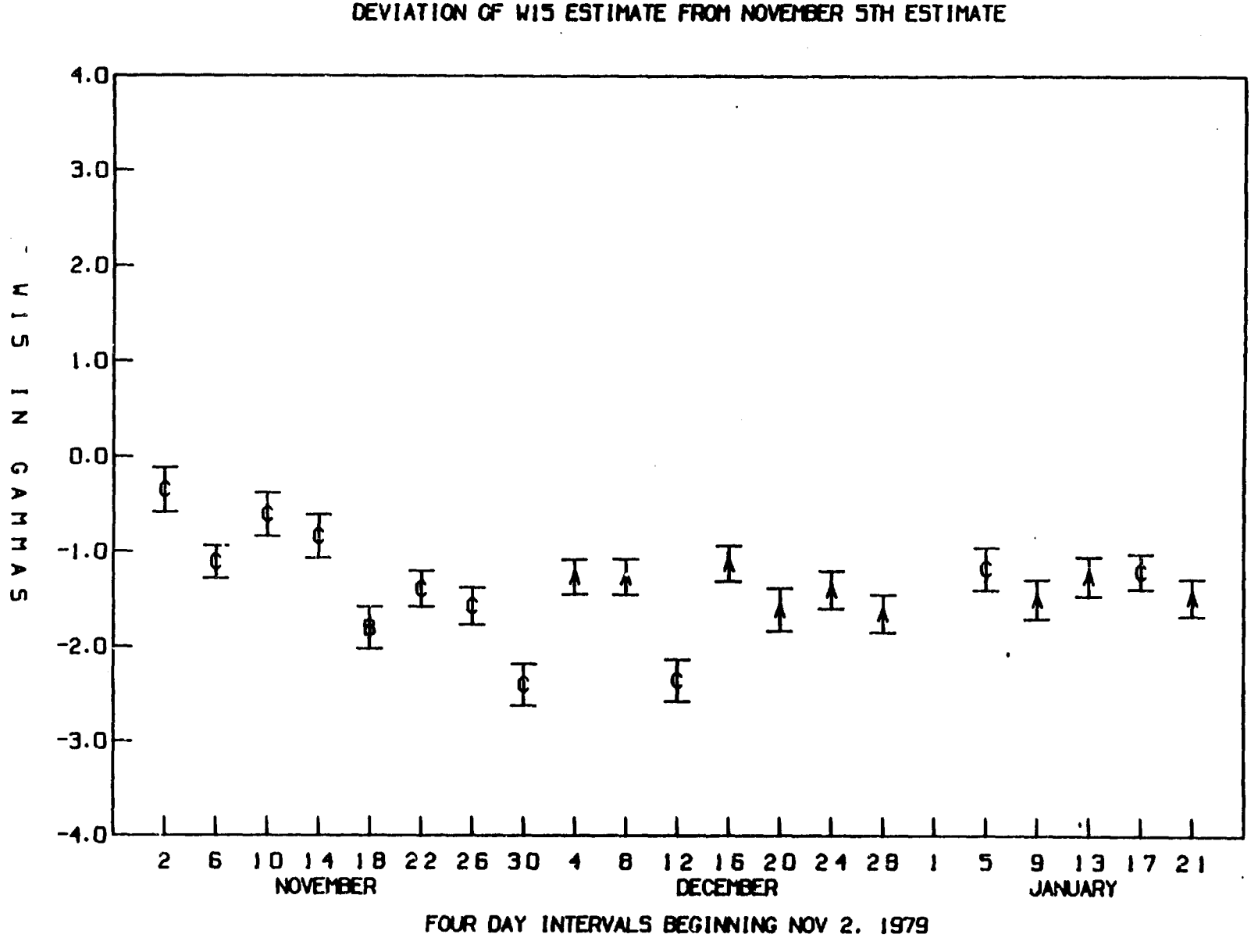
DEVIATION OF W15 ESTIMATE FROM NOVEMBER 5TH ESTIMATE
W15 IN GAMMAS
4.0
3.0
2.0
1.0
0.0
-1.0
-2.0
-3.0
-4.0
2 6 10 14 18 22 26 30 4 8 12 16 20 24 28 1 5 9 13 17 21
NOVEMBER
DECEMBER
JANUARY
FOUR DAY INTERVALS BEGINNING NOV 2. 1979

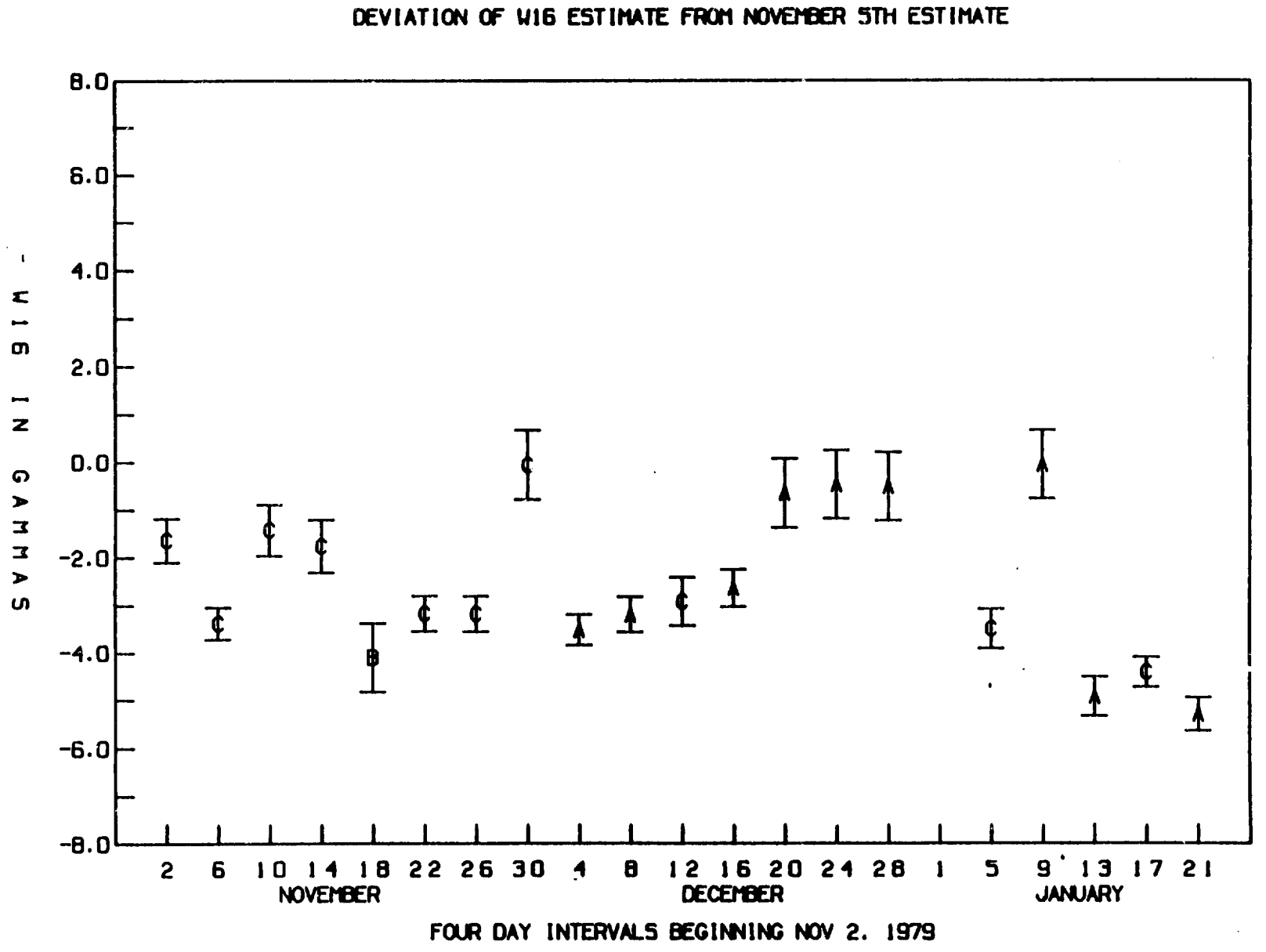
DEVIATION OF W16 ESTIMATE FROM NOVEMBER 5TH ESTIMATE
8.0
6.0
4.0
2.0
0.0
-2.0
-4.0
-6.0
-8.0
W16 IN GAMMAS
2 6 10 14 18 22 26 30 4 8 12 16 20 24 28 1 5 9 13 17 21
NOVEMBER
DECEMBER
JANUARY
FOUR DAY INTERVALS BEGINNING NOV 2. 1979

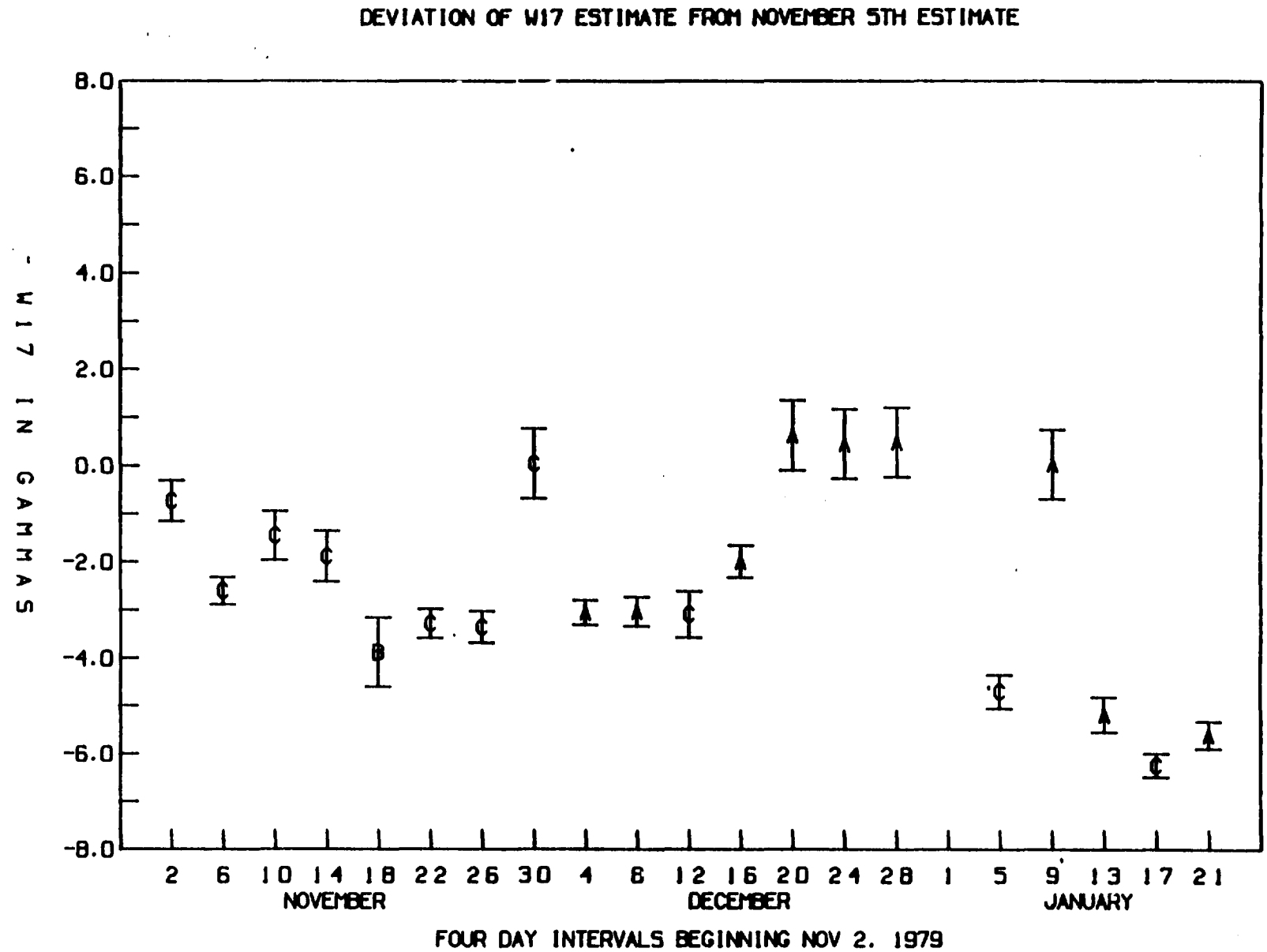
DEVIATION OF W17 ESTIMATE FROM NOVEMBER 5TH ESTIMATE
8.0
6.0
4.0
2.0
0.0
-2.0
-4.0
-6.0
-8.0
W17 IN GAMMAS
2 6 10 14 18 22 26 30 4 8 12 16 20 24 28 1 5 9 13 17 21
NOVEMBER
DECEMBER
JANUARY
FOUR DAY INTERVALS BEGINNING NOV 2. 1979

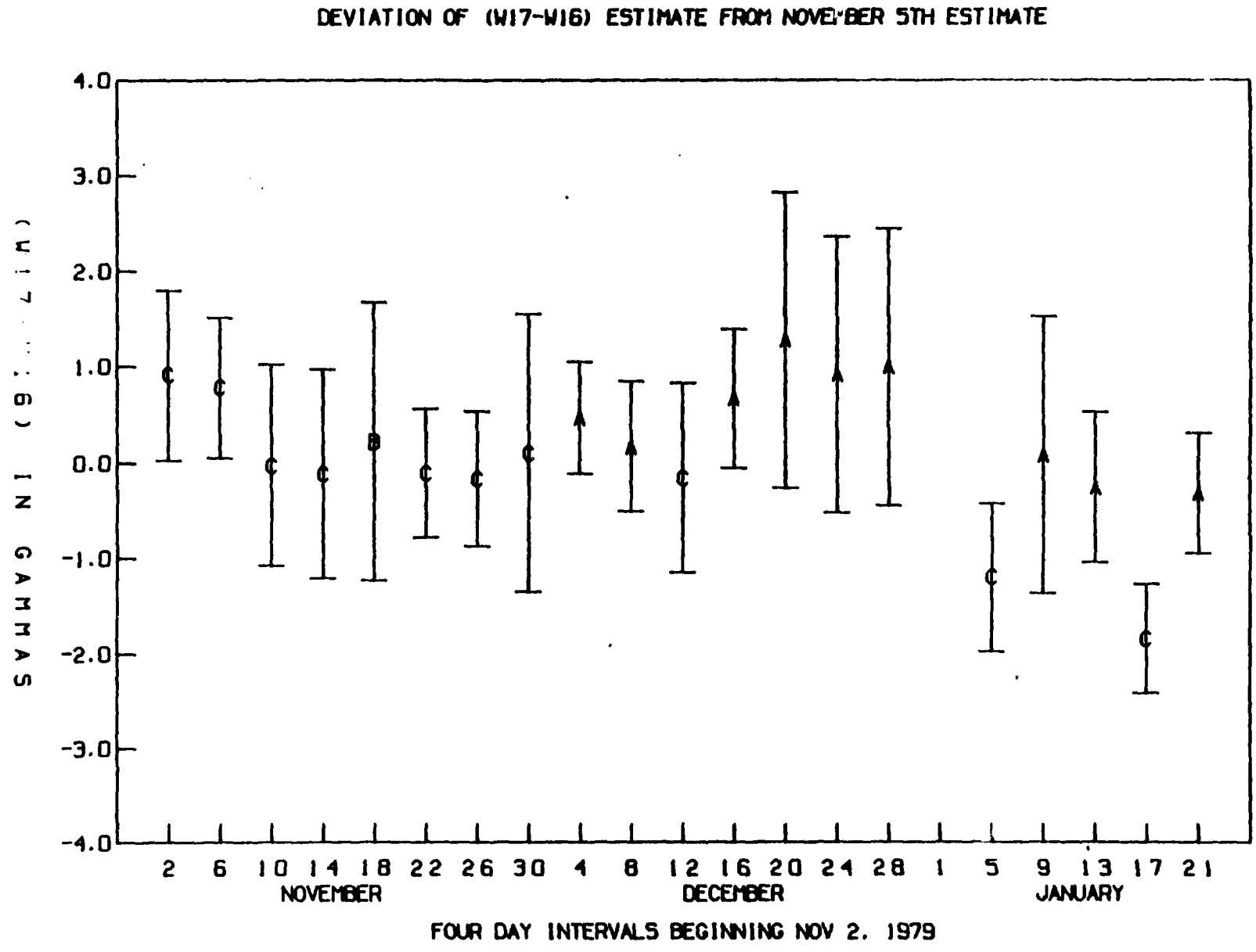
DEVIATION OF (W17-W16) ESTIMATE FROM NOVEMBER 5TH ESTIMATE
4.0
3.0
2.0
1.0
0.0
-1.0
-2.0
-3.0
-4.0
(W17-W16) IN GAMMAS
2 6 10 14 18 22 26 30 4 8 12 16 20 24 28 1 5 9 13 17 21
NOVEMBER
DECEMBER
JANUARY
FOUR DAY INTERVALS BEGINNING NOV 2. 1979

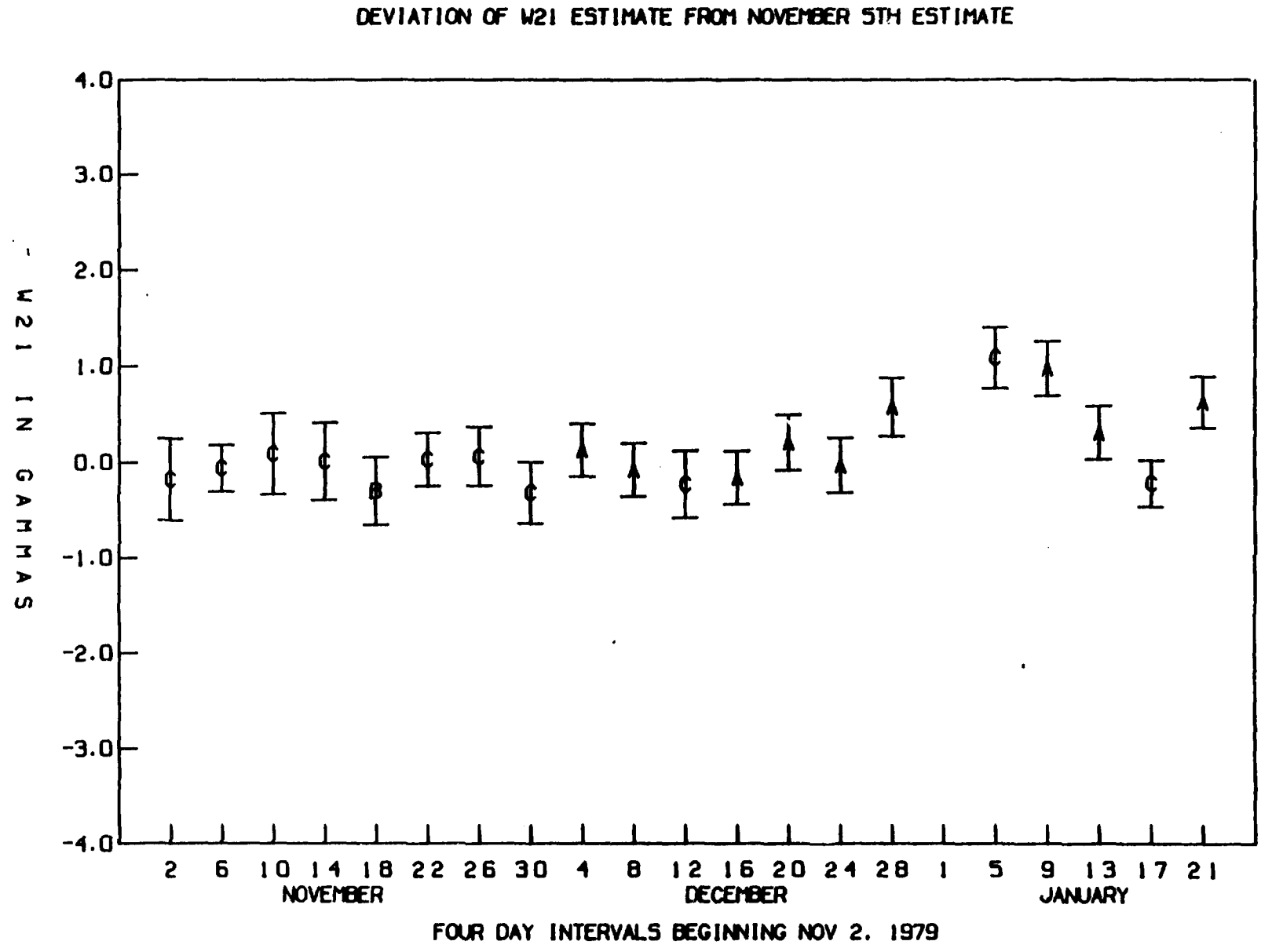
DEVIATION OF W21 ESTIMATE FROM NOVEMBER 5TH ESTIMATE
W21 IN GAMMAS
4.0
3.0
2.0
1.0
0.0
-1.0
-2.0
-3.0
-4.0
2 6 10 14 18 22 26 30 4 8 12 16 20 24 28 1 5 9 13 17 21
NOVEMBER
DECEMBER
JANUARY
FOUR DAY INTERVALS BEGINNING NOV 2. 1979

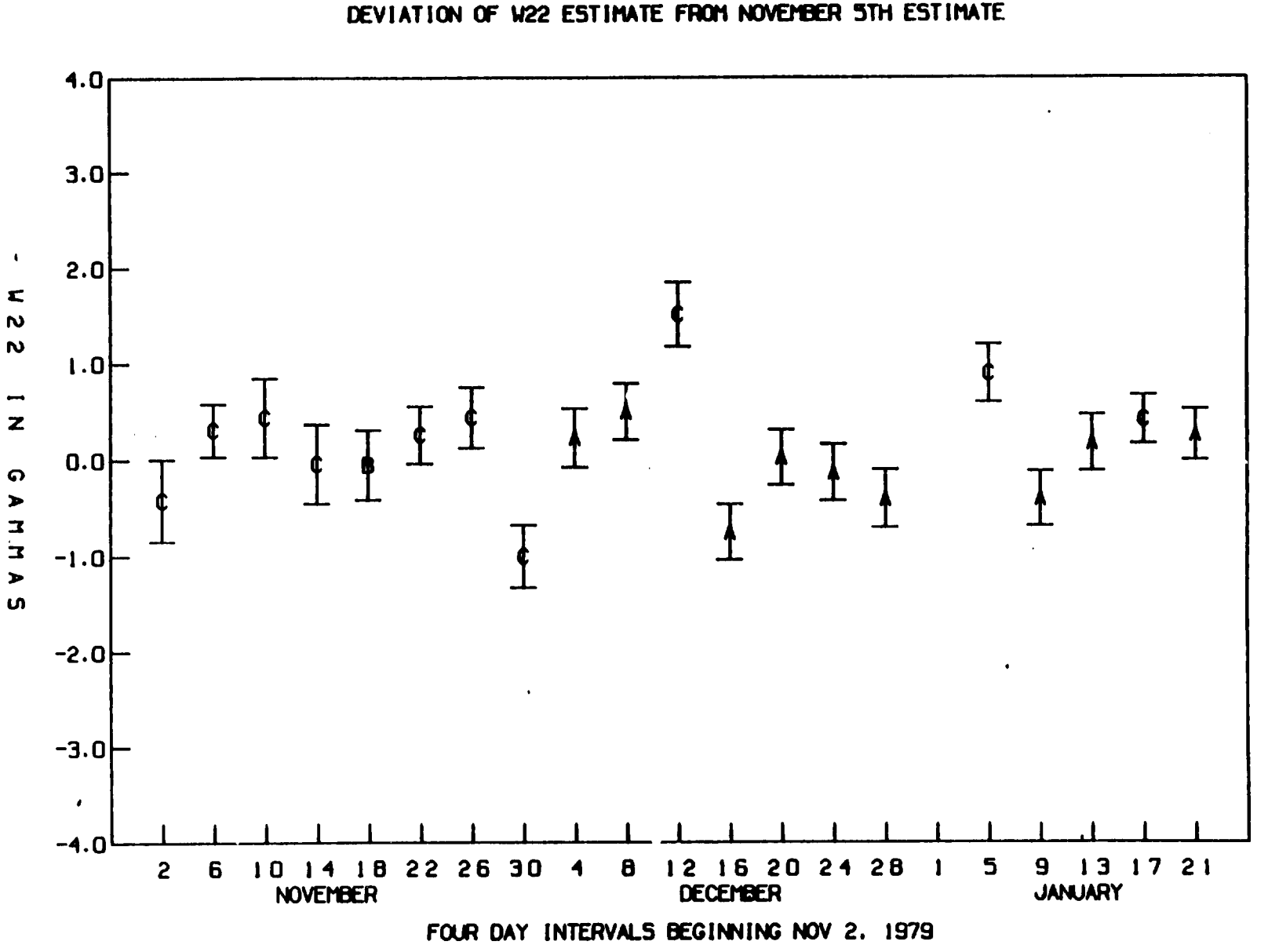
DEVIATION OF W22 ESTIMATE FROM NOVEMBER 5TH ESTIMATE
- W22 IN GAMMAS
4.0
3.0
2.0
1.0
0.0
-1.0
-2.0
-3.0
-4.0
2 6 10 14 18 22 26 30 4 8 12 16 20 24 28 1 5 9 13 17 21
NOVEMBER
DECEMBER
JANUARY
FOUR DAY INTERVALS BEGINNING NOV 2. 1979

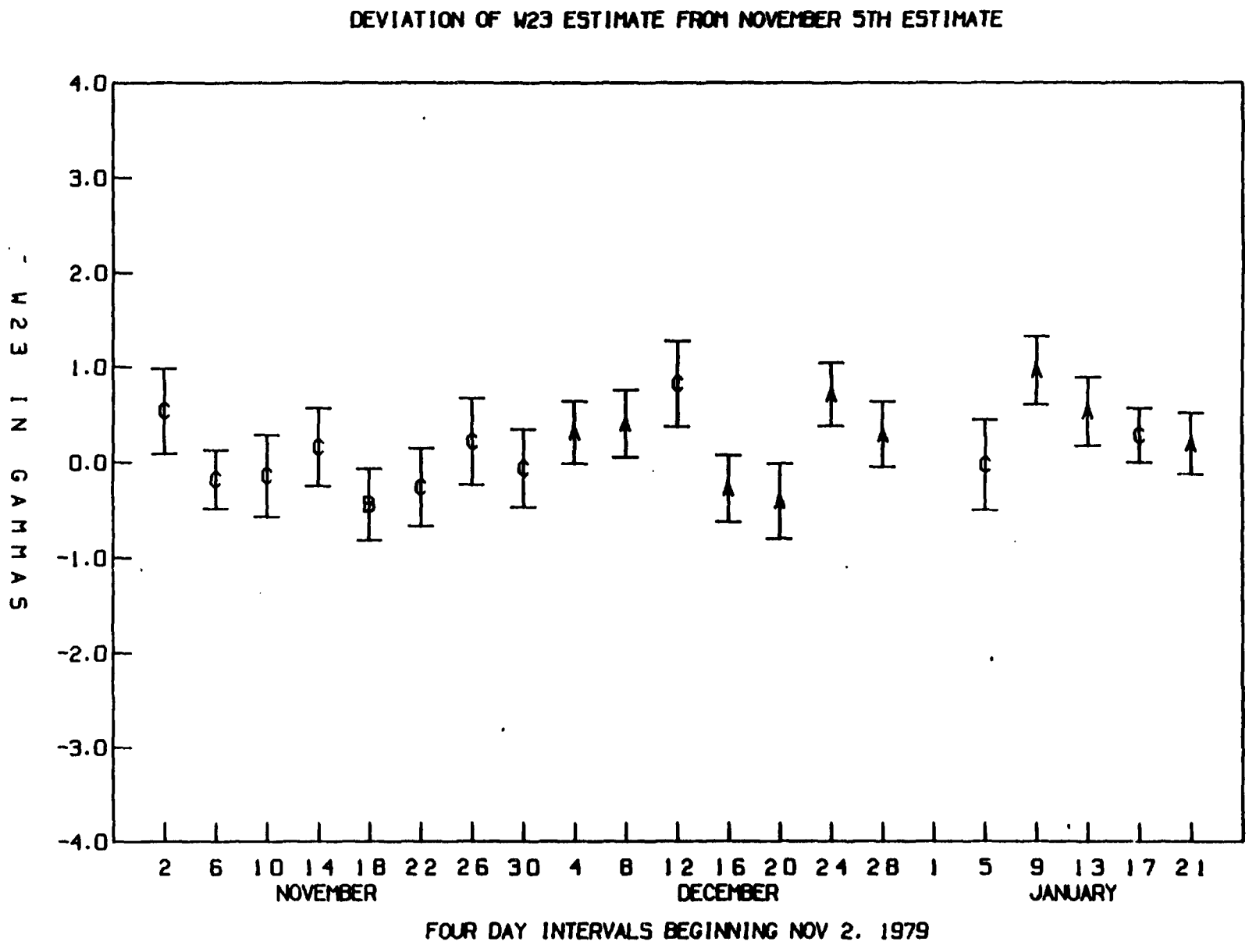
DEVIATION OF W23 ESTIMATE FROM NOVEMBER 5TH ESTIMATE
4.0
3.0
2.0
1.0
0.0
-1.0
-2.0
-3.0
-4.0
- W23 IN GAMMAS
2 6 10 14 18 22 26 30 4 8 12 16 20 24 28 1 5 9 13 17 21
NOVEMBER
DECEMBER
JANUARY
FOUR DAY INTERVALS BEGINNING NOV 2. 1979

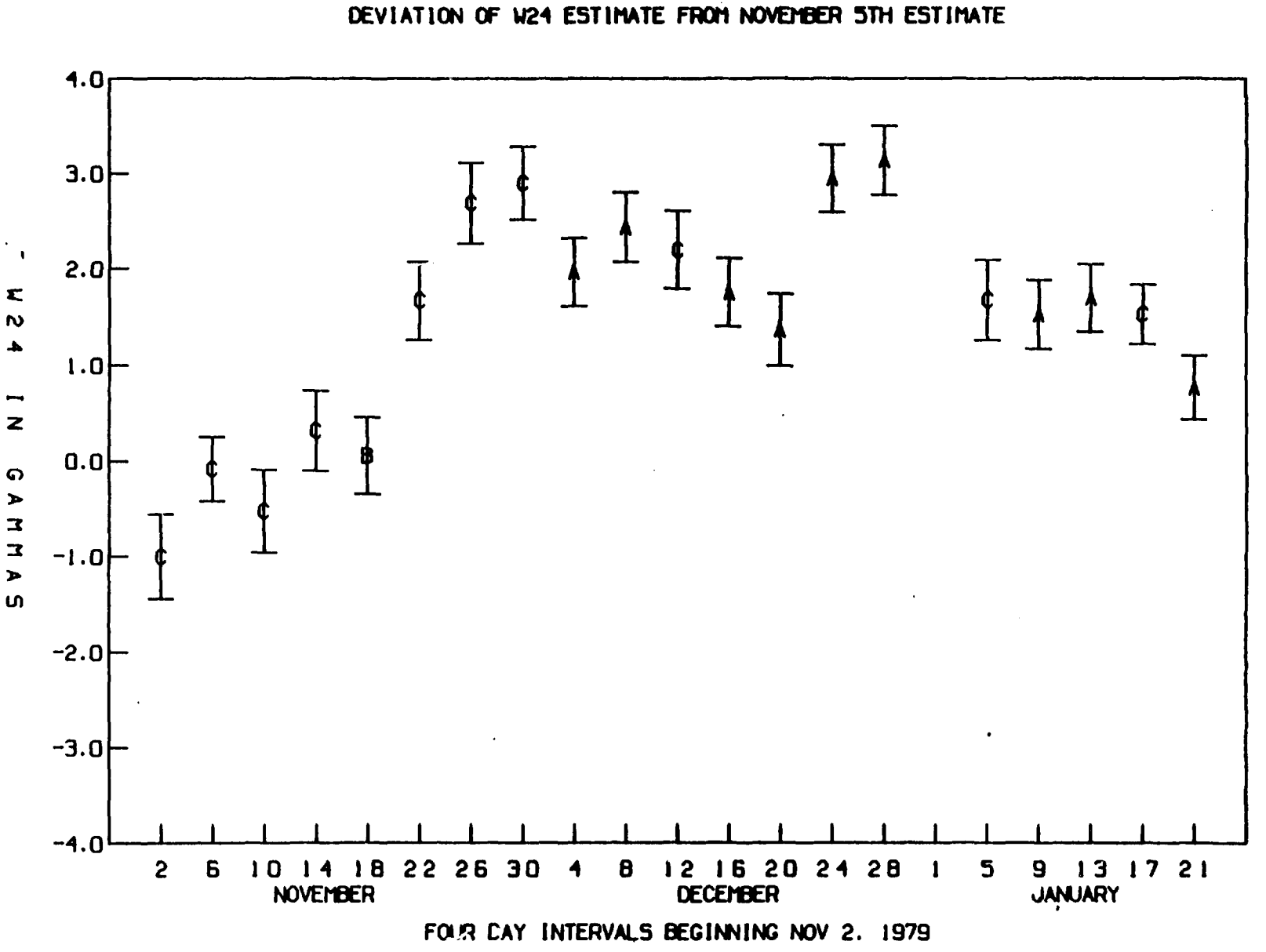
DEVIATION OF W24 ESTIMATE FROM NOVEMBER 5TH ESTIMATE
4.0
3.0
2.0
1.0
0.0
-1.0
-2.0
-3.0
-4.0
- W24 IN GAMMAS
2 6 10 14 18 22 26 30 4 8 12 16 20 24 28 1 5 9 13 17 21
NOVEMBER
DECEMBER
JANUARY
FOUR DAY INTERVALS BEGINNING NOV 2. 1979

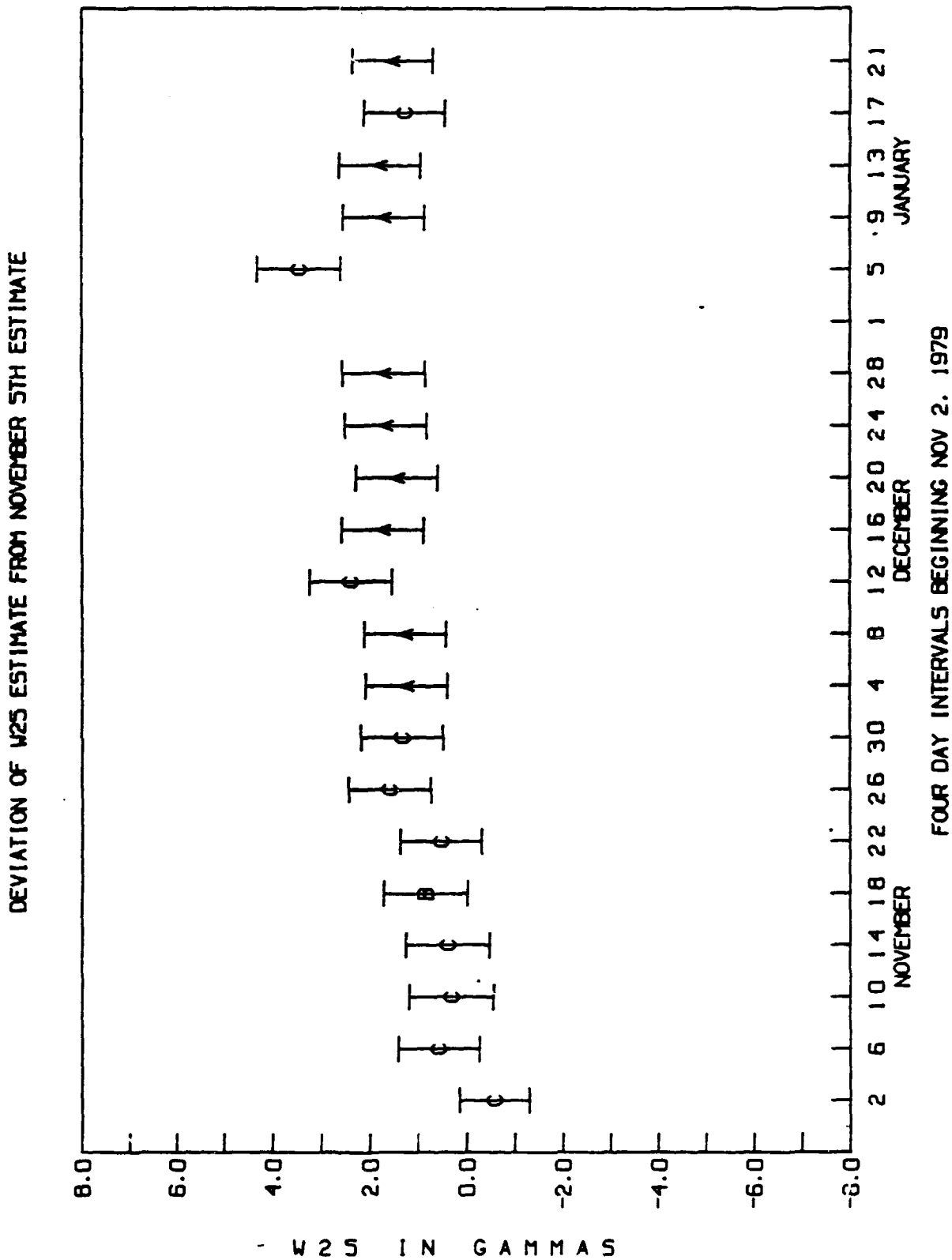
DEVIATION OF W25 ESTIMATE FROM NOVEMBER 5TH ESTIMATE
8.0
6.0
4.0
2.0
0.0
-2.0
-4.0
-6.0
W25 IN GAMMAS
2 6 10 14 18 22 26 30 4 8 12 16 20 24 28 1 5 9 13 17 21
NOVEMBER
DECEMBER
JANUARY
FOUR DAY INTERVALS BEGINNING NOV 2, 1979

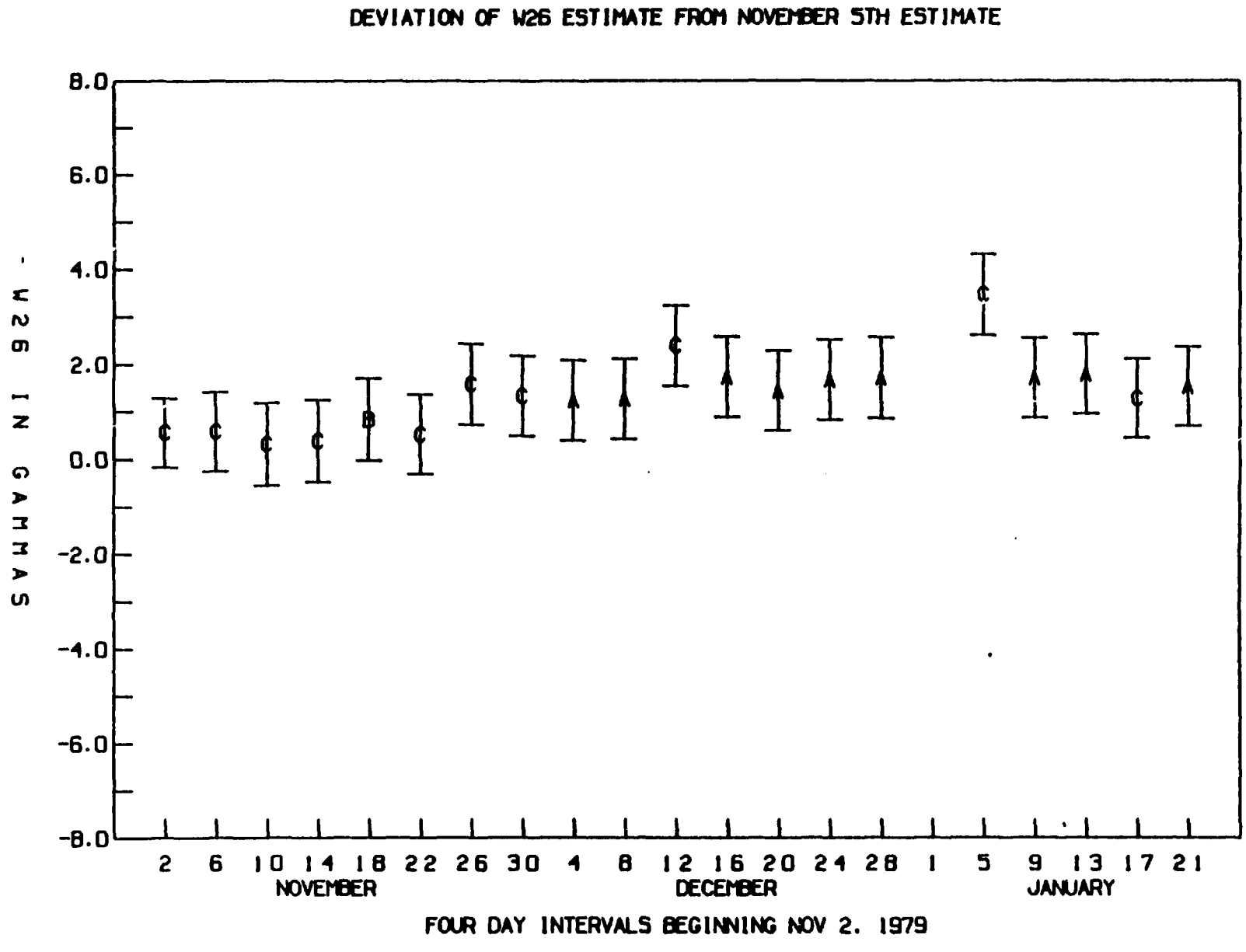
DEVIATION OF W26 ESTIMATE FROM NOVEMBER 5TH ESTIMATE
8.0
6.0
4.0
2.0
0.0
-2.0
-4.0
-6.0
-8.0
W26 IN GAMMAS
2 6 10 14 18 22 26 30 4 8 12 16 20 24 28 1 5 9 13 17 21
NOVEMBER
DECEMBER
JANUARY
FOUR DAY INTERVALS BEGINNING NOV 2. 1979

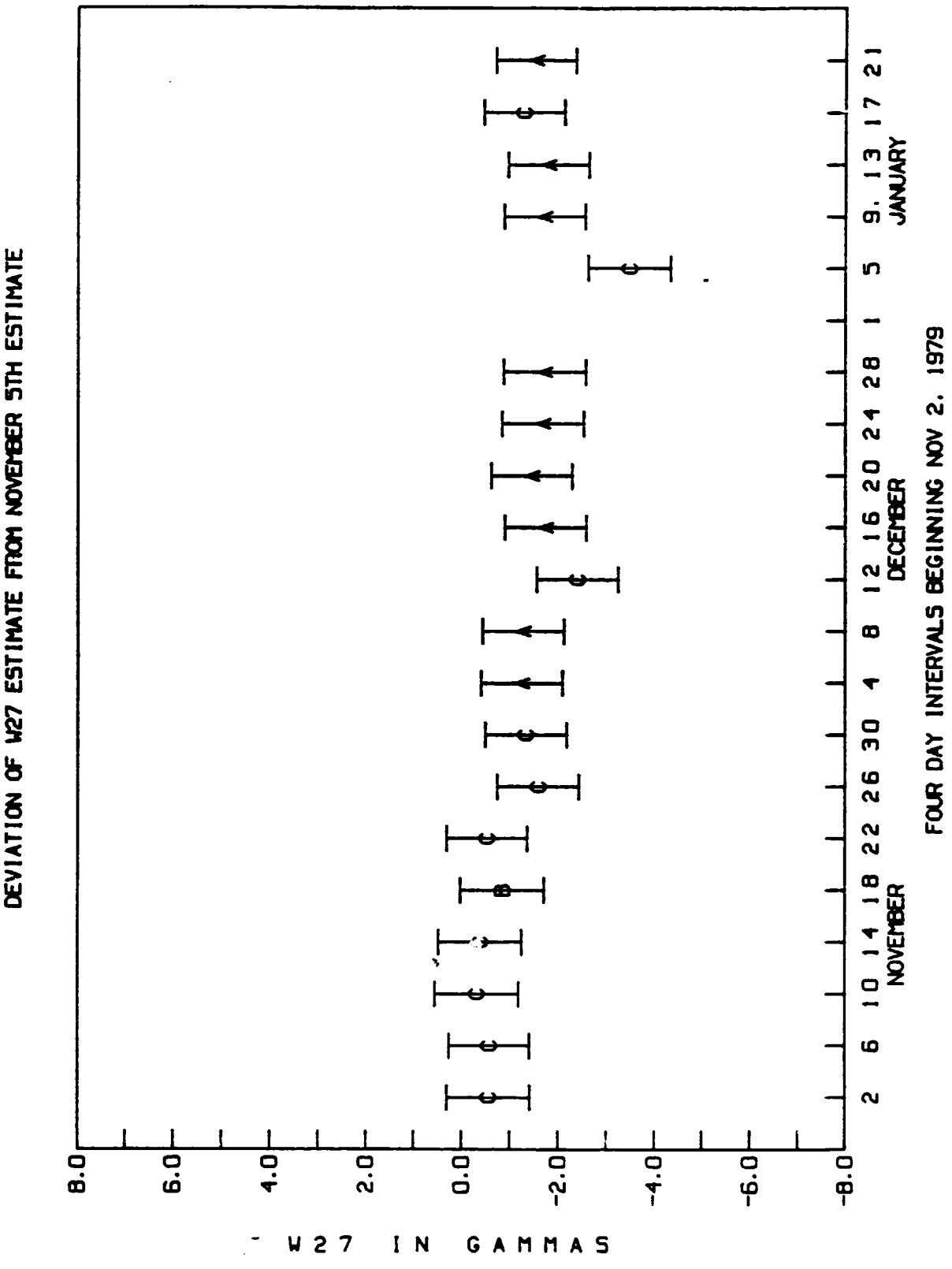
DEVIATION OF W27 ESTIMATE FROM NOVEMBER 5TH ESTIMATE
W27 IN GAMMAS
8.0
6.0
4.0
2.0
0.0
-2.0
-4.0
-6.0
-8.0
2 6 10 14 18 22 26 30 4 8 12 16 20 24 28 1 5 9 13 17 21
NOVEMBER
DECEMBER
JANUARY
FOUR DAY INTERVALS BEGINNING NOV 2, 1979

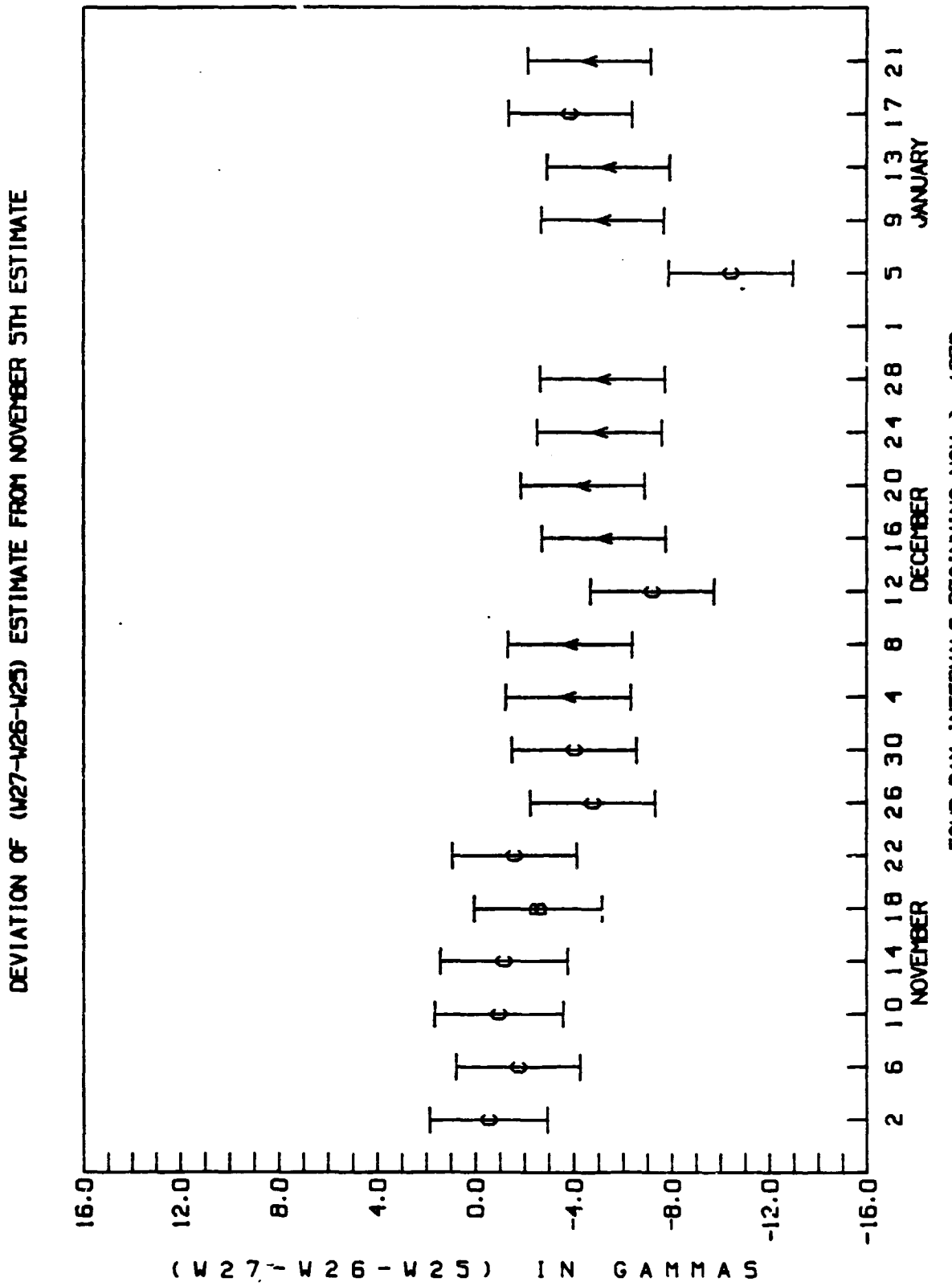
DEVIATION OF (W27-W26-W25) ESTIMATE FROM NOVEMBER 5TH ESTIMATE
(W27-W26-W25) IN GAMMAS
16.0
12.0
8.0
4.0
0.0
-4.0
-8.0
-12.0
-16.0
2 6 10 14 18 22 26 30 4 8 12 16 20 24 28 1 5 9 13 17 21
NOVEMBER
DECEMBER
JANUARY
FOUR DAY INTERVALS BEGINNING NOV 2, 1979

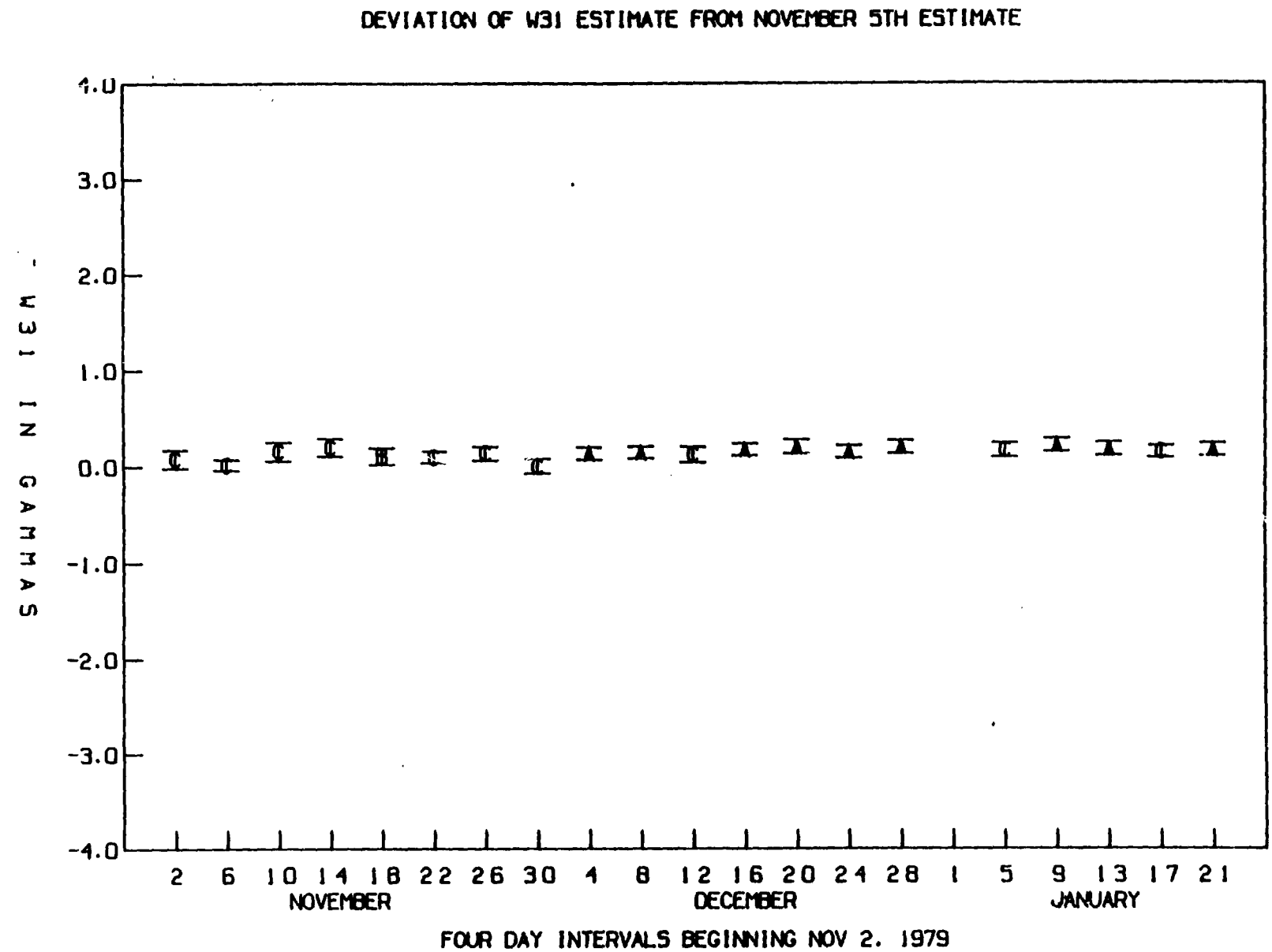
DEVIATION OF W31 ESTIMATE FROM NOVEMBER 5TH ESTIMATE
4.0
3.0
2.0
1.0
0.0
-1.0
-2.0
-3.0
-4.0
W31 IN GAMMAS
2 6 10 14 18 22 26 30 4 8 12 16 20 24 28 1 5 9 13 17 21
NOVEMBER
DECEMBER
JANUARY
FOUR DAY INTERVALS BEGINNING NOV 2. 1979

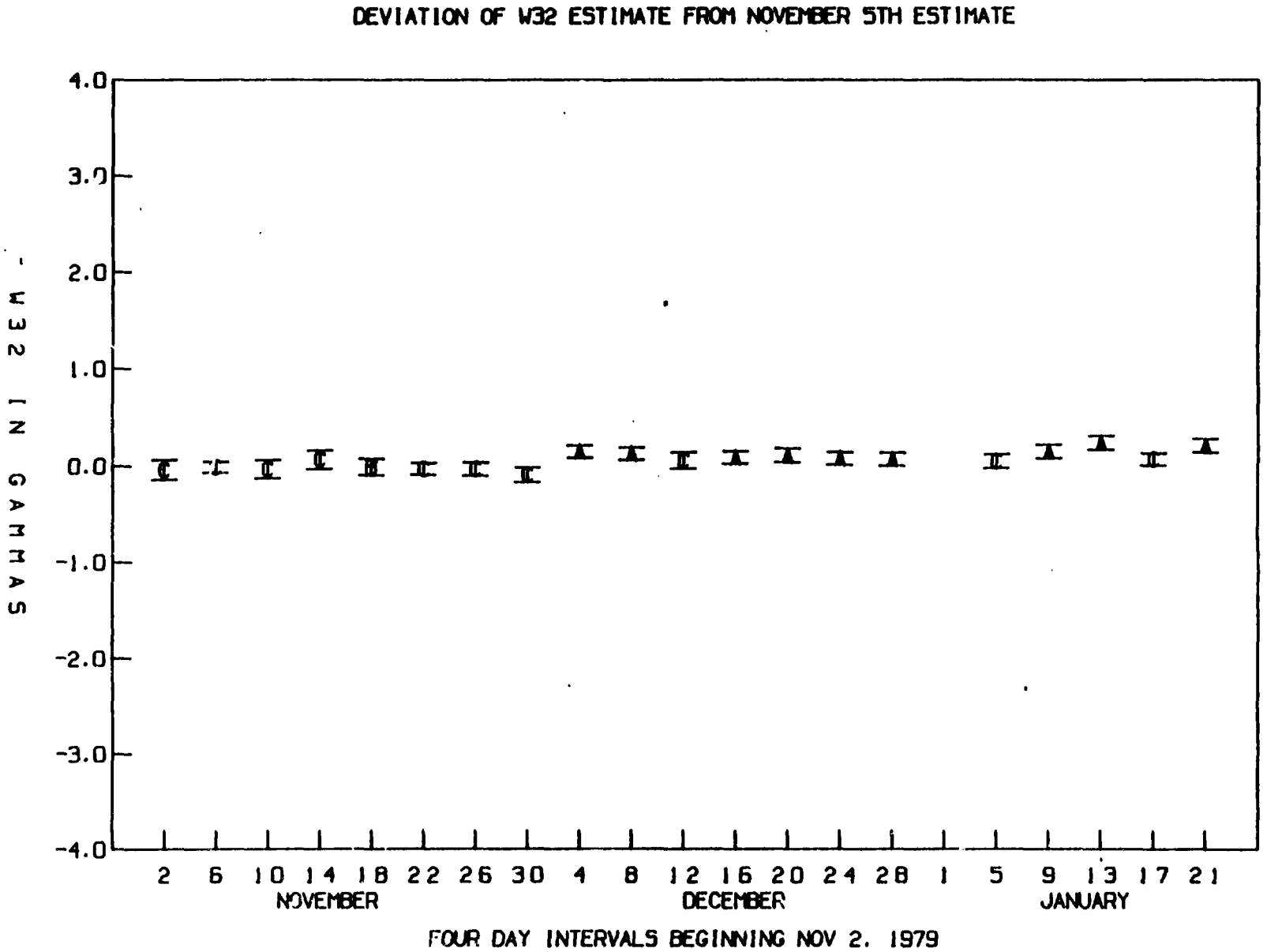
DEVIATION OF W32 ESTIMATE FROM NOVEMBER 5TH ESTIMATE
4.0
3.0
2.0
1.0
0.0
-1.0
-2.0
-3.0
-4.0
W32 IN GAMMAS
2 6 10 14 18 22 26 30 4 8 12 16 20 24 28 1 5 9 13 17 21
NOVEMBER
DECEMBER
JANUARY
FOUR DAY INTERVALS BEGINNING NOV 2. 1979

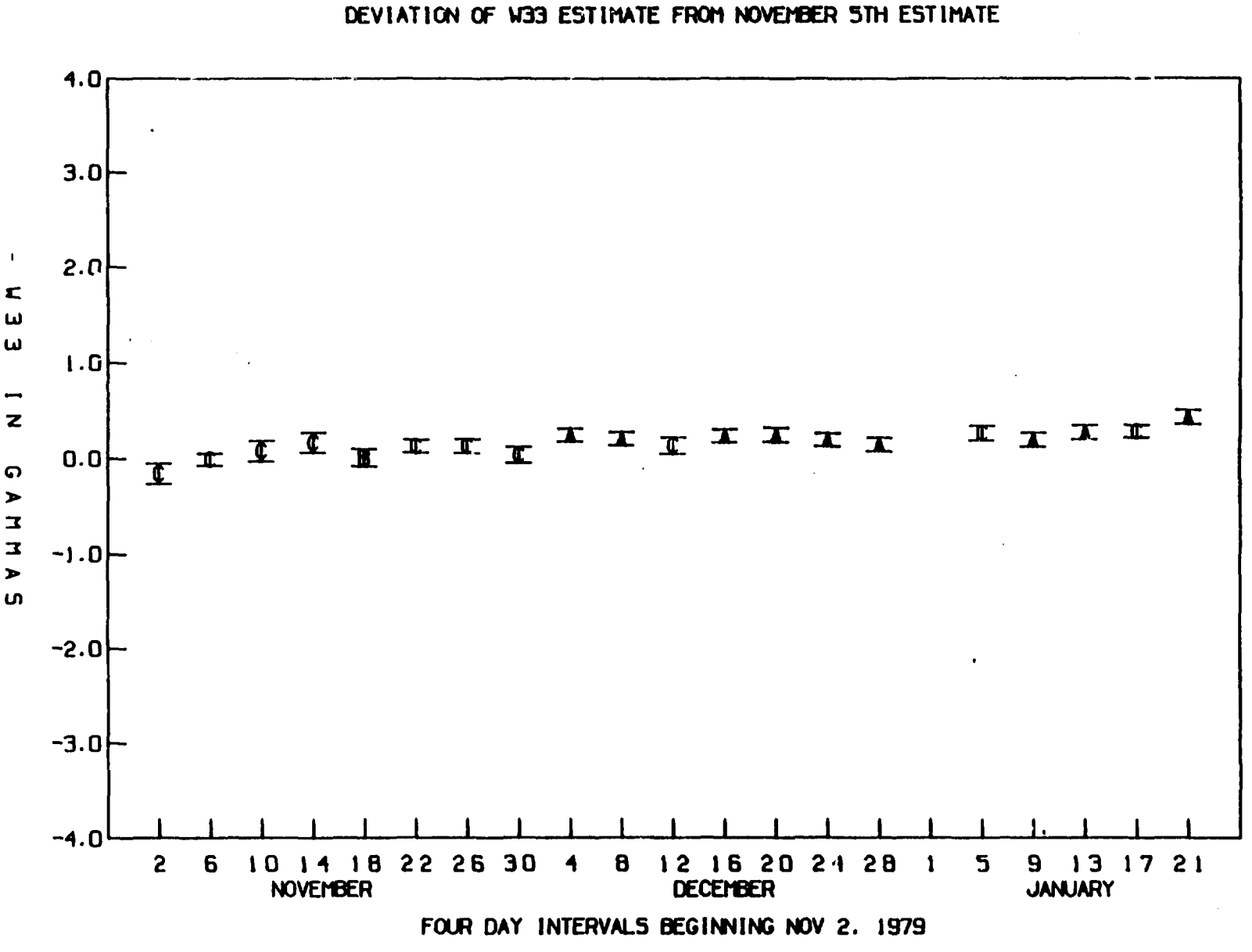
DEVIATION OF W33 ESTIMATE FROM NOVEMBER 5TH ESTIMATE
4.0
3.0
2.0
1.0
0.0
-1.0
-2.0
-3.0
-4.0
W33 IN GAMMAS
2 6 10 14 18 22 26 30 4 8 12 16 20 24 28 1 5 9 13 17 21
NOVEMBER
DECEMBER
JANUARY
FOUR DAY INTERVALS BEGINNING NOV 2. 1979

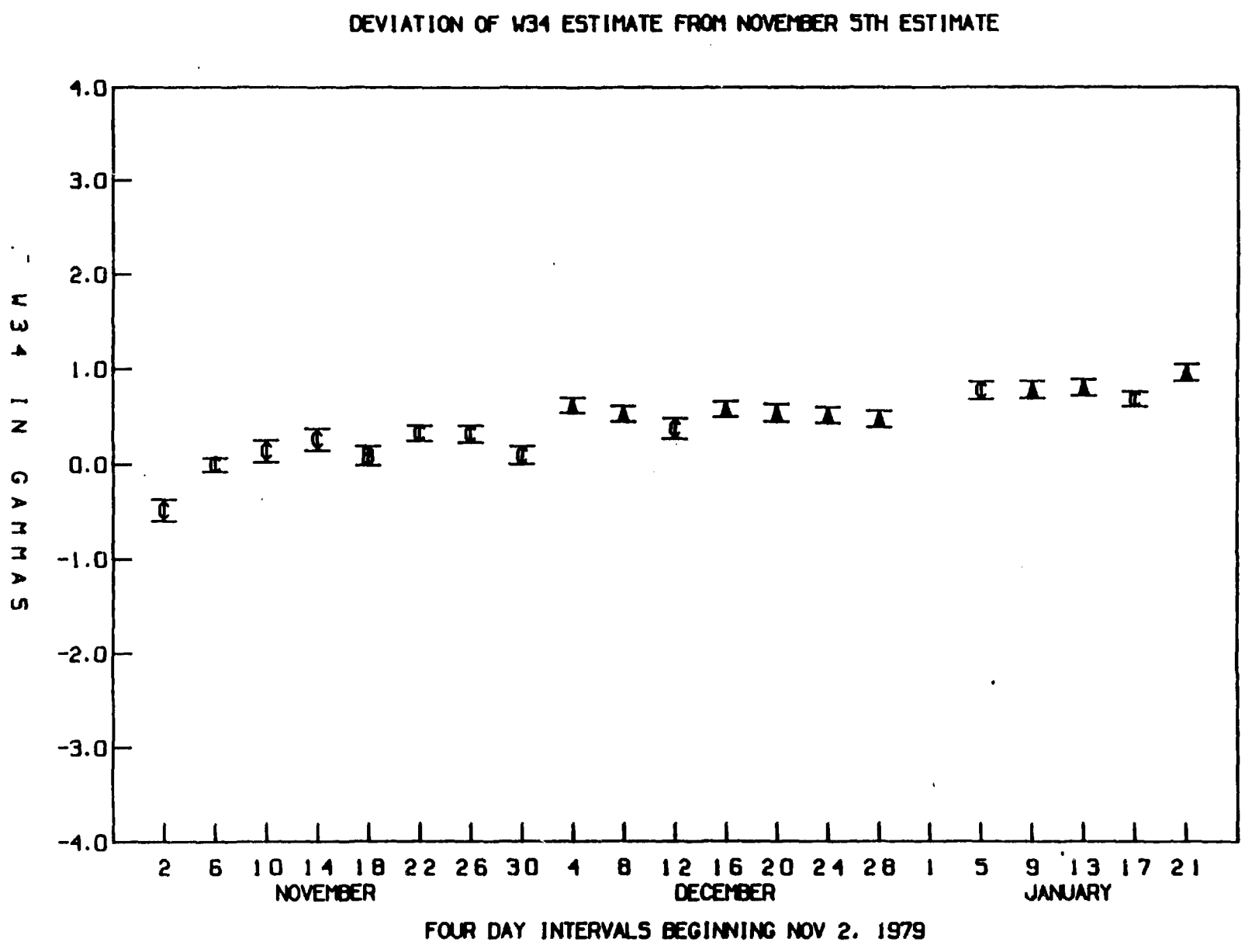
DEVIATION OF W34 ESTIMATE FROM NOVEMBER 5TH ESTIMATE
W34 IN GAMMAS
4.0
3.0
2.0
1.0
0.0
-1.0
-2.0
-3.0
-4.0
2 6 10 14 18 22 26 30 4 8 12 16 20 24 28 1 5 9 13 17 21
NOVEMBER
DECEMBER
JANUARY
FOUR DAY INTERVALS BEGINNING NOV 2. 1979

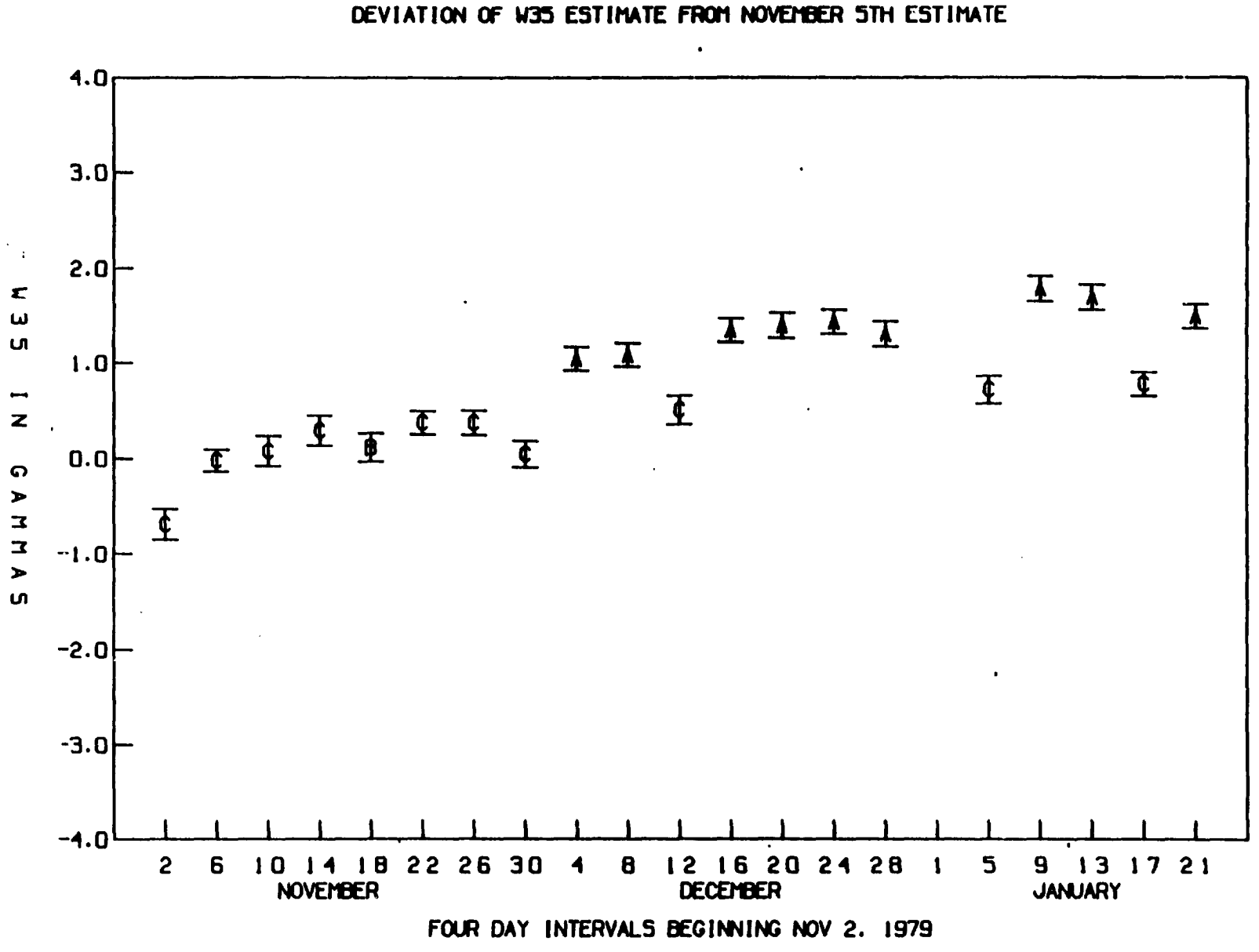
DEVIATION OF W35 ESTIMATE FROM NOVEMBER 5TH ESTIMATE
W35 IN GAMMAS
4.0
3.0
2.0
1.0
0.0
-1.0
-2.0
-3.0
-4.0
2 6 10 14 18 22 26 30 4 8 12 16 20 24 28 1 5 9 13 17 21
NOVEMBER
DECEMBER
JANUARY
FOUR DAY INTERVALS BEGINNING NOV 2. 1979

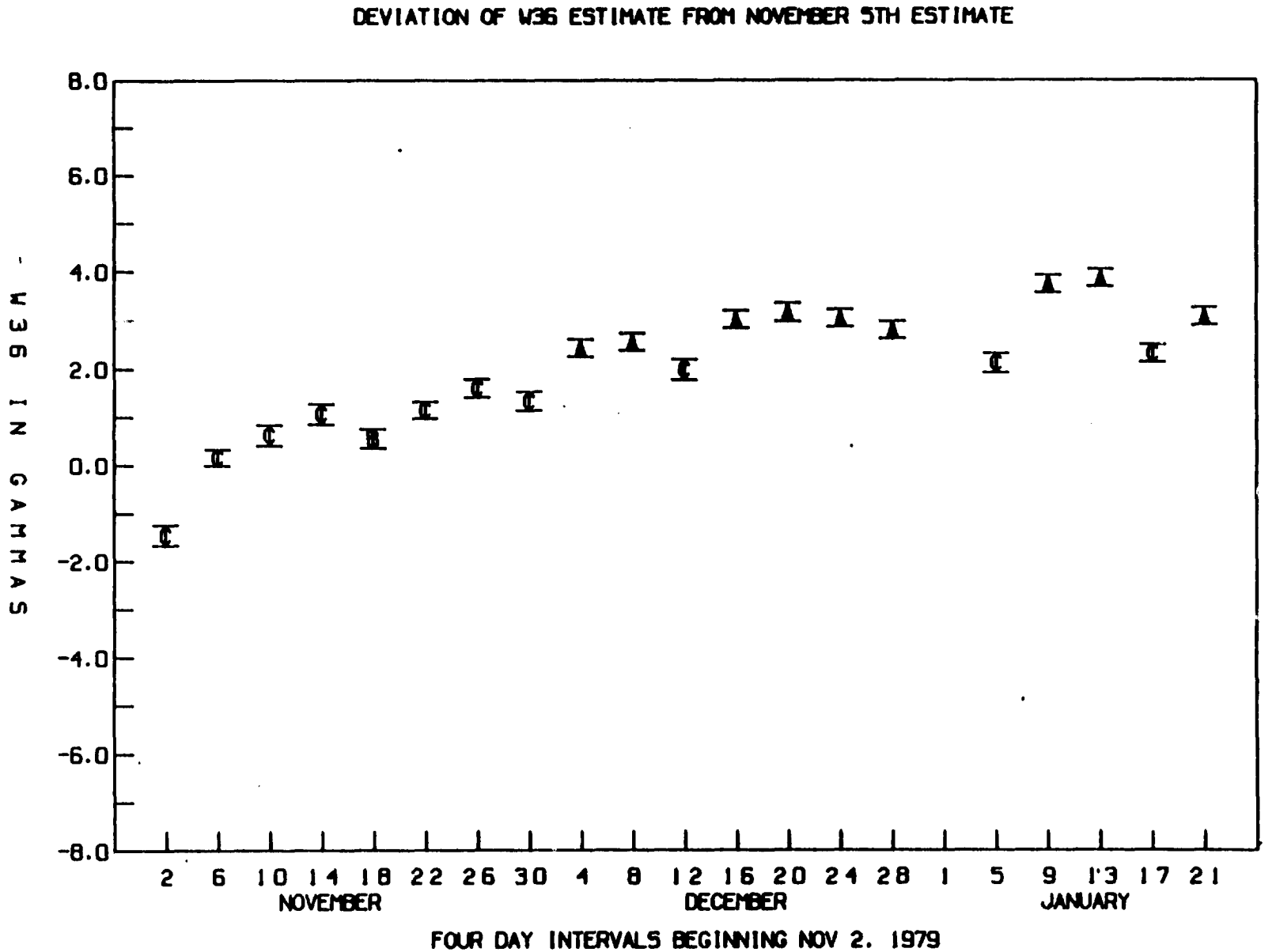
DEVIATION OF W36 ESTIMATE FROM NOVEMBER 5TH ESTIMATE
W36 IN GAMMAS
8.0
6.0
4.0
2.0
0.0
-2.0
-4.0
-6.0
-8.0
2 6 10 14 18 22 26 30 4 8 12 16 20 24 28 1 5 9 13 17 21
NOVEMBER
DECEMBER
JANUARY
FOUR DAY INTERVALS BEGINNING NOV 2. 1979

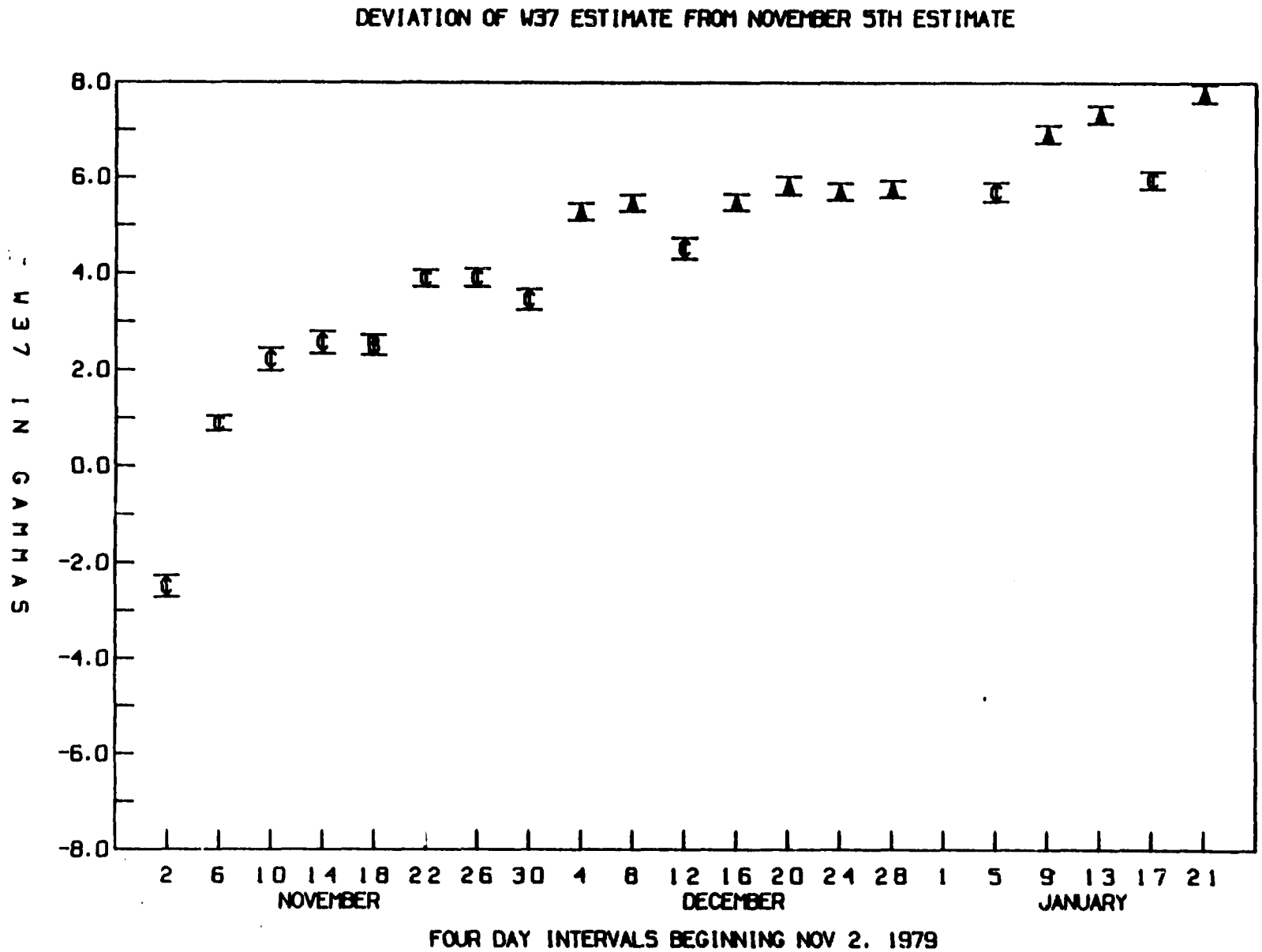
DEVIATION OF W37 ESTIMATE FROM NOVEMBER 5TH ESTIMATE
W37 IN GAMMAS
8.0
6.0
4.0
2.0
0.0
-2.0
-4.0
-6.0
-8.0
2 6 10 14 18 22 26 30 4 8 12 16 20 24 28 1 5 9 13 17 21
NOVEMBER
DECEMBER
JANUARY
FOUR DAY INTERVALS BEGINNING NOV 2. 1979

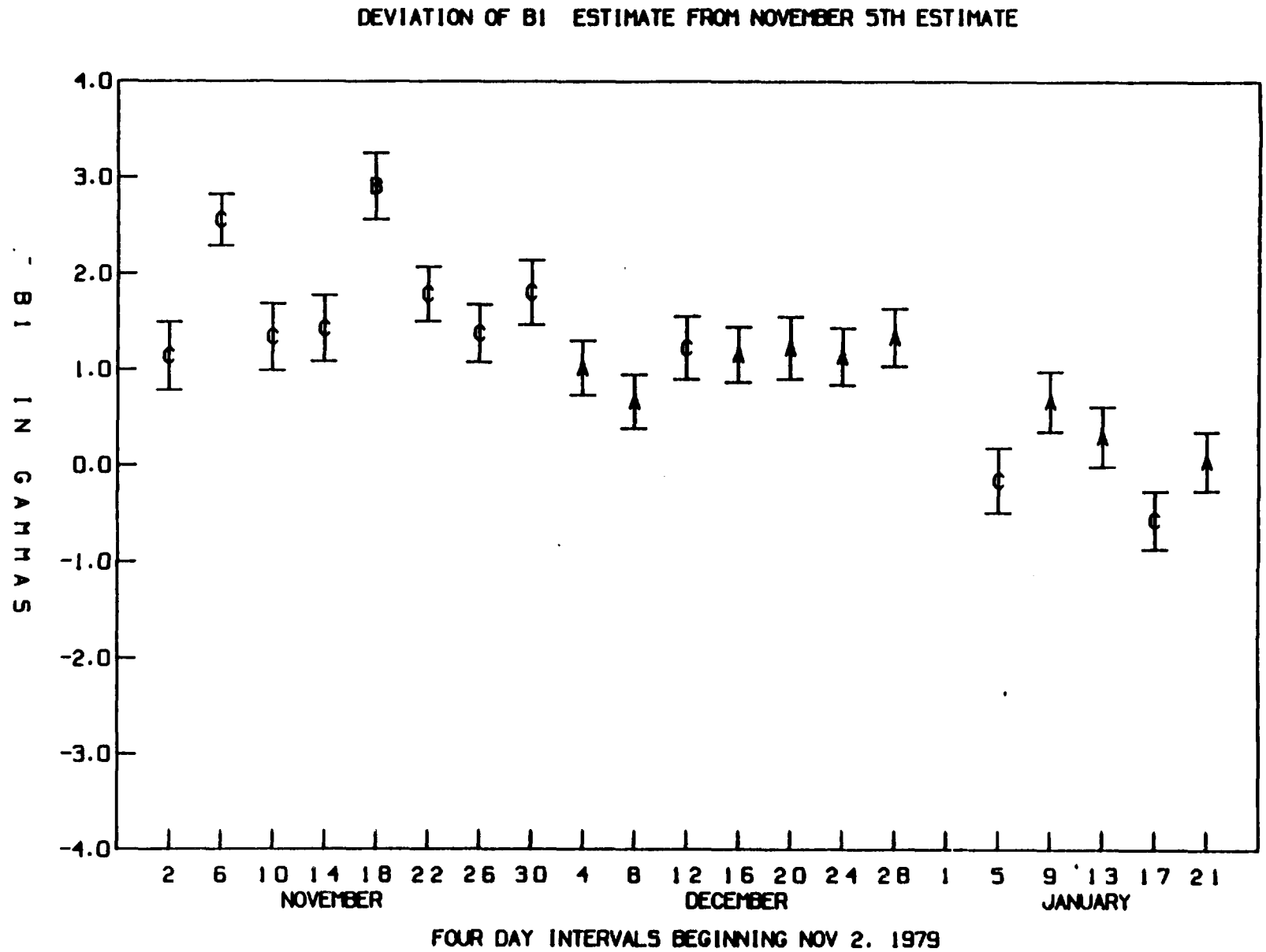
DEVIATION OF BI ESTIMATE FROM NOVEMBER 5TH ESTIMATE
4.0
3.0
2.0
1.0
0.0
-1.0
-2.0
-3.0
-4.0
BI - BI IN GAMMAS
2 6 10 14 18 22 26 30 4 8 12 16 20 24 28 1 5 9 13 17 21
NOVEMBER
DECEMBER
JANUARY
FOUR DAY INTERVALS BEGINNING NOV 2. 1979

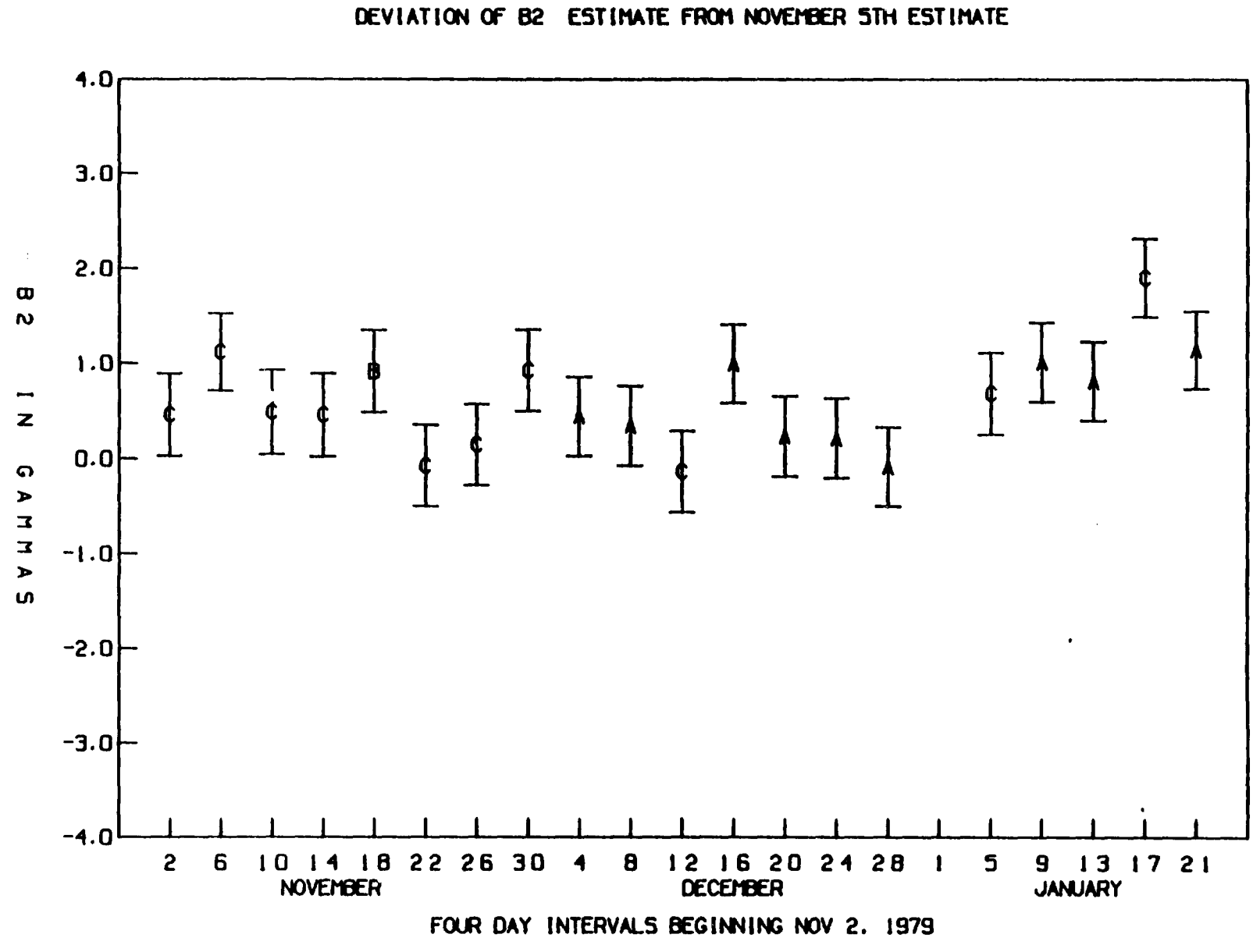
DEVIATION OF B2 ESTIMATE FROM NOVEMBER 5TH ESTIMATE
B2 IN GAMMAS
4.0
3.0
2.0
1.0
0.0
-1.0
-2.0
-3.0
-4.0
2 6 10 14 18 22 26 30 4 8 12 16 20 24 28 1 5 9 13 17 21
NOVEMBER
DECEMBER
JANUARY
FOUR DAY INTERVALS BEGINNING NOV 2. 1979

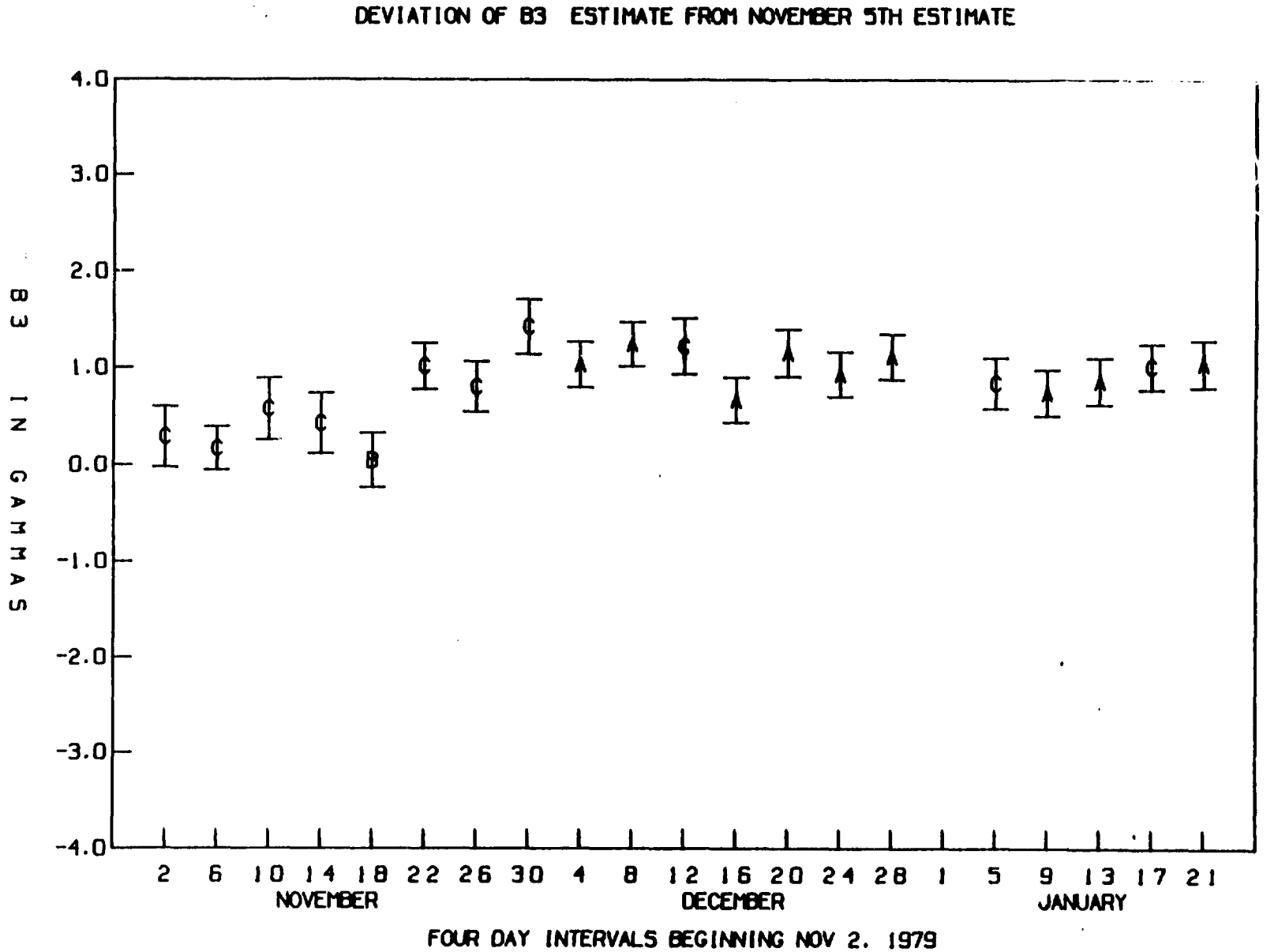
DEVIATION OF B3 ESTIMATE FROM NOVEMBER 5TH ESTIMATE
B3 IN GAMMAS
4.0
3.0
2.0
1.0
0.0
-1.0
-2.0
-3.0
-4.0
2 6 10 14 18 22 26 30 4 8 12 16 20 24 28 1 5 9 13 17 21
NOVEMBER
DECEMBER
JANUARY
FOUR DAY INTERVALS BEGINNING NOV 2. 1979

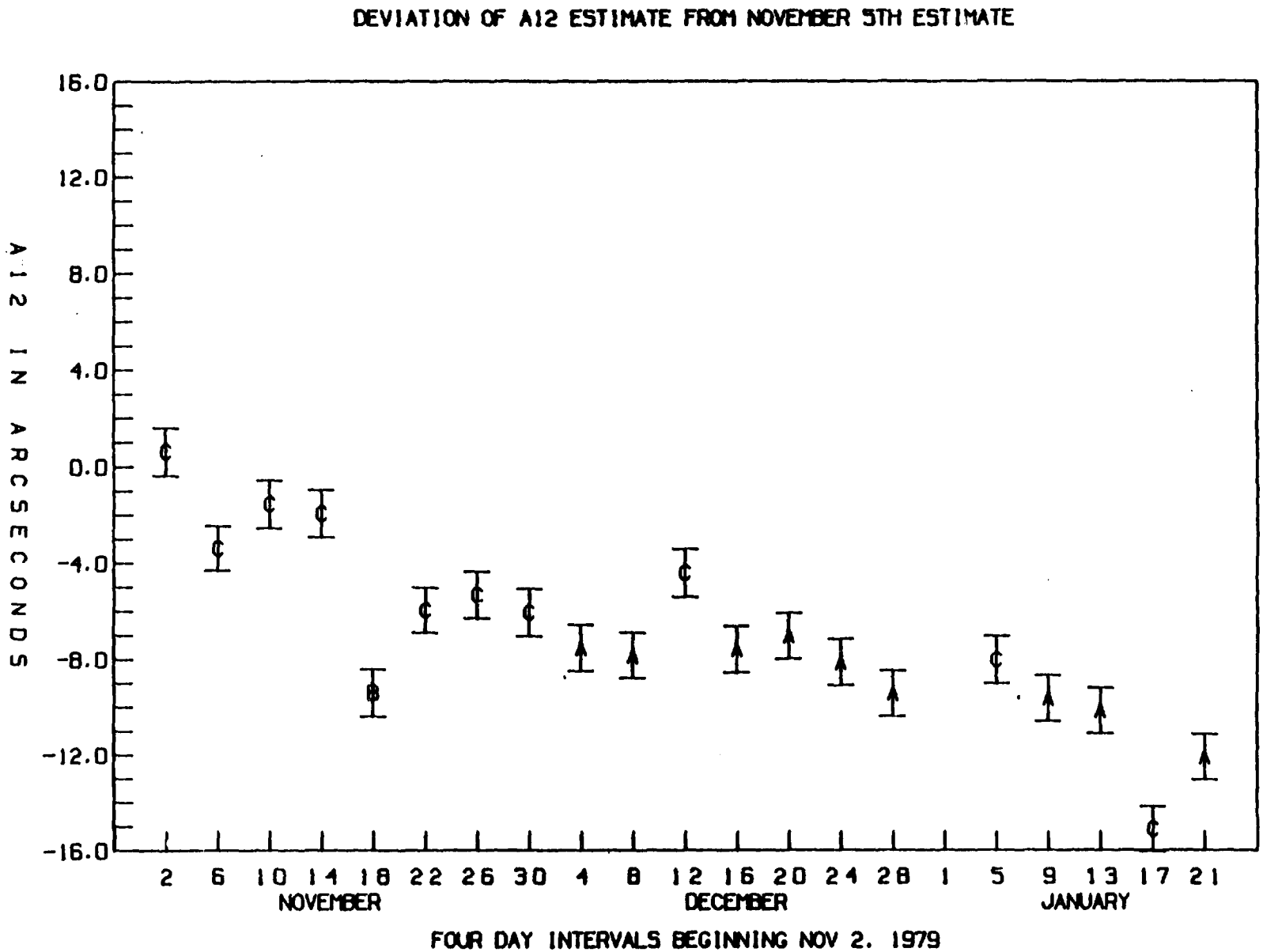
DEVIATION OF A12 ESTIMATE FROM NOVEMBER 5TH ESTIMATE
A12 IN ARCSECONDS
16.0
12.0
8.0
4.0
0.0
-4.0
-8.0
-12.0
-16.0
2 6 10 14 18 22 26 30 4 8 12 16 20 24 28 1 5 9 13 17 21
NOVEMBER
DECEMBER
JANUARY
FOUR DAY INTERVALS BEGINNING NOV 2. 1979

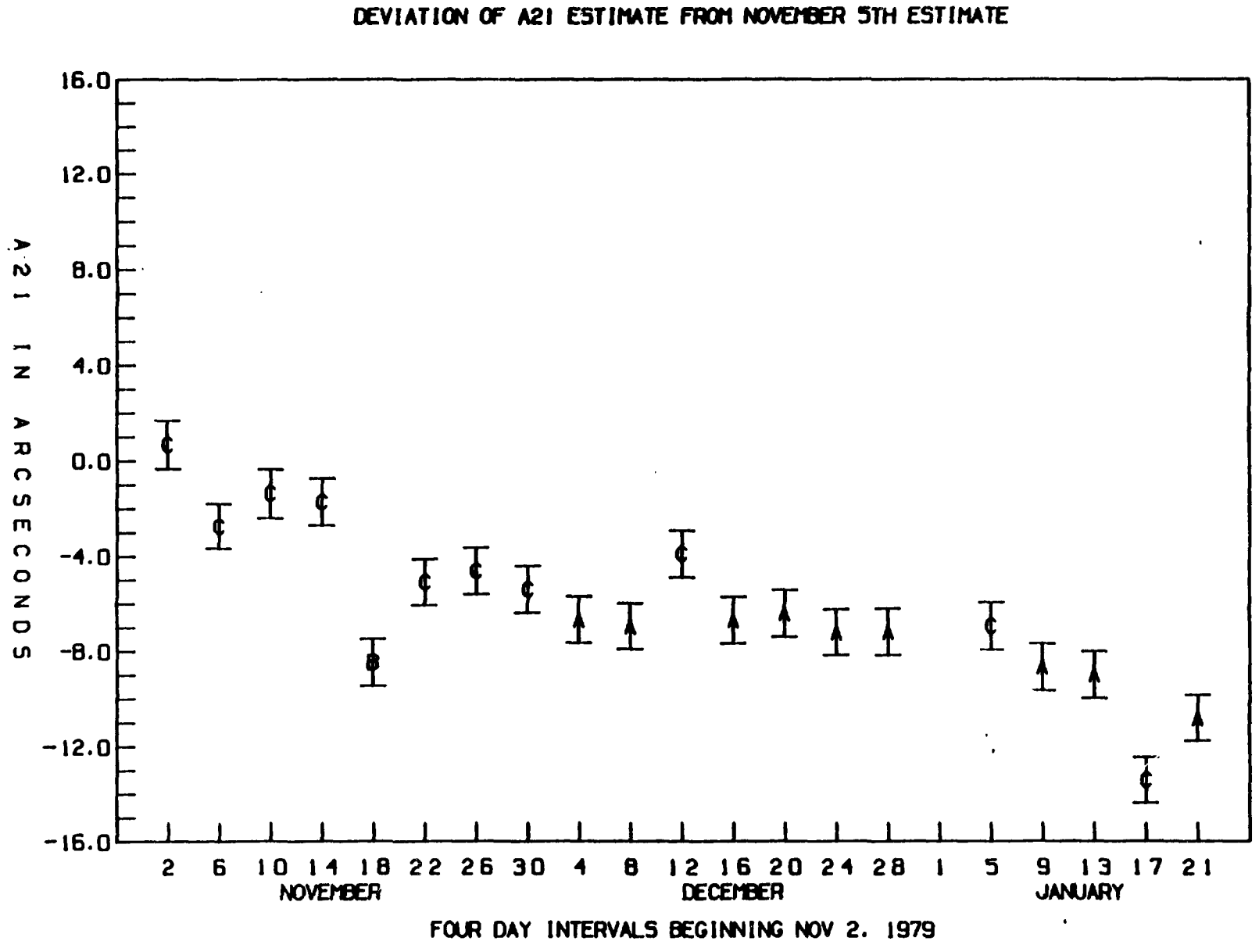
DEVIATION OF A21 ESTIMATE FROM NOVEMBER 5TH ESTIMATE
16.0
12.0
8.0
4.0
0.0
-4.0
-8.0
-12.0
-16.0
A21 IN ARCSECONDS
2 6 10 14 18 22 26 30 4 8 12 16 20 24 28 1 5 9 13 17 21
NOVEMBER
DECEMBER
JANUARY
FOUR DAY INTERVALS BEGINNING NOV 2. 1979

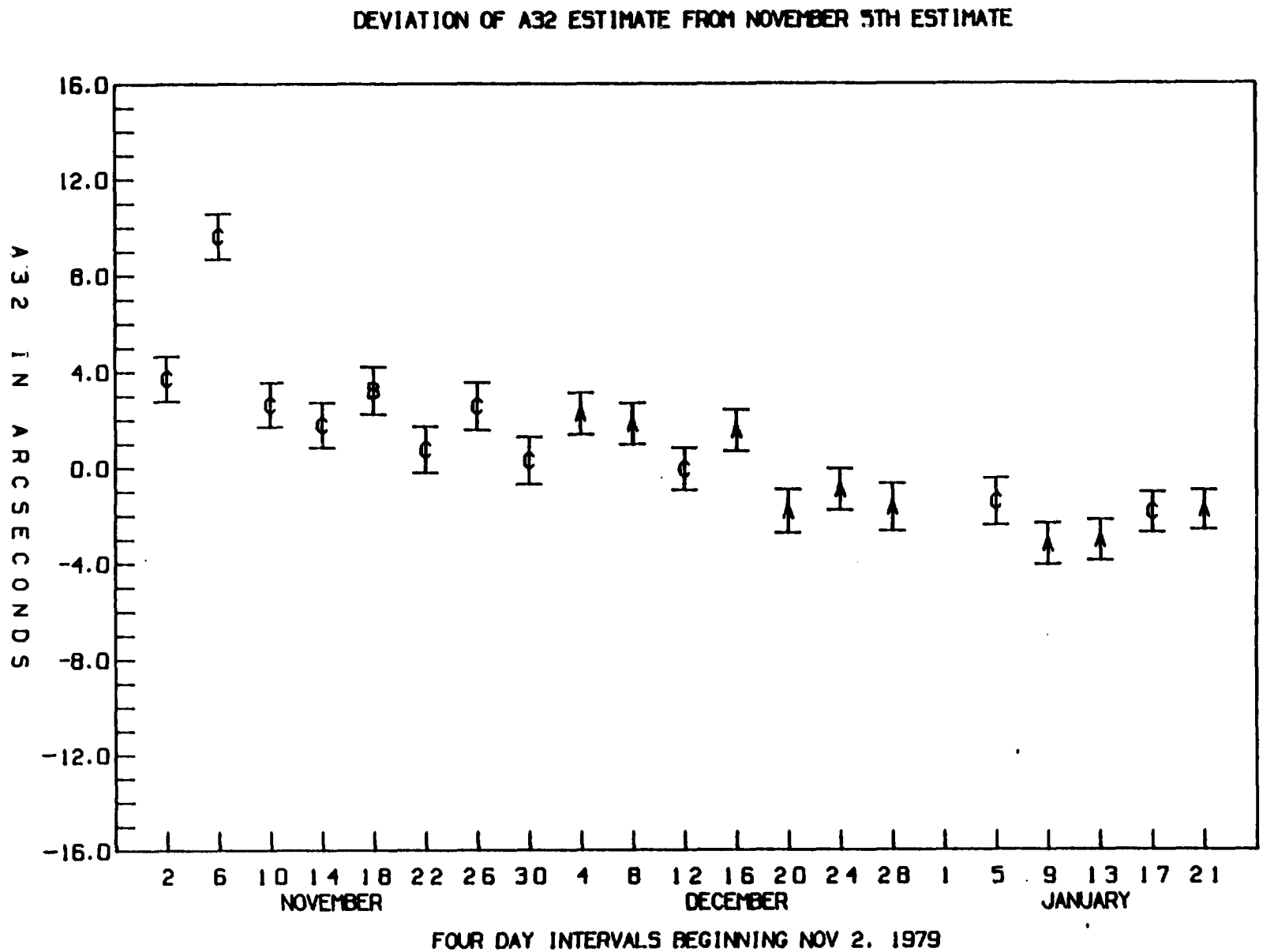
DEVIATION OF A32 ESTIMATE FROM NOVEMBER 5TH ESTIMATE
A32 IN ARCSECONDS
16.0
12.0
8.0
4.0
0.0
-4.0
-8.0
-12.0
-16.0
2 6 10 14 18 22 26 30 4 8 12 16 20 24 28 1 5 9 13 17 21
NOVEMBER
DECEMBER
JANUARY
FOUR DAY INTERVALS BEGINNING NOV 2. 1979

STATISTICS FOR CALIBRATION OF NOVEMBER 2, 1979

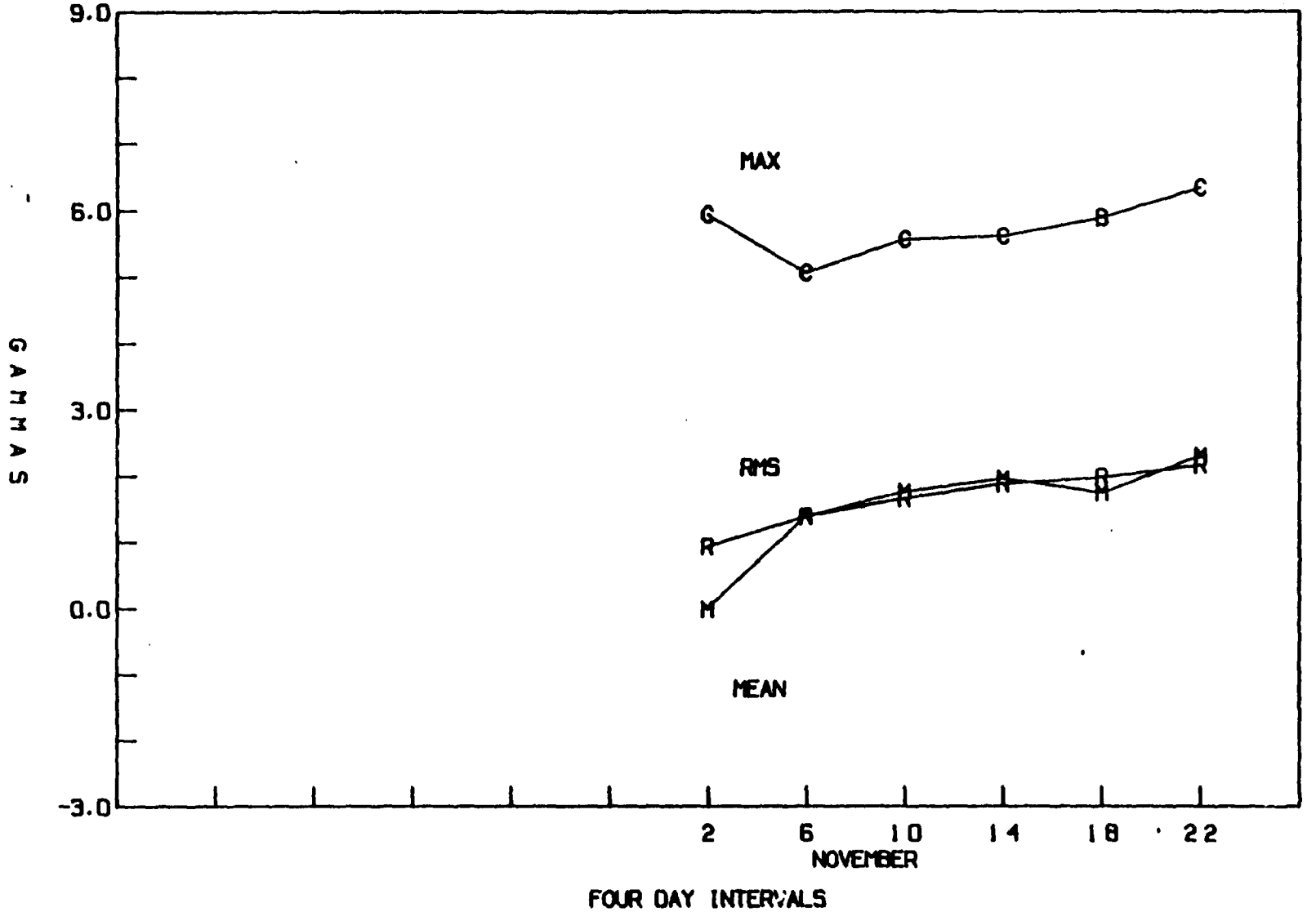

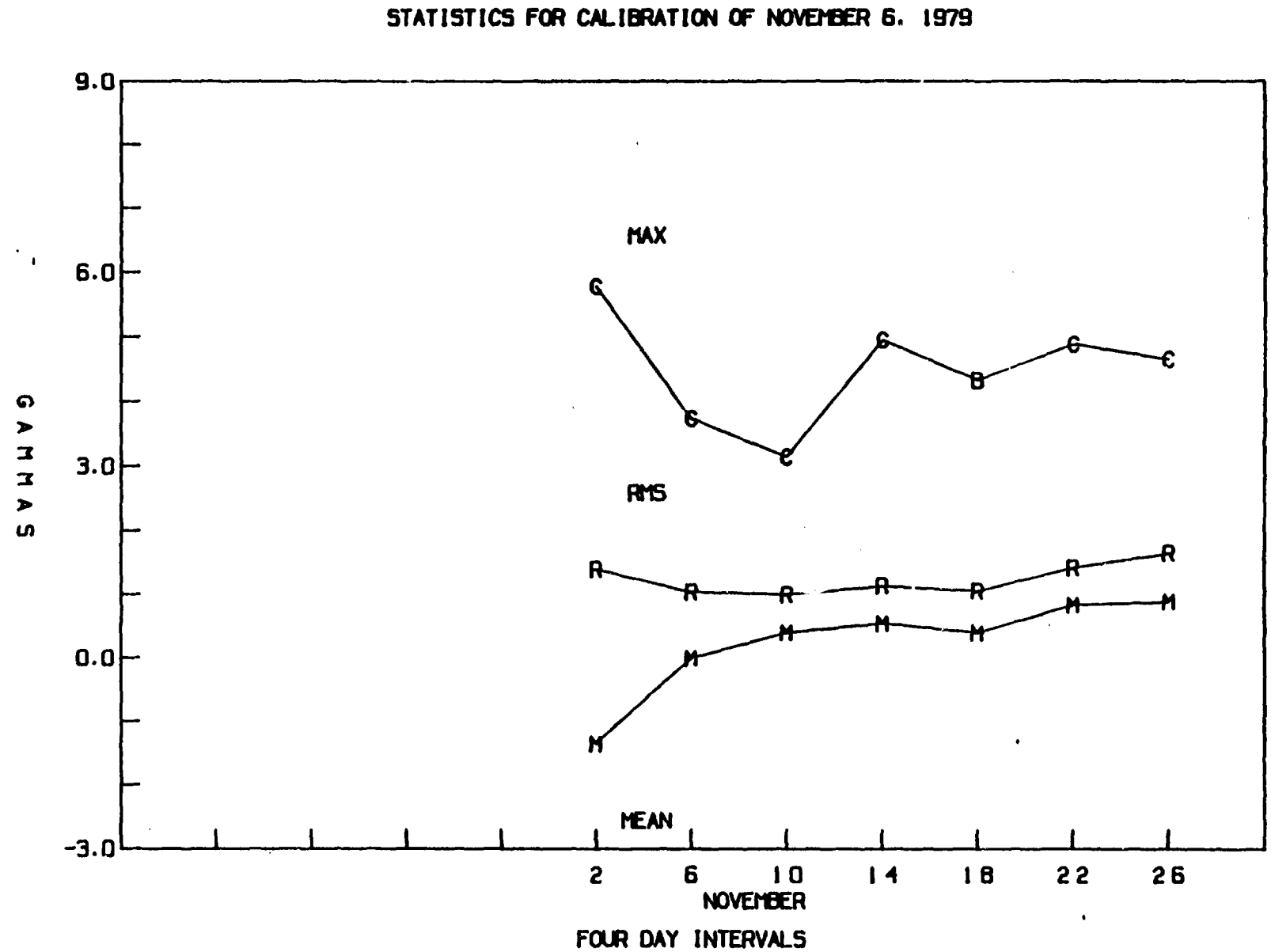
STATISTICS FOR CALIBRATION OF NOVEMBER 6. 1979
9.0
6.0
3.0
0.0
-3.0
GAMMAS
MAX
RMS
MEAN
2
6
10
14
18
22
26
NOVEMBER
FOUR DAY INTERVALS

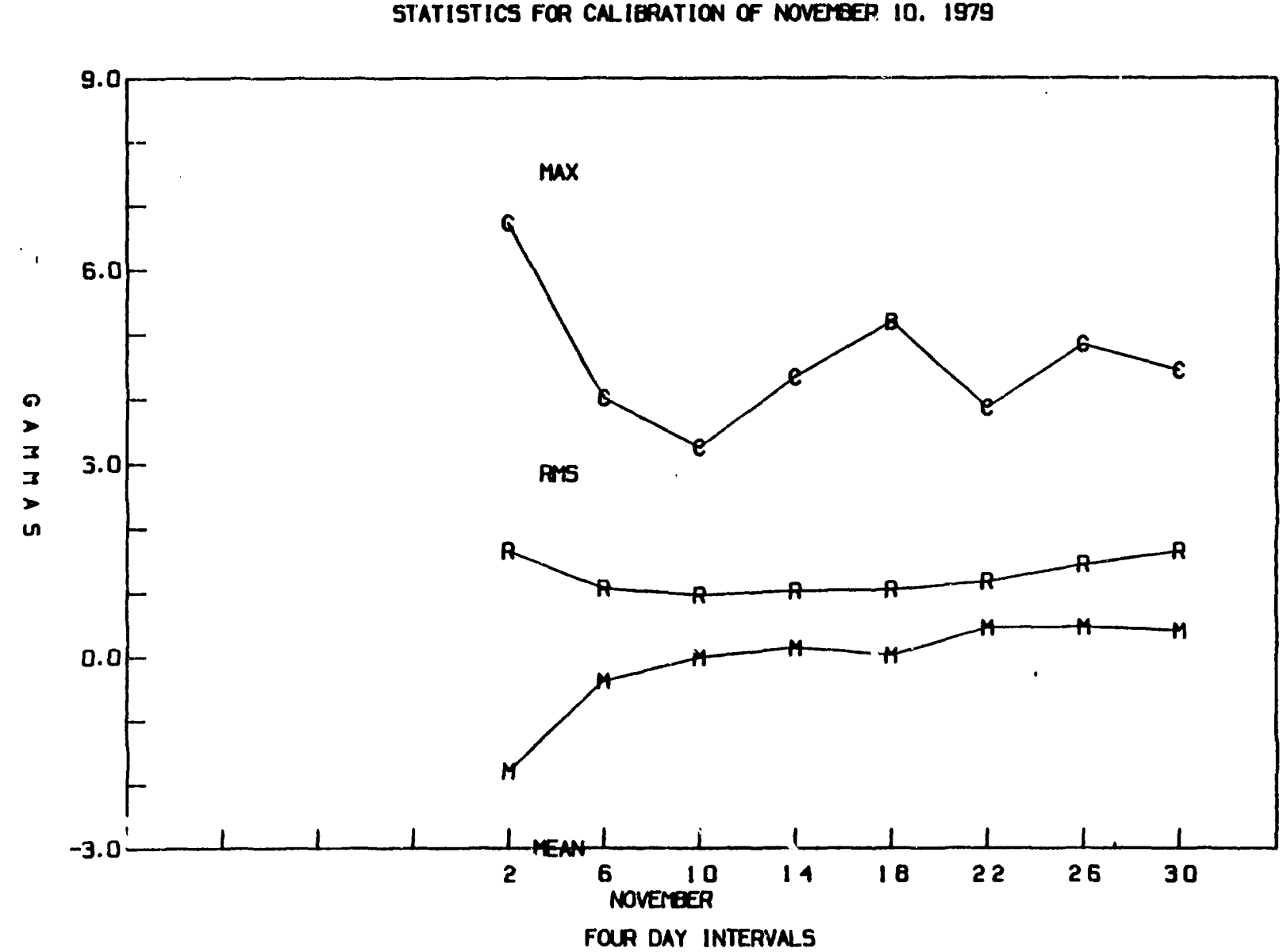
STATISTICS FOR CALIBRATION OF NOVEMBER 10, 1979
9.0
6.0
3.0
0.0
-3.0
GAMMAS
MAX
RMS
MEAN
2
6
10
14
18
22
26
30
NOVEMBER
FOUR DAY INTERVALS

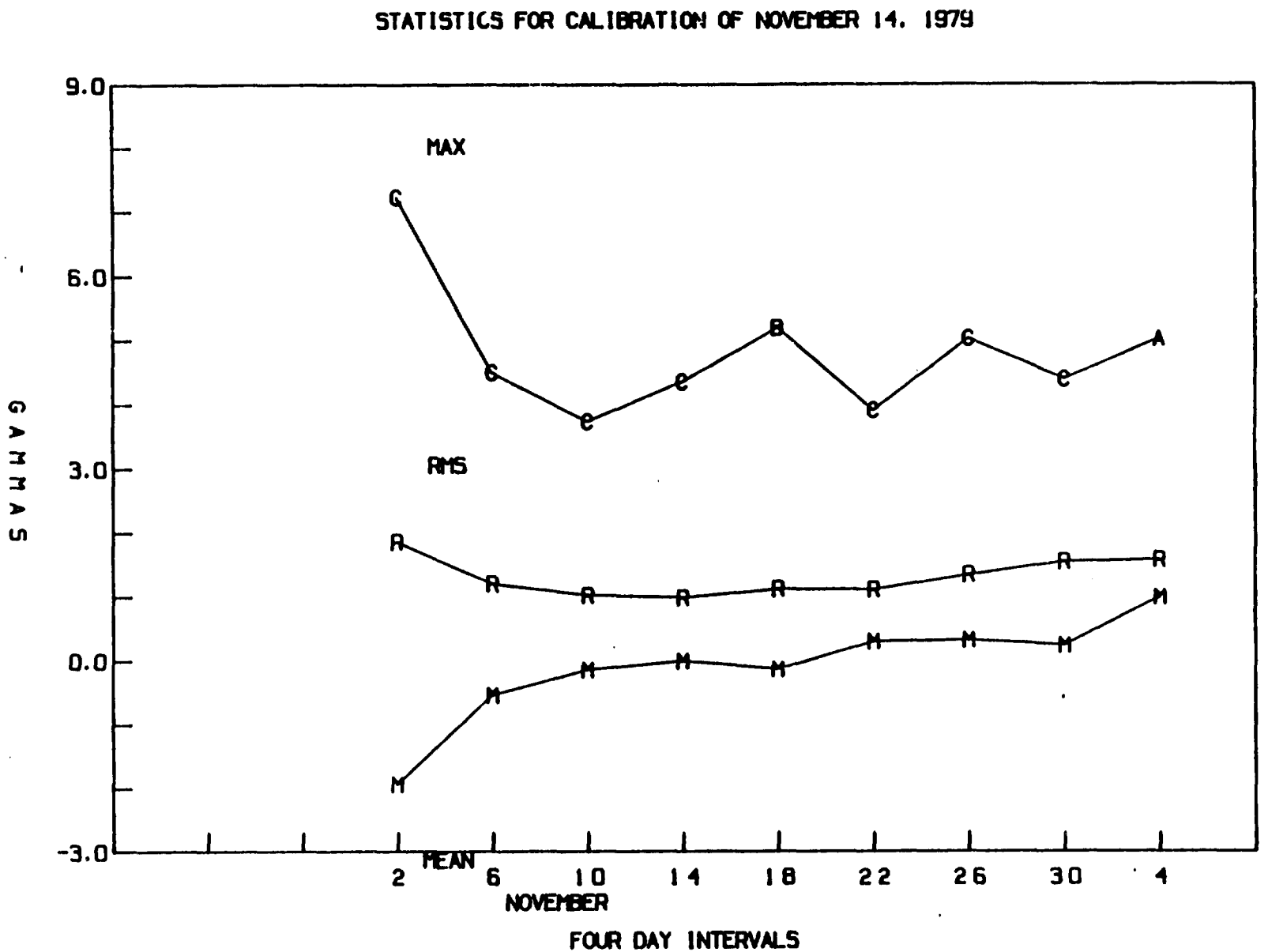
STATISTICS FOR CALIBRATION OF NOVEMBER 14, 1979
9.0
6.0
3.0
0.0
-3.0
GAMMAS
MAX
RMS
MEAN
2
6
10
14
18
22
26
30
4
NOVEMBER
FOUR DAY INTERVALS

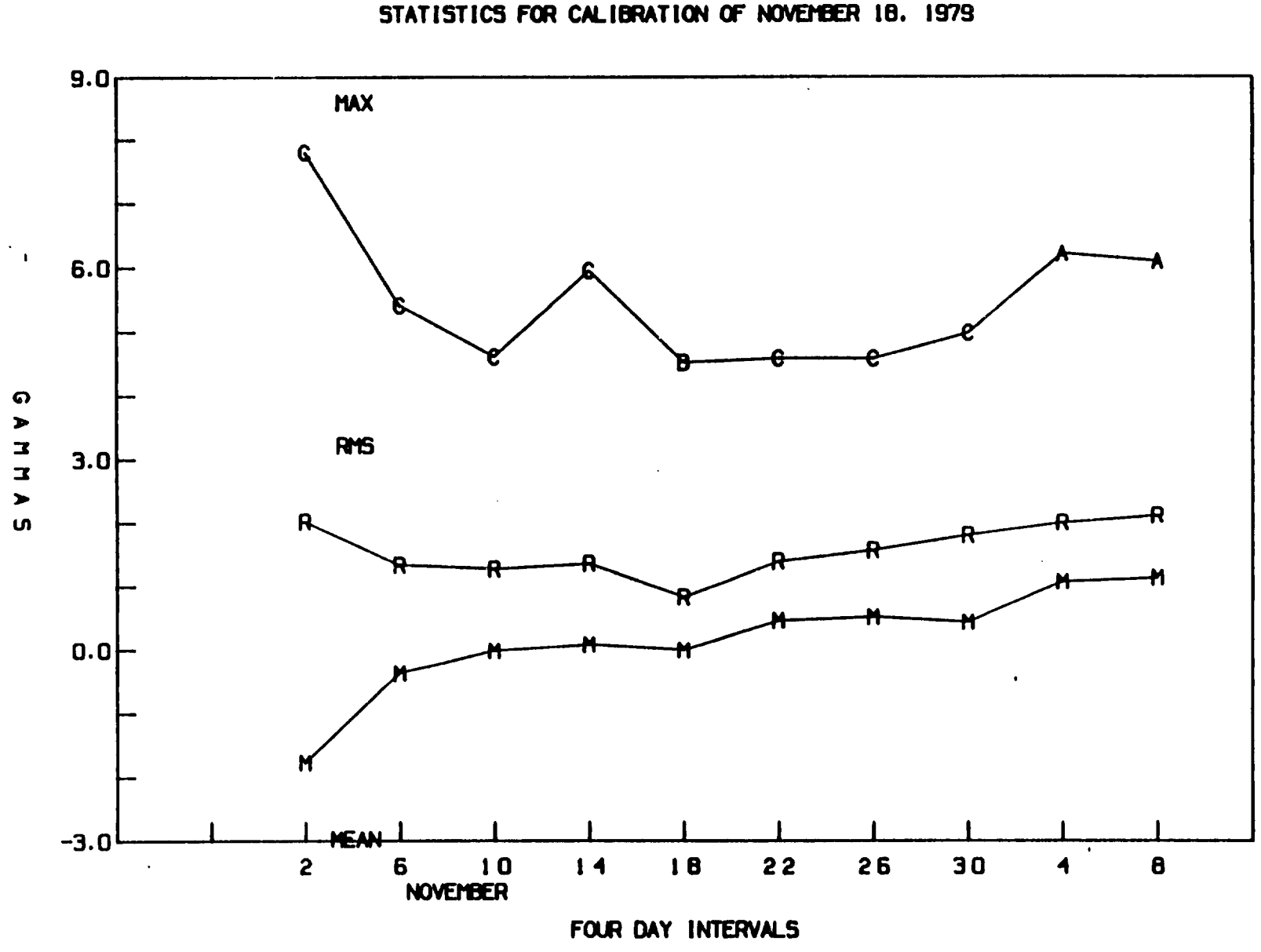
STATISTICS FOR CALIBRATION OF NOVEMBER 18, 1979
9.0
6.0
3.0
0.0
-3.0
GAMMAS
MAX
RMS
MEAN
2
6
10
14
18
22
26
30
4
8
NOVEMBER
FOUR DAY INTERVALS

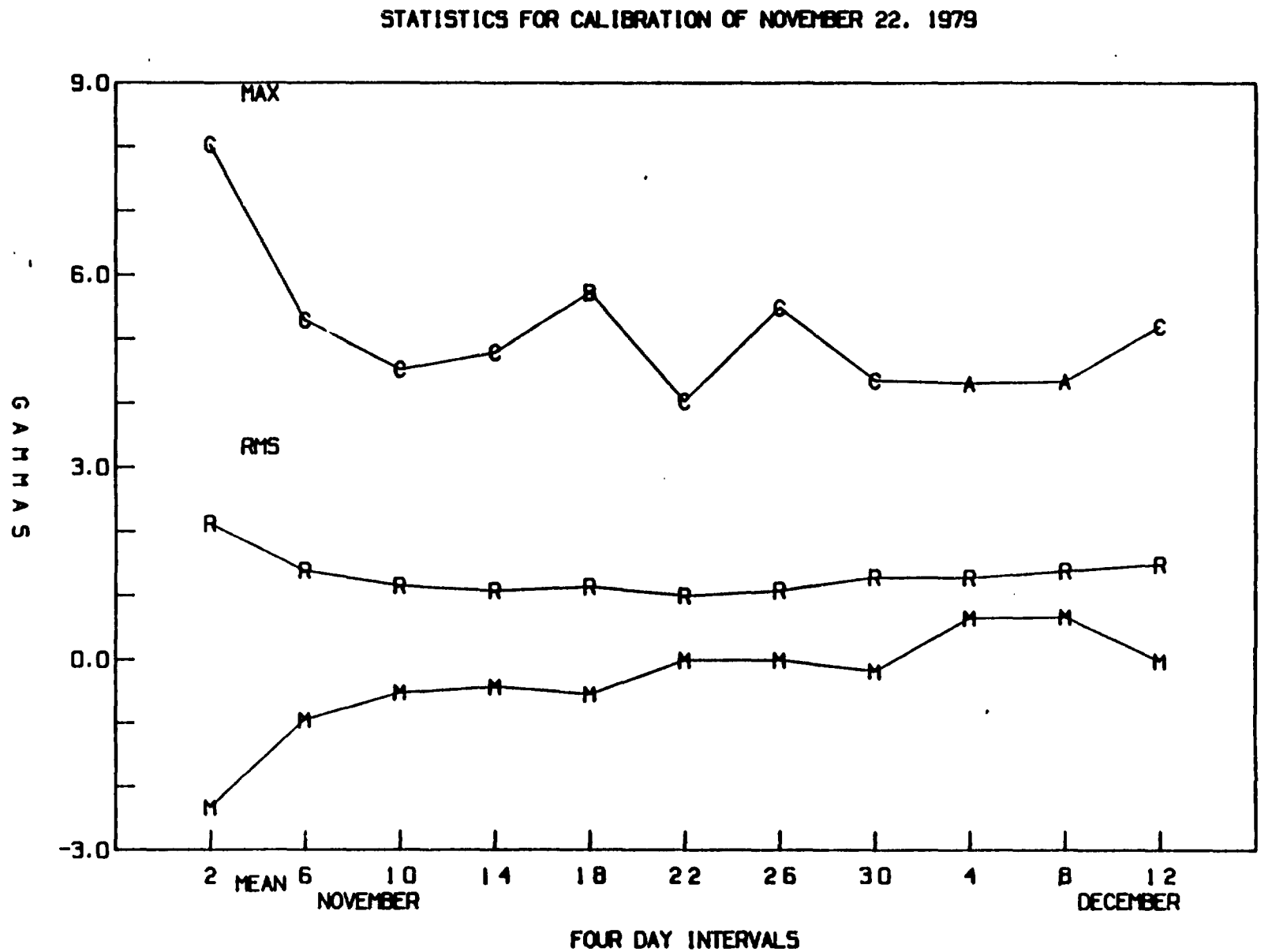
STATISTICS FOR CALIBRATION OF NOVEMBER 22. 1979
9.0
6.0
3.0
0.0
-3.0
MAX
RMS
GAMMAS
2
MEAN
6
10
14
18
22
26
30
4
8
12
NOVEMBER
DECEMBER
FOUR DAY INTERVALS

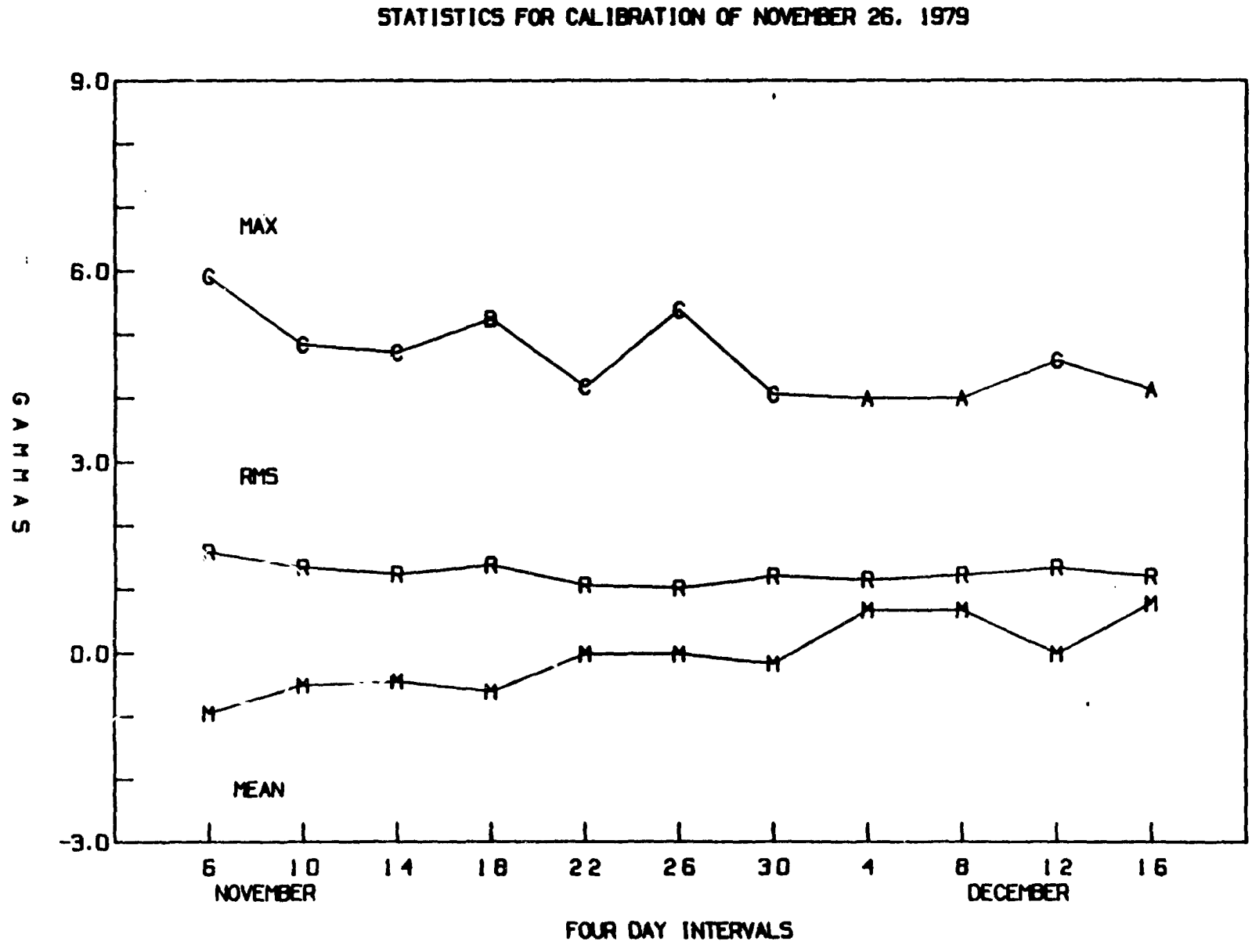
STATISTICS FOR CALIBRATION OF NOVEMBER 26. 1979
9.0
6.0
3.0
0.0
-3.0
GAMMAS
MAX
RMS
MEAN
6
10
14
18
22
26
30
4
8
12
16
NOVEMBER
DECEMBER
FOUR DAY INTERVALS

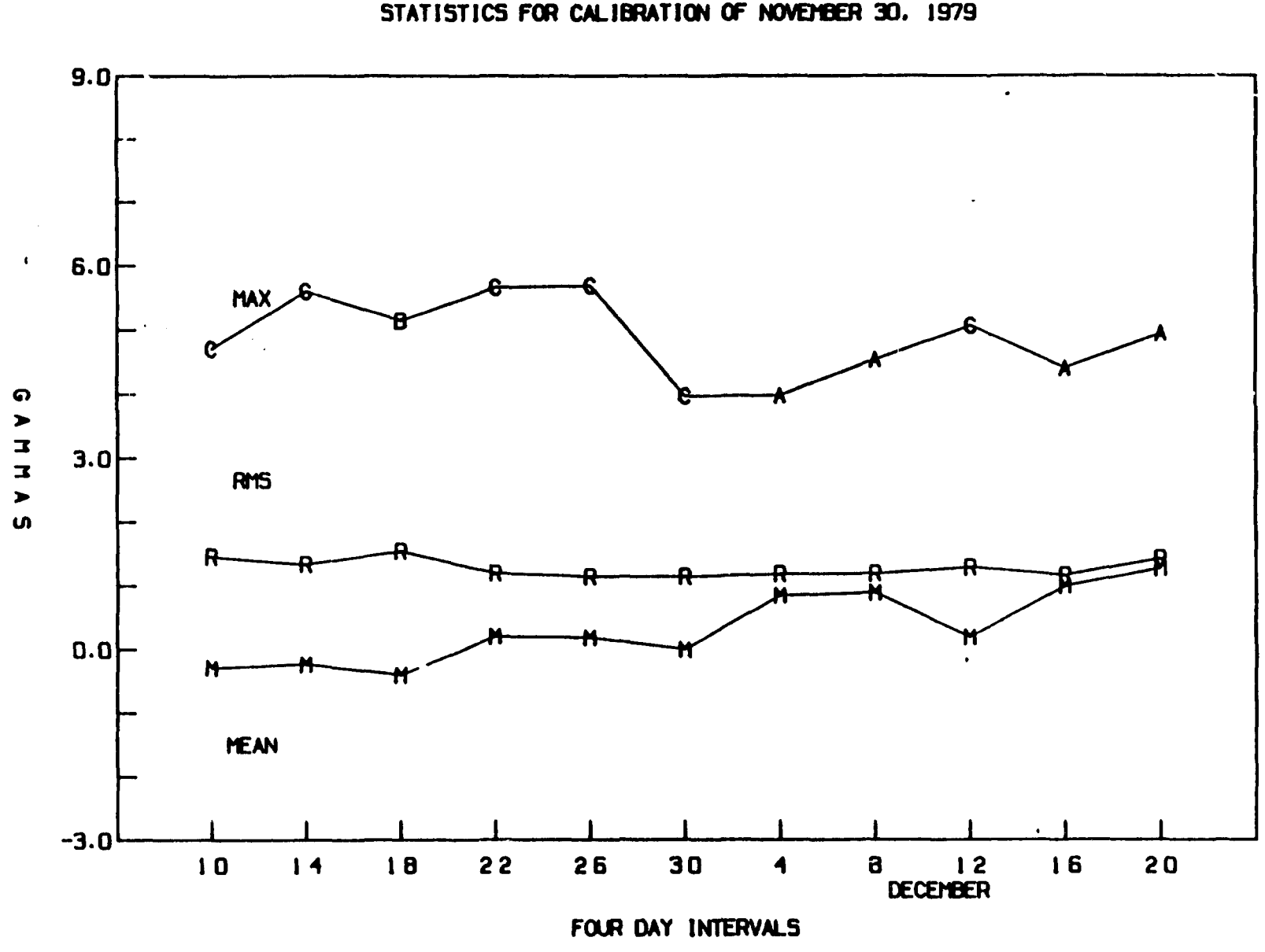
STATISTICS FOR CALIBRATION OF NOVEMBER 30, 1979
9.0
6.0
3.0
0.0
-3.0
GAMMAS
MAX
RMS
MEAN
10
14
18
22
26
30
4
8
12
16
20
DECEMBER
FOUR DAY INTERVALS

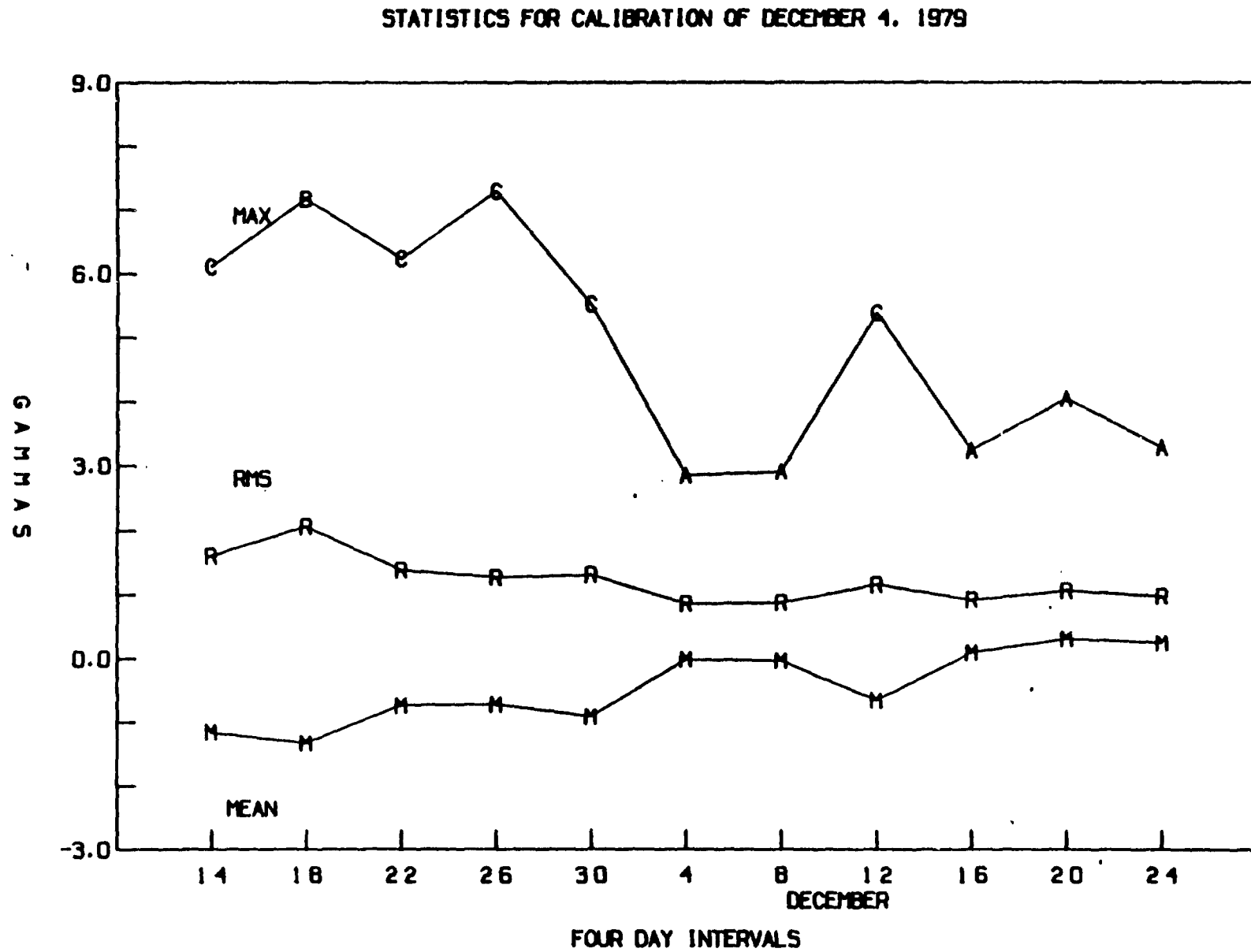
STATISTICS FOR CALIBRATION OF DECEMBER 4, 1979
9.0
6.0
3.0
0.0
-3.0
GAMMAS
MAX
RMS
MEAN
14
18
22
26
30
4
8
12
16
20
24
DECEMBER
FOUR DAY INTERVALS

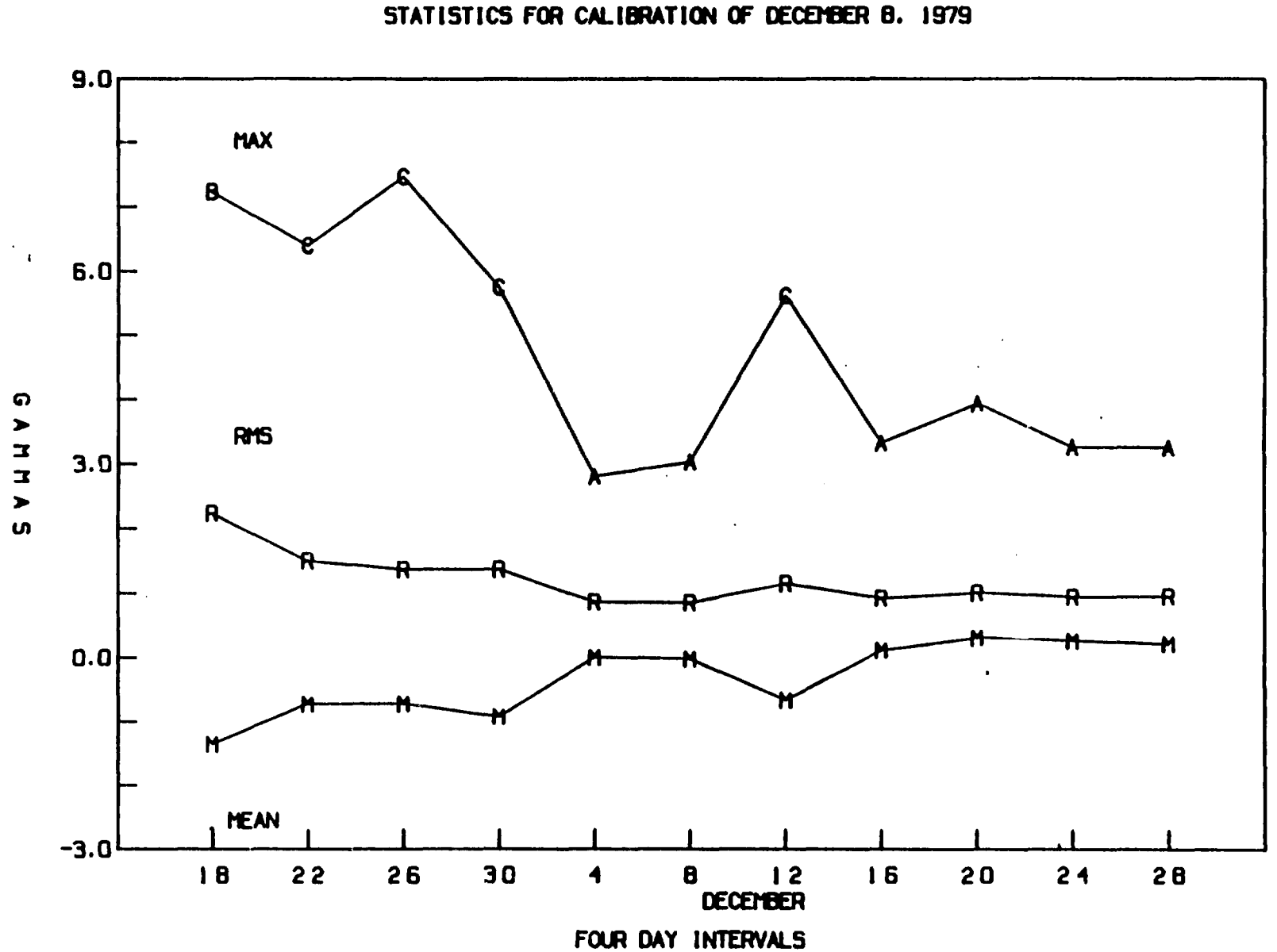
STATISTICS FOR CALIBRATION OF DECEMBER 8, 1979
9.0
6.0
3.0
0.0
-3.0
GAMMAS
MAX
RMS
MEAN
18
22
26
30
4
8
12
16
20
24
28
DECEMBER
FOUR DAY INTERVALS

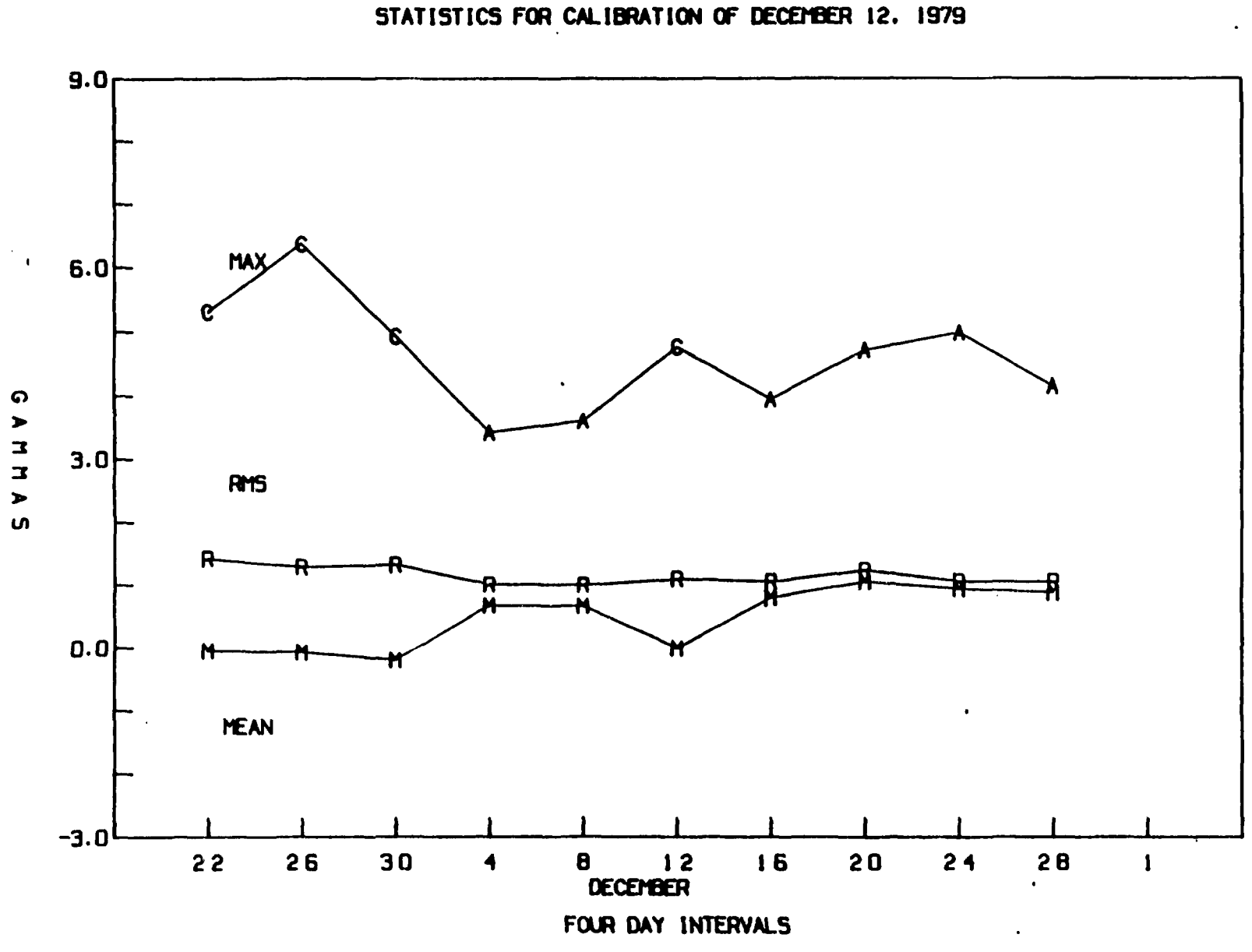
STATISTICS FOR CALIBRATION OF DECEMBER 12, 1979
9.0
6.0
3.0
0.0
-3.0
GAMMAS
MAX
RMS
MEAN
22
26
30
4
8
12
16
20
24
28
1
DECEMBER
FOUR DAY INTERVALS

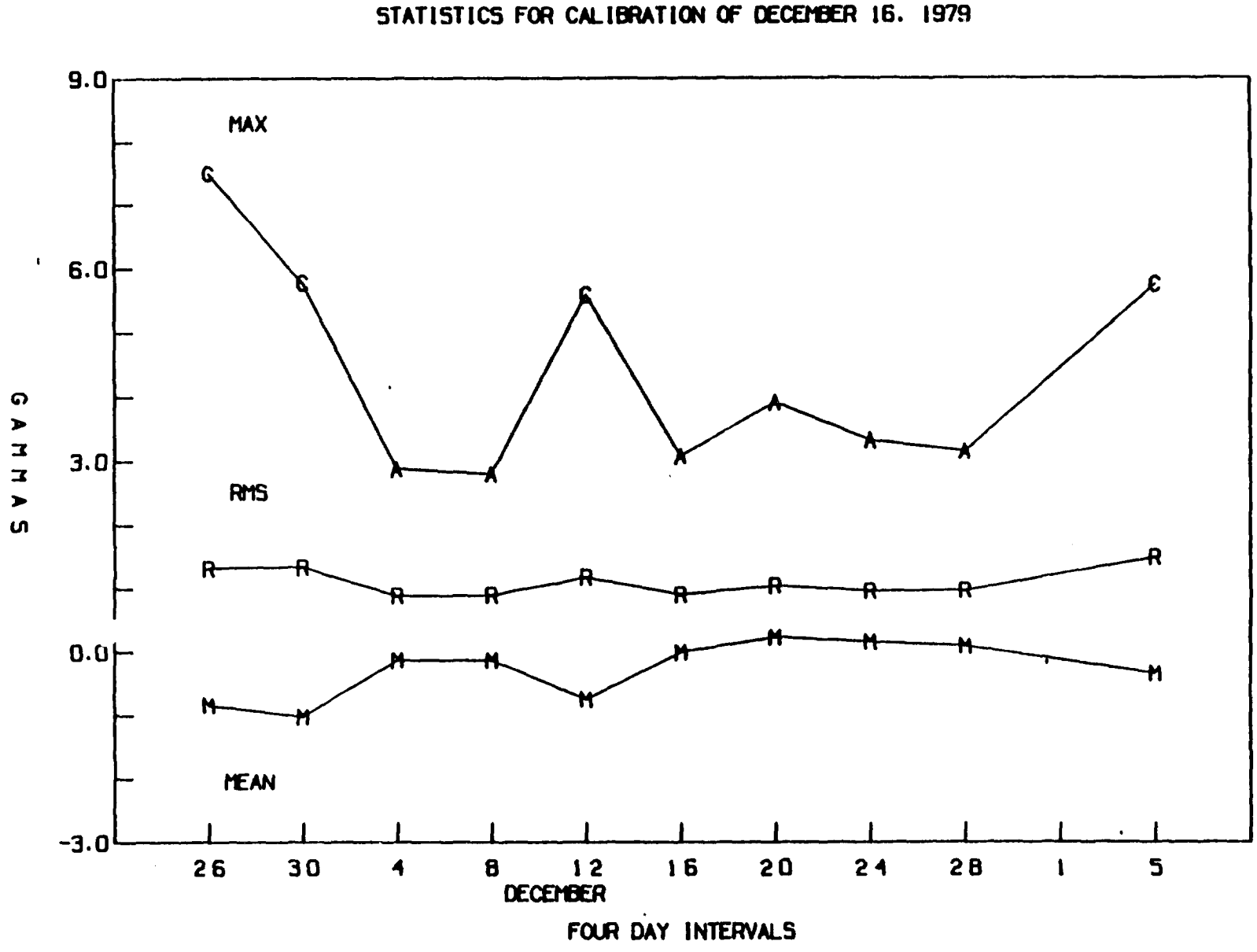
STATISTICS FOR CALIBRATION OF DECEMBER 16. 1979
9.0
6.0
3.0
0.0
-3.0
GAMMAS
MAX
RMS
MEAN
26
30
4
8
12
16
20
24
28
1
5
DECEMBER
FOUR DAY INTERVALS

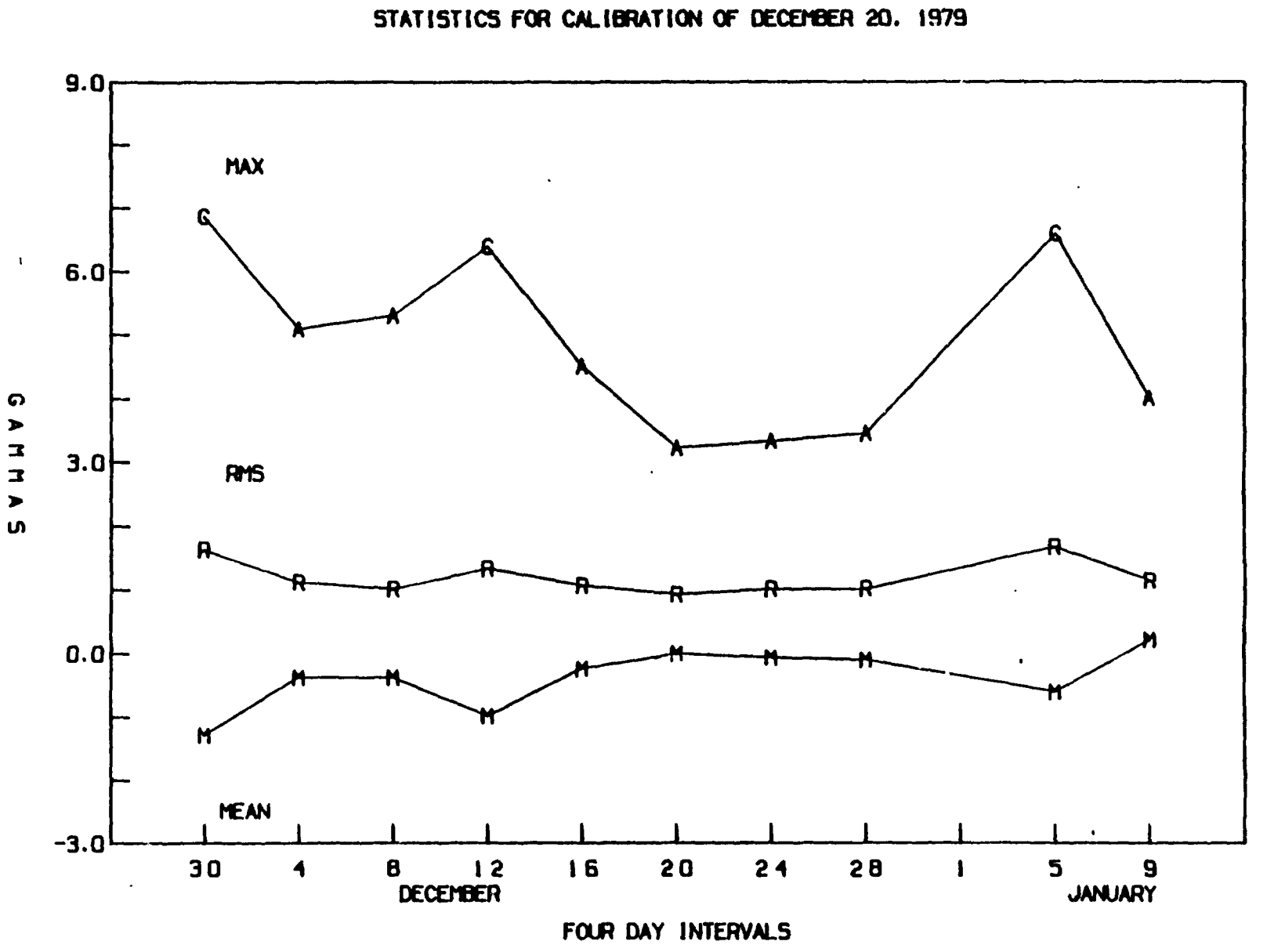
STATISTICS FOR CALIBRATION OF DECEMBER 20. 1979
9.0
6.0
3.0
0.0
-3.0
GAMMAS
MAX
RMS
MEAN
30
4
8
12
16
20
24
28
1
5
9
DECEMBER
JANUARY
FOUR DAY INTERVALS

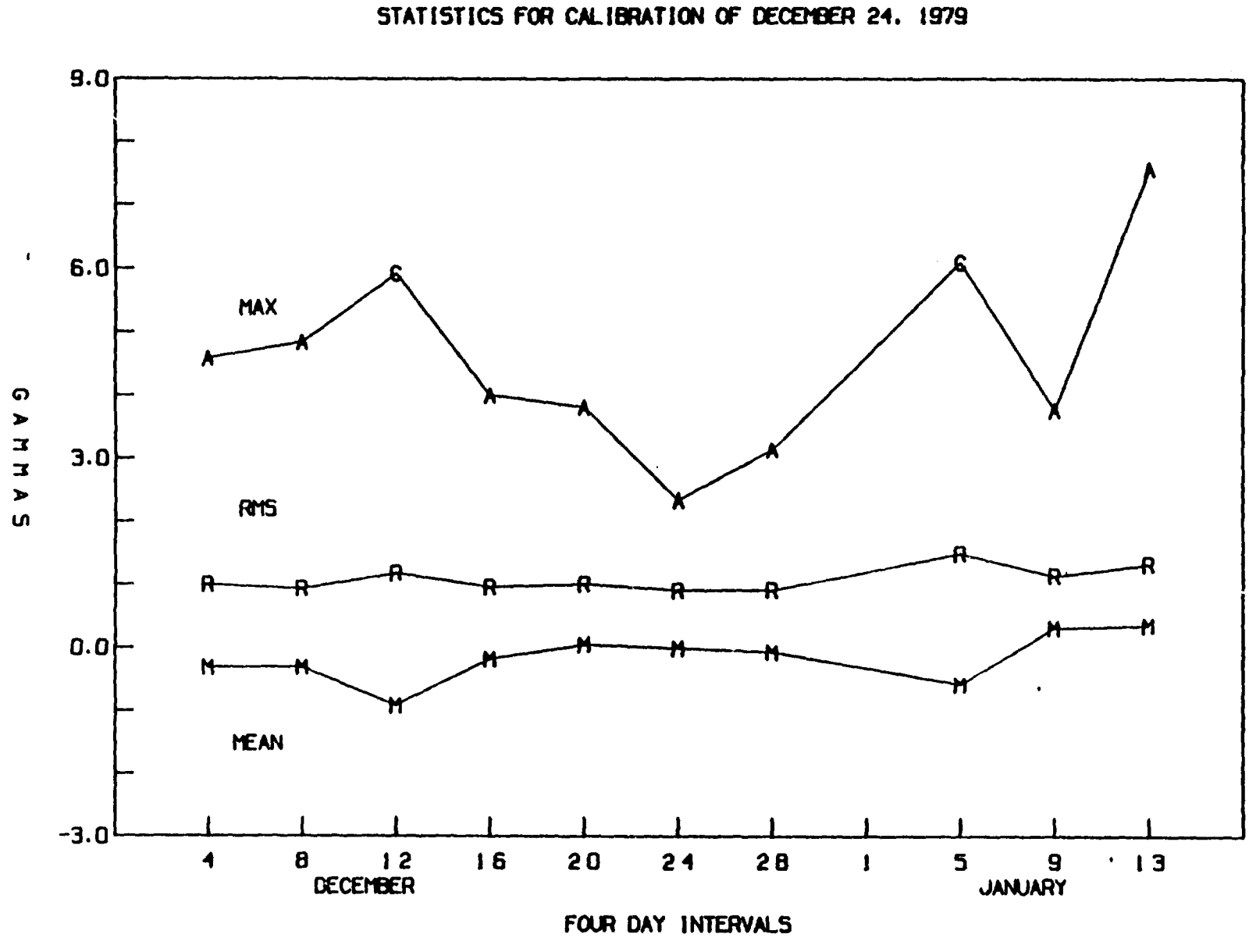
STATISTICS FOR CALIBRATION OF DECEMBER 24, 1979
9.0
6.0
3.0
0.0
-3.0
GAMMAS
MAX
RMS
MEAN
4
8
12
16
20
24
28
1
5
9
13
DECEMBER
JANUARY
FOUR DAY INTERVALS

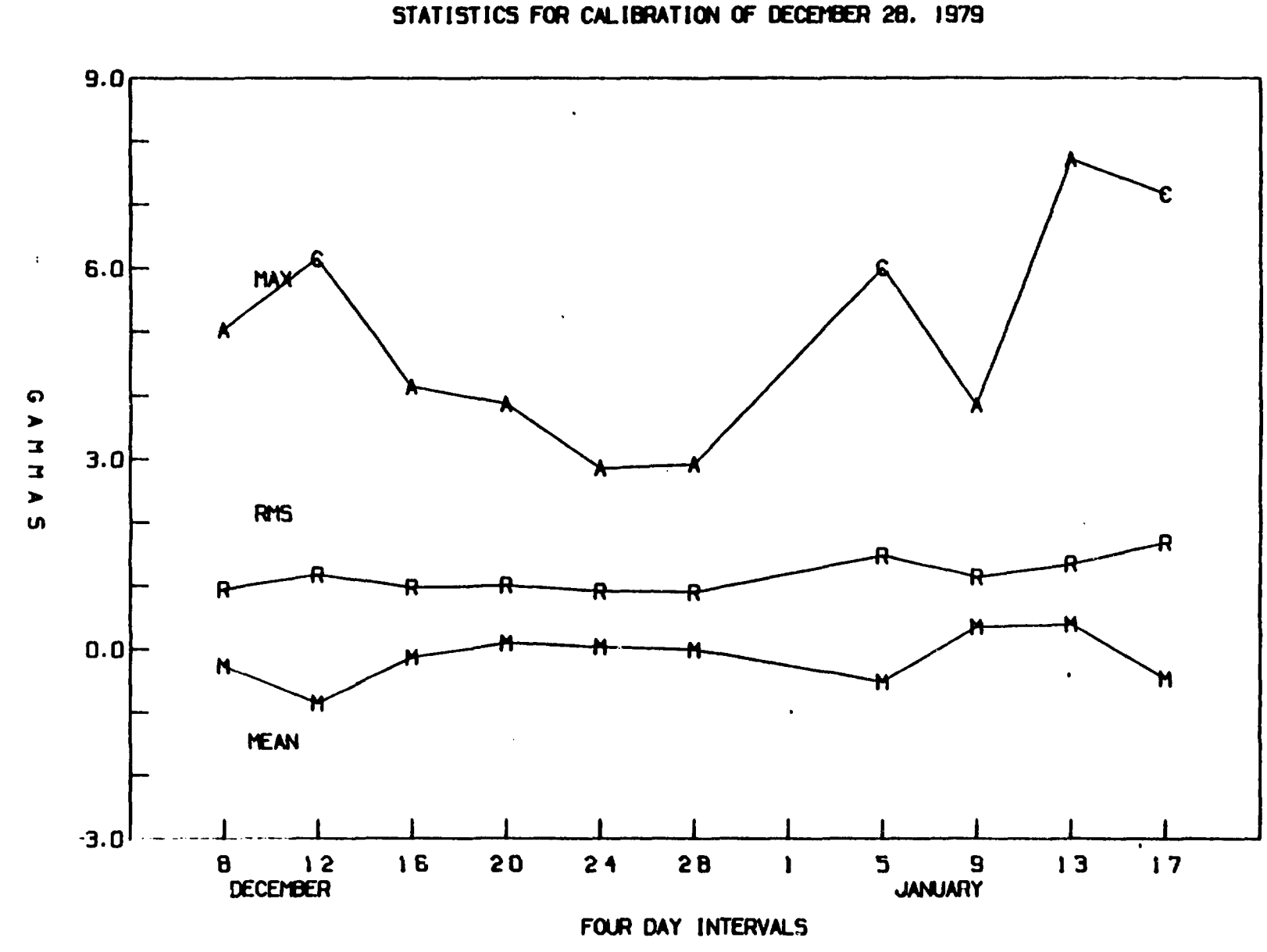
STATISTICS FOR CALIBRATION OF DECEMBER 28. 1979
9.0
6.0
3.0
0.0
-3.0
GAMMAS
MAX
RMS
MEAN
8
12
16
20
24
28
1
5
9
13
17
DECEMBER
JANUARY
FOUR DAY INTERVALS

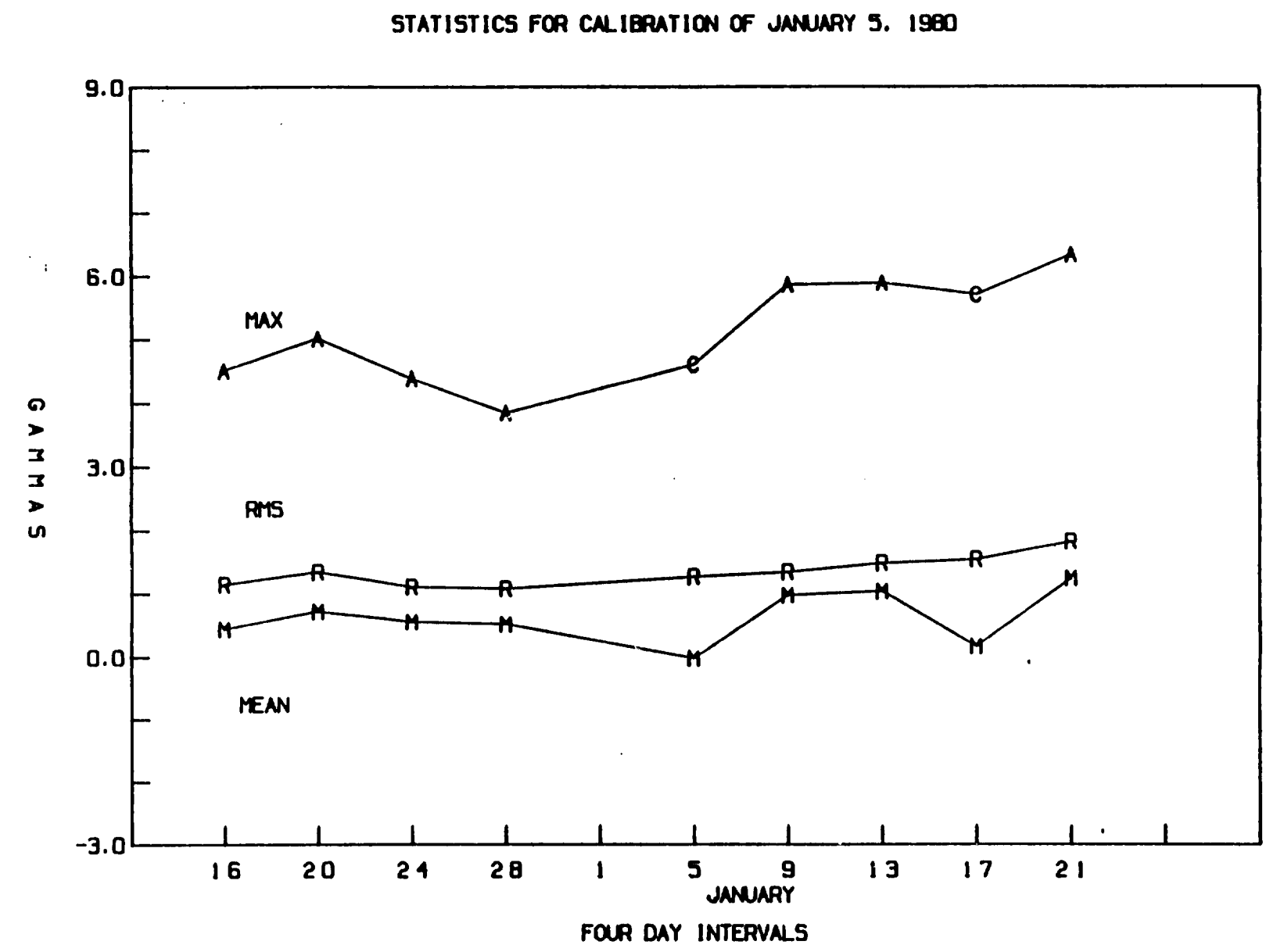
STATISTICS FOR CALIBRATION OF JANUARY 5. 1980
9.0
6.0
3.0
0.0
-3.0
GAMMAS
MAX
RMS
MEAN
16
20
24
28
1
5
9
13
17
21
JANUARY
FOUR DAY INTERVALS

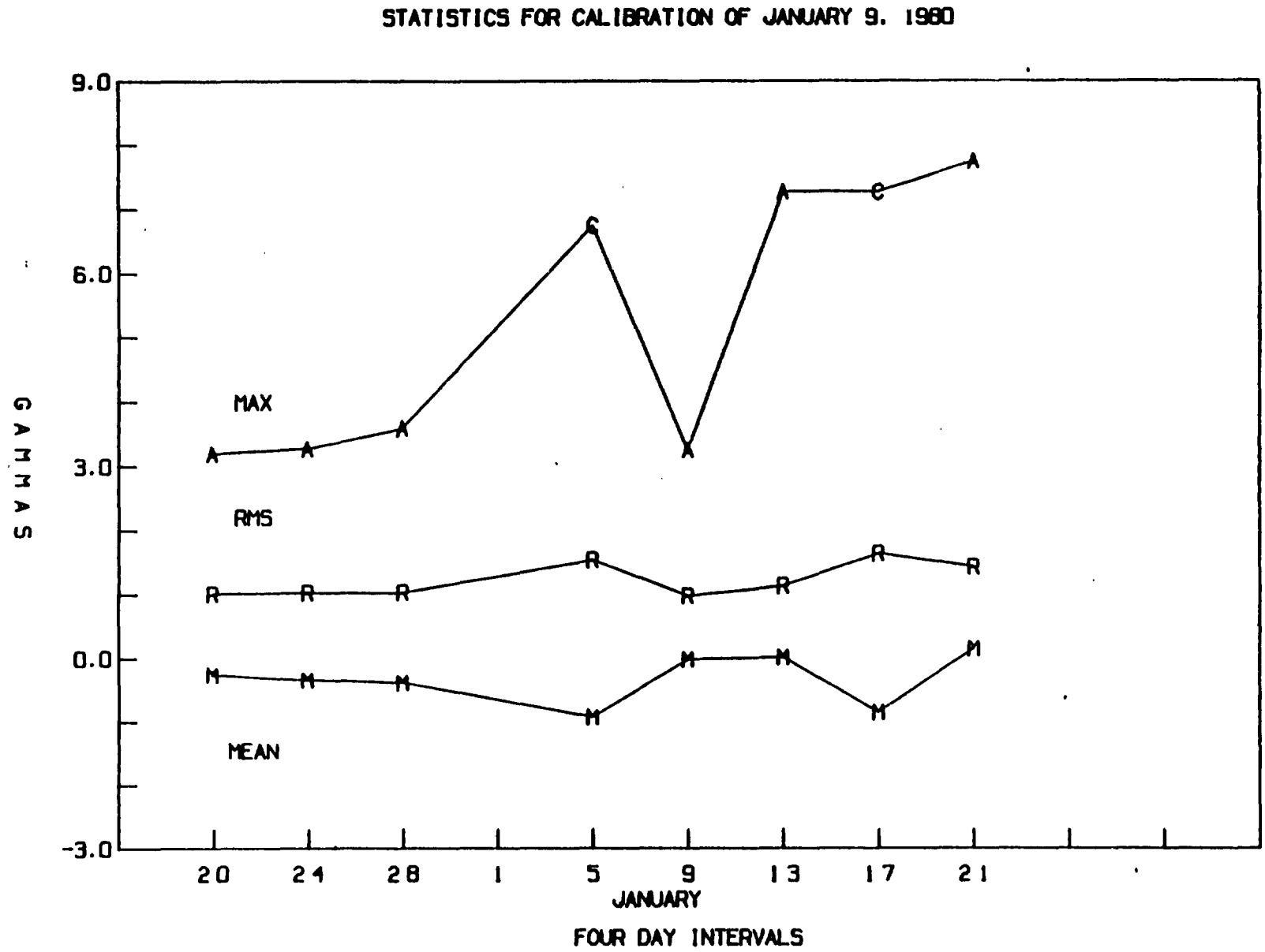
STATISTICS FOR CALIBRATION OF JANUARY 9. 1980
9.0
6.0
3.0
0.0
-3.0
GAMMAS
MAX
RMS
MEAN
20
24
28
1
5
9
13
17
21
JANUARY
FOUR DAY INTERVALS

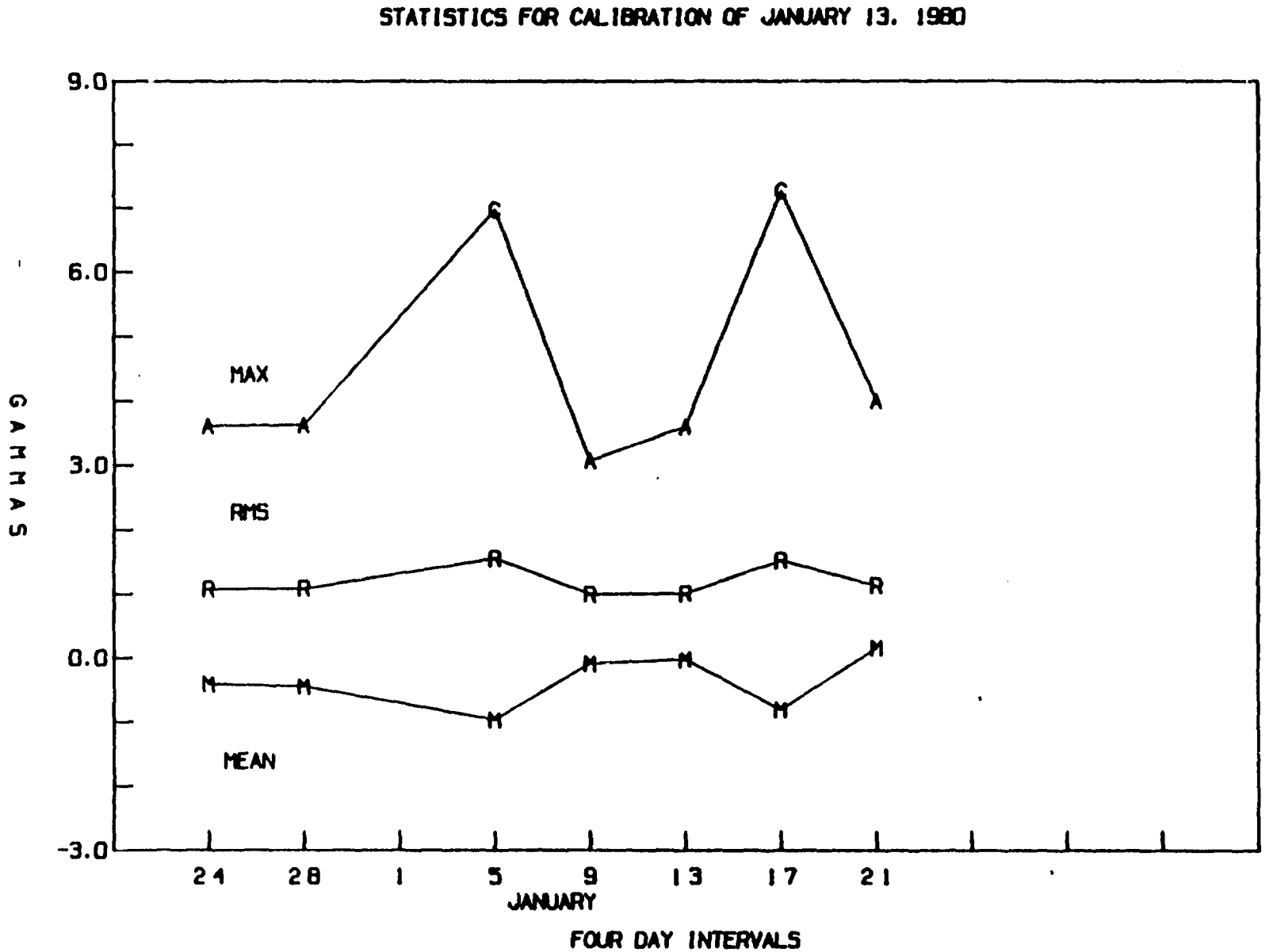
STATISTICS FOR CALIBRATION OF JANUARY 13, 1980
9.0
6.0
3.0
0.0
-3.0
GAMMAS
MAX
RMS
MEAN
24
28
1
5
9
13
17
21
JANUARY
FOUR DAY INTERVALS

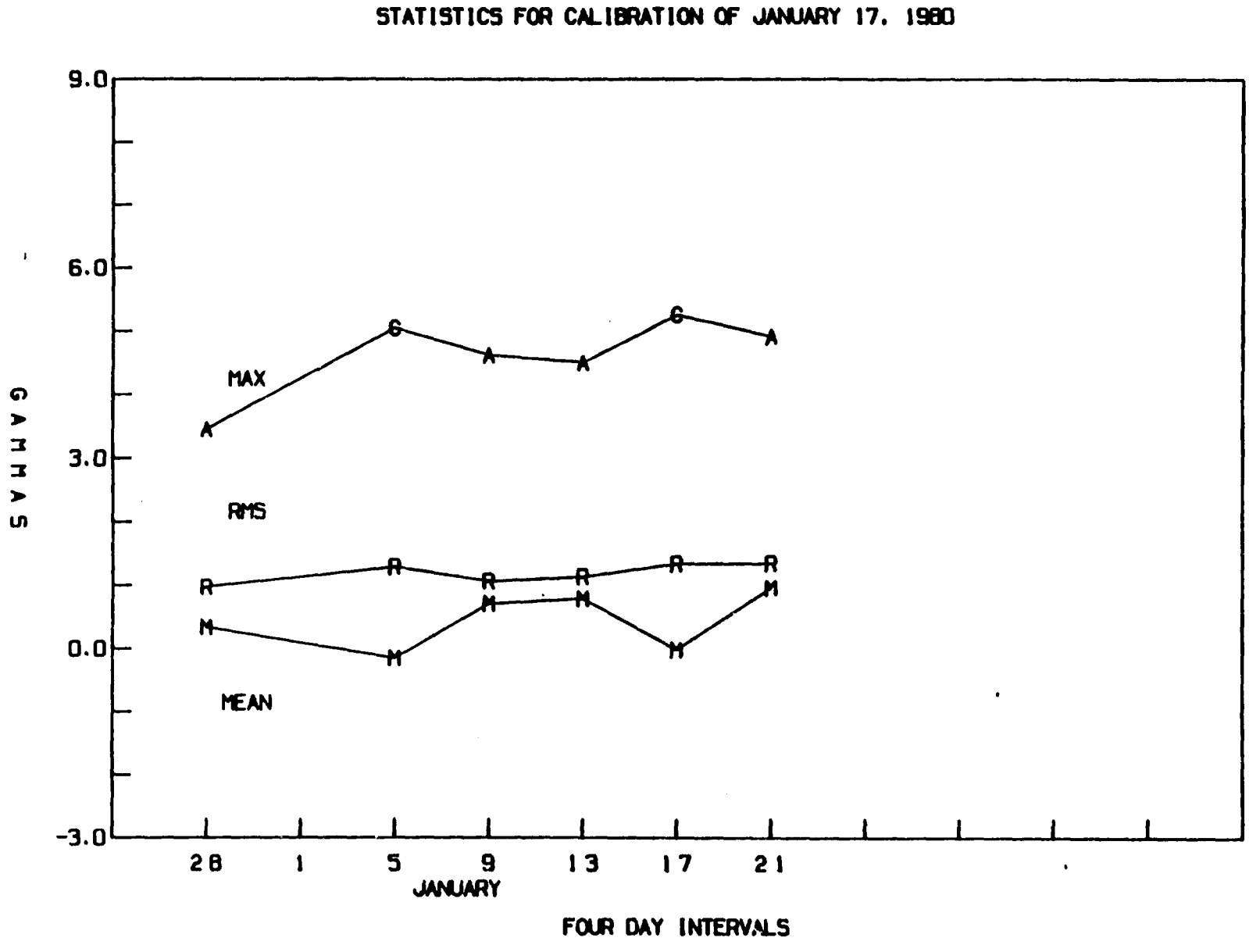
STATISTICS FOR CALIBRATION OF JANUARY 17, 1980
9.0
6.0
3.0
0.0
-3.0
GAMMAS
MAX
RMS
MEAN
28
1
5
9
13
17
21
JANUARY
FOUR DAY INTERVALS

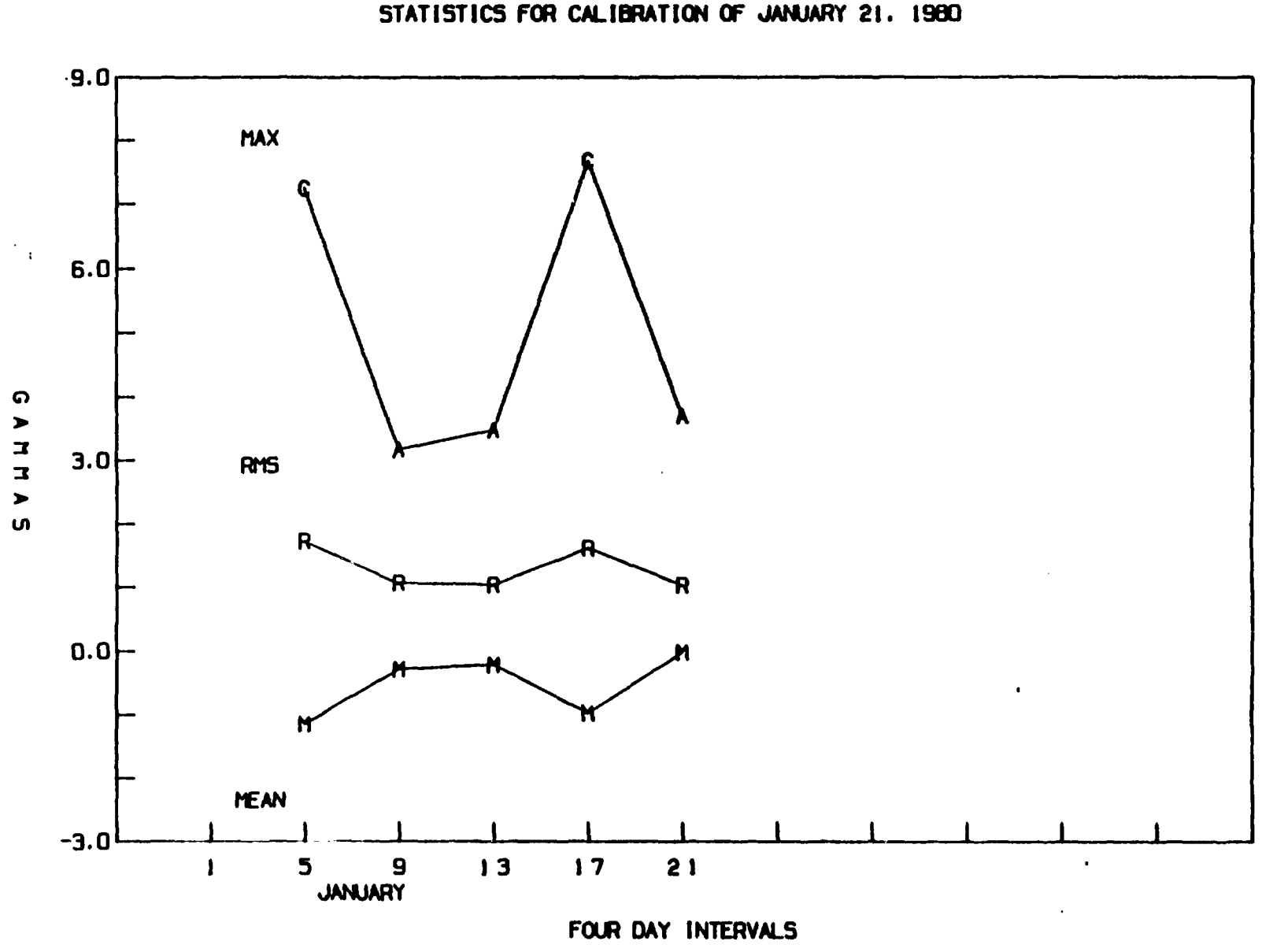
STATISTICS FOR CALIBRATION OF JANUARY 21. 1980
9.0
6.0
3.0
0.0
-3.0
GAMMAS
MAX
RMS
MEAN
1
5
9
13
17
21
JANUARY
FOUR DAY INTERVALS

SUMMARY

In summary, the results we have described indicate first that the calibration parameters of the MAGSAT vector magnetometer, particularly those associated with the third (z) axis, changed significantly between the pre-launch calibration and the first post-launch calibration. This can possibly be attributed to slight mechanical shifts due to the difference in stresses between a vacuum and non-vacuum environment. Second, some of the calibration parameters underwent small and slow systematic changes during the mission lifetime; and third, the calibration parameters determined from intercomparison with the scalar instrument are slightly different (~1 gamma) between the cases when both sensor A and sensor B of the scalar magnetometer are operating, when only sensor A is operating, and when only sensor B is operating. There are three possible causes for differences in vector calibration with respect to the scalar sensor configuration:

1. The change in null-zone configuration of the scalar instrument results in a bias in the distribution of vector directions visible in the calibration. This could cause imprecise determination of some calibration parameters, particularly those defining cross-coupling between axes of the vector instrument.
2. With only one sensor operable, heading errors on the scalar magnetometer are increased. Such errors will be geographically preferential, which means they will also occur at systematic directions of the field with respect to the vector magnetometer. That is, for certain field directions the scalar magnetometer would give an erroneous reading of up to 1.5 gammas, with a corresponding change in the determination of the vector magnetometer calibration parameters.
3. An interference of the scalar magnetometer with the vector magnetometer which changes with the scalar magnetometer configuration. Such an interference was experienced during pre-launch magnetic testing. In that case, the R. F. excitation signal from the scalar instrument caused a sensitivity shift in the vector instrument. This was most pronounced in the second (y) axis, still noticeable in the third (z) axis, and least discernable in the first (x) axis. Subsequent radio frequency shielding reduced the effect to less than one gamma at full scale.

In addition to knowing that the calibration parameters differ with the scalar configuration, we know that the calibration constants determined under a specific scalar configuration result in a larger mean difference when applied to data with a different scalar configuration. This would seem to rule out the first hypothesized cause for the difference. We need, however, to distinguish between causes 2 and 3 because if cause 2 is correct then we should utilize the more accurate calibrations from times when both sensors A and B were operating. If, on the other hand, radio frequency interference differences are affecting the measurements, then the calibration actually does change and the calibration parameters should be those derived from the scalar data with the same configuration that was in effect at the time of the data being calibrated.

Examination of the calibration parameter plots indicates that all axes are affected by scalar configuration changes. This seems to indicate that cause 2 is operable. However, more analysis is required before a final verdict is in.

REFERENCES

1. R. A. Langel, R. D. Reagan, J. P. Murphy, MAGSAT: A Satellite for Measuring Near Earth Magnetic Fields, GSFC X-922-77-199, July 1977.
2. M. H. Acuna, C. S. Scearce, J. B. Seek and J. Scheifele, The MAGSAT Vector Magnetometer – A Precision Fluxgate Magnetometer for the Measurement of the Geomagnetic Field, GSFC TM-79656, October 1978. (Revised October 1980.)
3. M. H. Acuna, MAGSAT-Vector Magnetometer Absolute Sensor Alignment Determination, NASA-GSFC TM-79648, September 1978. (Revised October 1980.)

BIBLIOGRAPHIC DATA SHEET

1. Report No.	2. Government Accession No.	3. Recipient's Catalog No.
TM 82046		

4. Title and Subtitle	5. Report Date
Magsat Vector Magnetometer Calibration Using Magsat Geomagnetic Field Measurements	November 1980
	6. Performing Organization Code
7. Author(s) E. R. Lancaster, Timothy Jennings, Martha Morrissey and Robert Langel	8. Performing Organization Report No.
9. Performing Organization Name and Address	10. Work Unit No.
Goddard Space Flight Center Greenbelt, Maryland 20771	11. Contract or Grant No.
	13. Type of Report and Period Covered
12. Sponsoring Agency Name and Address	Technical Memorandum
NASA	14. Sponsoring Agency Code

15. Supplementary Notes

16. Abstract

The Magnetic Field Satellite (Magsat) was launched on Oct. 30, 1979 into a nearly polar, sun-synchronous orbit, carrying a scalar magnetometer and a vector magnetometer. The satellite reentered the earth's atmosphere on June 11, 1980, having measured and transmitted more than three complete sets of global magnetic field data. The data obtained from the mission will be used primarily to compute a currently accurate model of the earth's main magnetic field, to update and refine world and regional magnetic charts, and to develop a global scalar and vector crustal magnetic anomaly map.

This report describes the in-flight calibration procedure used for 39 vector magnetometer system parameters and gives results obtained from some data sets and the numerical studies designed to evaluate the results.

17. Key Words (Selected by Author(s))	18. Distribution Statement
Magsat, Magnetometer, Magnetic Field Measurement, Calibration	

19. Security Classif. (of this report)	20. Security Classif. (of this page)	21. No. of Pages	22. Price*
Unclassified	Unclassified		

*For sale by the National Technical Information Service, Springfield, Virginia 22151.

GSFC 25-44 (10/77)

FILMED

JAN 29 1998